Characterization of Solid Waste in a Bioreactor Landfill Using Seismic Borehole Techniques

A thesis submitted to
the Faculty of Graduate Studies and Research
in partial fulfillment of the requirements for the degree

Masters of Applied Science in Environmental Engineering

By

Taryn Glancy

B.Eng Environmental Engineering

Department of Civil and Environmental Engineering
Carleton University

Ottawa-Carleton Institute of Civil and Environmental Engineering

May 2009

Your file Votre référence
ISBN: 978-0-494-52039-0
Our file Notre référence
ISBN: 978-0-494-52039-0

Abstract

Optimization of biodegradation in bioreactor landfills will allow for faster waste stabilization and enhanced methane production. A key parameter affecting the rate of biodegradation is moisture content. Currently there is no method to measure bulk moisture content within the landfill. This study evaluates the seismic tomography approach in order to map the seismic velocity distribution between two boreholes within a bioreactor landfill. Compressional wave velocity is dependant on a number of different factors including water content. A surface 5.4 kg hammer source proved more effective than a buffalo gun and a borehole hammer source. Compressional waves ranged from 300 – 500 m/s and shear waves ranged from 140-210 m/s, both having a velocity gradient increasing with depth. Seismic tomography was not as successful as anticipated. Data was noisy and difficult to pick. Difficulties with the seismic sources resulted in limited coverage. Wavelengths of generated waves result in near-field conditions making it difficult to note changes in waveform. The addition of 7000 m^3 of water between the boreholes did not result in a detectable increase in compressional wave velocity. It was difficult to control the flow of water between the boreholes. Waste conditions may not have been in a saturation range sensitive to velocity changes.

Acknowledgements

I would like to give my greatest thanks to both of my supervisors Dr. Paul Van Geel and Dr. Claire Samson. They have both been extremely supportive and helpful throughout the duration of this project. They both were very pro-active during field surveys despite the long hours and cold weather. They have made my experience as a Master's student very rewarding and I could not have done it without them.

I would like to acknowledge our industry partners for both their cash and in-kind contributions including Michael Pullen from Waste Management of Canada, Michael Snow from Golder Associates, and David Harding from WESA Inc. I would like to thank Chris Phillips from Golder Associates for his assistance during Survey 1. I would also like the thank Erwan Gloaguen and his team from Institut National de la Recherche Scientifique for their support in the GPR field survey. I would like to thank Houle-Chevrier Engineering Ltd for lending the team equipment during two field surveys.

I would extend my gratitude to Ghyslain Lecours and the staff at the Ste. Sophie landfill for their assistance during our field surveys. I would like thank Susan Pullan and Jim Hunter from the Geological Survey of Canada (GSC) for the loan of equipment and providing feedback on our results and survey plans. I would also like to thank Heather Crow from the GSC for taking the time to show me how to use equipment and answering many of my questions while I was analyzing the data.

Last but not least, I would like to thank my parents Lorna and Brian, my sister Brianna, and my best friend Laura for all of their love and support throughout my time as a graduate student. I would like to thank Pat for the many hours spent helping me resolve computer issues and assisting in the CAD figures presented in this thesis.

Table of Contents

List of Figures

List of Tables

1.0 Introduction

1.1 Problem Statement

Bioreactor landfills offer many advantages over conventional landfills. Bioreactors utilize enhanced microbiological processes to degrade the waste at a much faster rate. This enhanced degradation is mainly encouraged by maintaining the waste at a higher moisture content. The moisture content for conventional landfills usually falls within the range of 20-30 % (by weight), which is below the optimum range for waste biodegradation. Moisture contents in the range of 40-70% (by weight) have been shown to be much more effective (Reinhart and Townsend, 1998). Added moisture enhances biodegradation by serving as a reactant in hydrolysis, transporting enzymes and nutrients, dissolving metabolites, providing pH buffering, diluting inhibitory compounds and stimulating the methanogenic fermentation phase of solid waste (Reinhart and Townsend, 1998). A higher level of moisture content can be achieved by means of leachate recirculation via a series of leachate recirculation pipes installed throughout the landfill, or by the addition of water to the waste at the tipping face. Other processes such as waste shredding, pH adjustment, nutrient addition and temperature control can also aid the biodegradation process (Warith, 2002).

Enhanced biodegradation results in faster waste stabilization leading to improved leachate quality and a shorter contaminating lifespan. The financial burden of post-closure care is greatly reduced. Settlement also occurs at a faster rate which then results in more available landfill airspace and extends the landfill life. Landfill gas generation is increased and landfill gas collection becomes a financially feasible option. In this case,

greenhouse gas emissions are greatly reduced (Warith, 2002). A key issue in bioreactor landfill operations is to maintain uniform degradation throughout the waste. If this is achieved, landfill reclamation becomes a feasible option. In this case, the degraded waste can be removed from the landfill, sorted for potential recyclables such as metals, and then placed into a less engineered facility. The bioreactor can then be reused to degrade new waste. In this case, bioreactors landfills would then become much more economical (Warith, 2002).

To ensure uniform degradation throughout the landfill, operators must ensure a uniform moisture content. In order to know where to recirculate leachate, operators must first have knowledge of the moisture distribution throughout the landfill. There are also some cases in which the waste becomes saturated and leachate seeps out the sides of the landfill. Saturated waste also impedes the flow of the landfill gas generated, thereby reducing economic benefits. It would be useful to delineate the boundaries of this saturation in the landfill so operators know where to avoid recirculating leachate. Currently there is no effective method to measure bulk moisture content in a landfill. A number of techniques have been attempted in the past. The limitations of these methods are discussed in Chapter 2.

1.2 Research Objectives

The proposed research is an evaluation of seismic borehole techniques to detect changes in compressional wave velocity under variable moisture contents. Yang (2002) was able to relate compressional wave velocity through sand to saturation in laboratory

experiments. The assumption is that solid waste would have a similar response. An earlier surface seismic study conducted by Catley et al. (2006) provided a proof of concept. It was concluded that it was possible to record compressional wave reflections from the landfill base and that the velocity of compressional waves increased after the recirculation of leachate. A surface survey is limited in that, the measured velocity is an average velocity over the entire waste column. There is no way to determine exactly where vertically the higher-velocity, moister waste is located.

In order to more accurately delineate the moisture distribution within the waste, two vertical boreholes were installed on top of the landfill. These boreholes were then used to house seismic instruments to allow for the recording of seismic waves propagating throughout the waste between the boreholes. A seismic tomography approach was utilized to map the moisture distribution between the two boreholes. Tomography inverts the traveltimes of seismic waves propagating along multiple raypaths into a velocity distribution.

1.3 Site Description

Three surveys were conducted at the bioreactor landfill located in Ste. Sophie, Quebec. The bioreactor is owned and operated by Waste Management of Canada Inc., and accepted both municipal and industrial waste from 2000 to 2005. The bioreactor is considered one of the largest in North America. The cell where the study was conducted is 450m long by 325m wide by 30m deep. A final cover consisting of about 30 cm of top soil, 90 cm of clay and 150 cm of sand was placed on the landfill in 2006. The sides of

the landfill are sloped at approximately 30%. The bioreactor has four horizontal series of gravel trenches with a vertical spacing of 6-8 m and a horizontal spacing of 15-20 m. The exact locations of all the trenches are illustrated in Figure 1.1. The bottom three trench series contain both leachate injection pipes and biogas collection pipes. The top series trench contains only biogas collection pipes. Each gravel trench is approximately 1 m wide and 1.5 m deep. The biogas collection pipes are constructed from perforated HDPE with a diameter of 150 mm. The leachate injection pipes are constructed from perforated HDPE with a diameter of 75 mm.

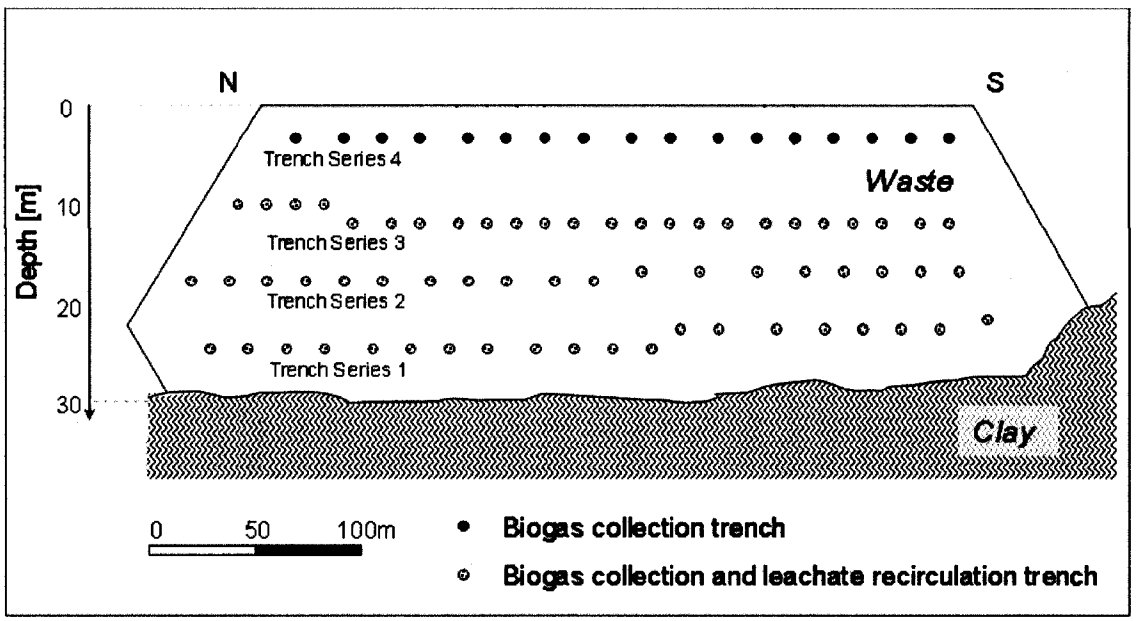

Figure 1.1: North-South cross-section of the Ste. Sophie bioreactor landfill (Catley et al., 2006).

1.4 Thesis Overview

Following the introduction, Chapter 2 is a literature review which provides an overview of the different methods that have been used to measure moisture content in solid waste. The theory of seismic waves, factors affecting seismic wave velocity, and typical seismic wave velocities in solid waste are discussed. Also provided is a review of seismic surveying techniques, including a description of equipment used and of different types of borehole surveys. A brief outline of data processing and analysis is included.

Chapter 3 provides detailed data acquisition descriptions for the three field surveys conducted. Survey 1 conducted in November of 2007 was a preliminary field survey to test equipment with the newly installed boreholes and obtain a data set to detect changes in compressional wave velocity with changes in moisture. Survey 2 was conducted in June of 2008 to test equipment and obtain data in order to characterize the waste in terms of seismic wave propagation in the absence of moisture content changes. Survey 3 was conducted in November of 2008 to again attempt to detect changes in compressional wave velocity with changes in moisture content and to further characterize the waste. A different geophysical technique, Ground Penetrating Radar, was attempted to detect changes in moisture content.

Chapter 4 provides a discussion of seismic wave propagation in solid waste. The discussion includes filtering of seismic data, wave type identification, dominant wave types, comparison of seismic sources, quality of data at variable offsets and tomography.

Chapter 5 focuses of seismic velocity in waste under variable moisture conditions. A discussion on the moisture distribution within a landfill is provided. During Survey 1 and Survey 3 several seismic experiments were conducted before and after water addition in an attempt to detect changes in P-wave velocity due to moisture content.

Chapter 6 provides conclusions from the analysis conducted for all surveys. It also discusses some recommendations for potential future work.

2.0 Background Theory and Literature Review

2.1 Overview of Seismic Waves

If an unbalanced stress is applied to an elastic body, strain is propagated outwards as a seismic wave. Stress can originate from an artificial impulse, like a hammer strike used in near-surface seismology or from a natural phenomenon like a fault rupture at an earthquake hypocentre.

The two types of seismic waves are body and surface waves; however, this research deals exclusively with body waves. Body waves include compressional waves and shear waves, which are referred to herein as P-waves (primary-waves) and S-waves (secondary-waves), respectively.

2.1.1 Body Waves

For P-waves, the particles of the medium move in the direction of wave propagation, while expanding and contracting the medium. For S-waves, the particles of the medium move perpendicular to the direction of wave propagation. These particle motions are illustrated in Figure 2.1. S-waves can be polarized in two orthogonal planes: when particle motion is in the vertical plane, they are referred to as SV-waves, and when the particle motion is in the horizontal plane, they are referred to as SH-waves.

Seismic energy can convert between P-waves and S-waves when reflecting at a boundary between media of different elastic properties. Mode conversion is small at normal incidence, and therefore not as prominent at short offsets (Schuck and Lange, 2007).

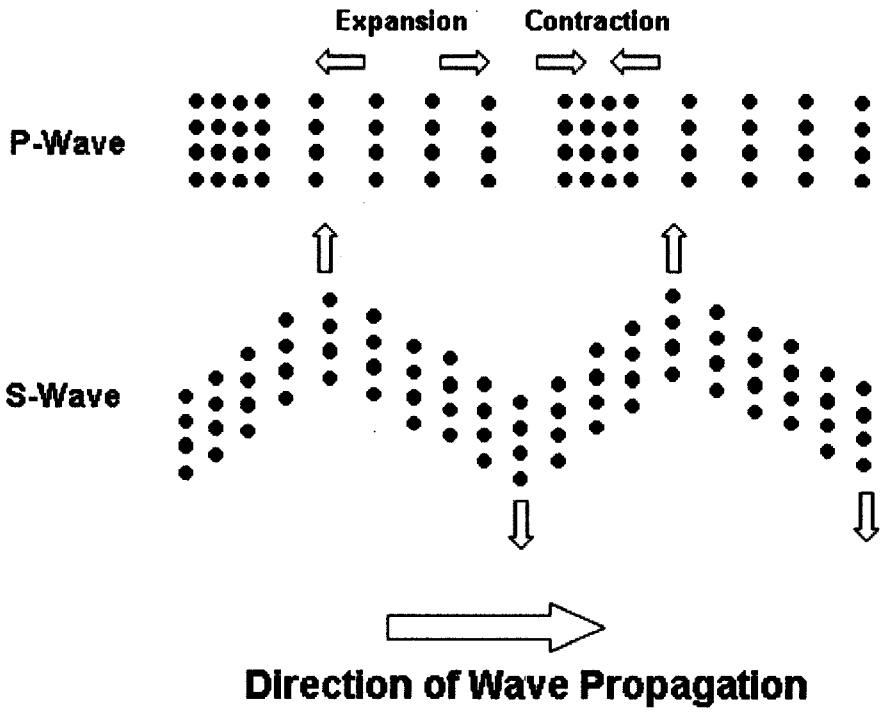

Figure 2.1: Particle motion during the propagation of P-waves (top) and S-waves (bottom). Adapted from (Sharma, 1997).

2.2 Velocity of Seismic Waves

In homogeneous solids, the velocity of both P-waves and S-waves, denoted V_P and V_S respectively, are dependant on density and elastic properties. In heterogeneous solids, factors such as porosity, fracturing, fluid density, solid density and the chemical composition of the medium itself can all affect seismic wave velocity. A good

mathematical description of seismic wave velocity can be found in Sharma (1997). An overview of the different equations and associated parameters shown is provided below.

2.2.1 Homogeneous Solids

In homogeneous solids, the velocity of P-waves and S-waves is dependant on density and elastic properties as described in Equations 2-1 and 2-2:

$$V_p = \sqrt{\left(\frac{K + \frac{4G}{3}}{\rho} \right)} \tag{2-1}$$

$$V_s = \sqrt{\frac{G}{\rho}} \tag{2-2}$$

where:

V_P = Compressional wave (P-wave) velocity (m/s)

V_S = Shear wave (S-wave) velocity (m/s)

K = bulk modulus = volume stress/volume strain (Pa)

G = shear modulus = shear stress/shear strain (Pa)

ρ = density (kg/m^3)

Using the fact that the elastic moduli are always positive, a simple visual inspection of Equation 2-1 and Equation 2-2 reveals that V_P is always greater than V_S and therefore P-waves are the first wave to be recorded. Most media are not homogeneous and therefore

Equations 2-1 and 2-2 cannot be directly applied. In these cases, empirical relationships are derived.

2.2.2 Seismic Velocity in Solid and Porous Media

In heterogeneous solids, factors such as interstitial fluids, porosity and density of the medium itself can all affect seismic wave velocity. In porous media, saturation can have a large effect on P-wave velocity.

Interstitial Fluids

In the case of liquids and gases, the shear modulus becomes equal to 0. S-waves cannot propagate through fluids and, for a given medium, S-wave velocity will essentially be the same for dry or saturated conditions (Sharma, 1997). P-waves are able to propagate through fluids and are largely affected by fluid content within the medium.

Depending on the contrast in velocity between the fluid and the solid matrix, interstitial fluid content can either increase or decrease P-wave velocity. For rocks, P-wave velocity decreases if the rocks are porous or highly fractured. This is because P-wave velocity through air (≈0.3 km/s) and water (≈1.5 km/s) is much lower than in solid rock (2.5-6.5 km/s). In highly porous and unconsolidated media such as sand, P-wave velocity increases with saturation. This is because P-wave velocity is much faster in water compared to unsaturated consolidated media.

Porosity

As porosity increases, density will decrease and the elastic properties will change, which could largely affect seismic velocity (Sheriff and Geldart, 1995). Wyllie et al. (1958) gives the relationship in Equation 2-3 for P-wave velocity in saturated sandstone, used extensively in borehole-log interpretation.

$$\frac{1}{V_{SAT}} = \frac{n}{V_F} + \frac{1-n}{V_M} \tag{2-3}$$

where:

V_{SAT} = P-wave velocity in saturated rock (m/s)

V_F = P-wave velocity in the fluid (m/s)

V_M = P-wave velocity in the solid rock matrix (m/s)

n = porosity

Density

Variations in density are mainly due to changes in porosity (Sheriff and Geldart, 1995). For sedimentary rocks, Gardner et al. (1974) provides the empirical relationship shown in Equation 2-4 relating P-wave velocity and density.

$$\rho = \alpha V_p^{\frac{1}{4}} \tag{2-4}$$

where:

ρ = density (kg/m^3)

α = 1670

V_p = P-wave velocity (km/s)

The effect of saturation in porous media

A key working assumption of this study is that seismic waves will travel through solid waste in a manner similar to propagation through sand. Sharma (1997) reports a P-wave velocity of 300-1000 m/s for dry sand and 1200-1900 m/s for saturated sand. The high porosity nature of sand results in a higher P-wave velocity with increasing saturation.

Yang (2002) has developed a series of equations to quantify the relationship between P-wave velocity and the degree of saturation in sand. These relationships make use of Equation 2-5 developed by Skempton (1954) to define the pore pressure coefficient. Equation 2-6 for P-wave velocity was shown to be valid in the field (Yang & Sato, 2000). Finally, combining Equations 2-5 and 2-6 yields the relationship between P-wave velocity and pore pressure coefficient given in Equation 2-7. It may be more useful to use the degree of saturation instead of pore water pressure, and therefore Equation 2-8 expresses the relationship between these two parameters.

$$B = \left[1 + n\frac{K_b}{K_f}\right]^{-1} \tag{2-5}$$

where:

B = pore pressure coefficient

n = porosity

K_b = bulk modulus of the soil skeleton (Pa)

K_f = bulk modulus of the fluid (Pa)

$$V_p = \left(\frac{K_b + \frac{4}{3}G + \frac{K_f}{n}}{\rho} \right)^{\frac{1}{2}} \tag{2-6}$$

where:

V_p = P-wave velocity (m/s)

G = shear modulus (Pa)

ρ = density (kg/m^3)

$$V_p = \left(\frac{\frac{4}{3}G + \frac{K_b}{(1-B)}}{\rho} \right)^{\frac{1}{2}} \tag{2-7}$$

$$B = \left[1 + n\frac{K_b}{K_w} + n\frac{K_b}{P_a}(1 - S_r) \right] \tag{2-8}$$

where:

S_r = degree of saturation

K_w = bulk modulus of the pore water (Pa)

P_a= absolute fluid pressure (Pa)

Yang (2002) provides graphical illustrations of these relationships including Figure 2.2 showing the change in P-wave velocity with the pore pressure coefficient. Figure 2.3 taken from Hatanaka and Masuda (2008) illustrates the change in P-wave velocity with saturation (Sr) for different grain sizes of sand. In all cases, P-wave velocity is most

sensitive to change in the range of 85-100% saturation. It is hoped that the relationship between P-wave velocity and the degree of saturation for waste is more sensitive at lower saturation levels.

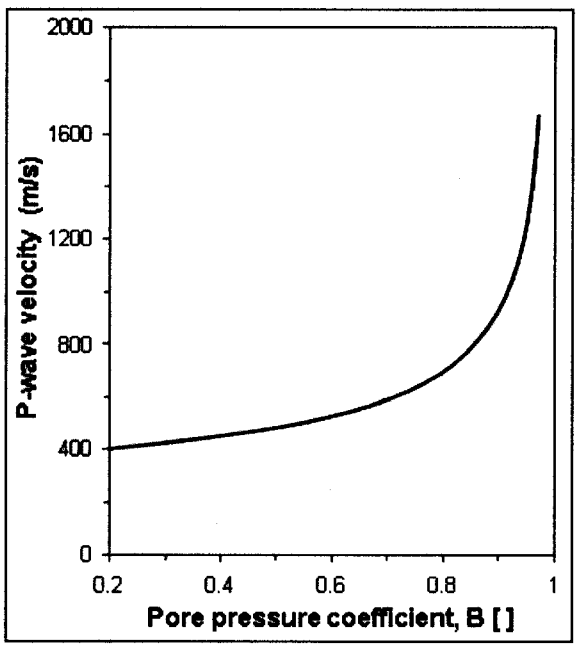

Figure 2.2: The relationship between P-wave velocity and the pore pressure coefficient for a sand (Yang, 2002).

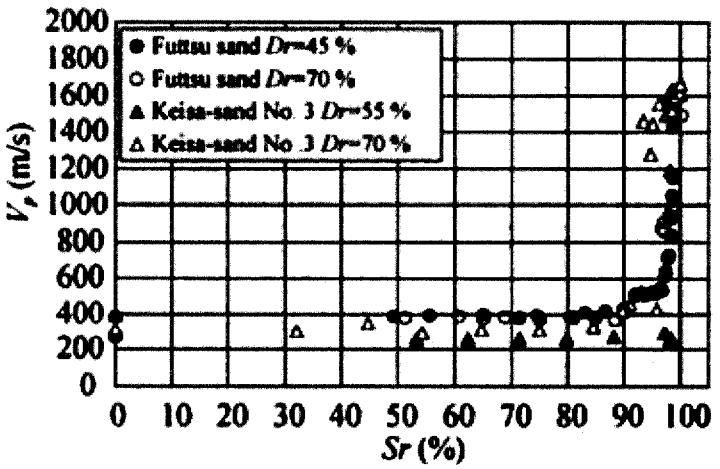

Figure 2.3: The relationship between P-wave velocity and Sr for a sand (Hatanaka and Masuda, 2008)

2.3 Seismic Wave Velocity in Solid Waste

Older landfills often have unknown geometric and physical parameters. Seismic refraction and reflection surveying can help provide information on the waste depth, cover thickness, boundary locations, unit weight versus depth profiles and the nature of the host sediments. Choudhury and Savoikar (2009) provide profiles of S-wave velocity versus depth for various landfill sites in Figure 2.4. Many of the S-wave velocity profiles from Figure 2.4 have been taken from Kavazanjian et al (1996). A number of studies have been reviewed and a summary of measured P-wave and S-wave velocities is presented in Table 2.1.

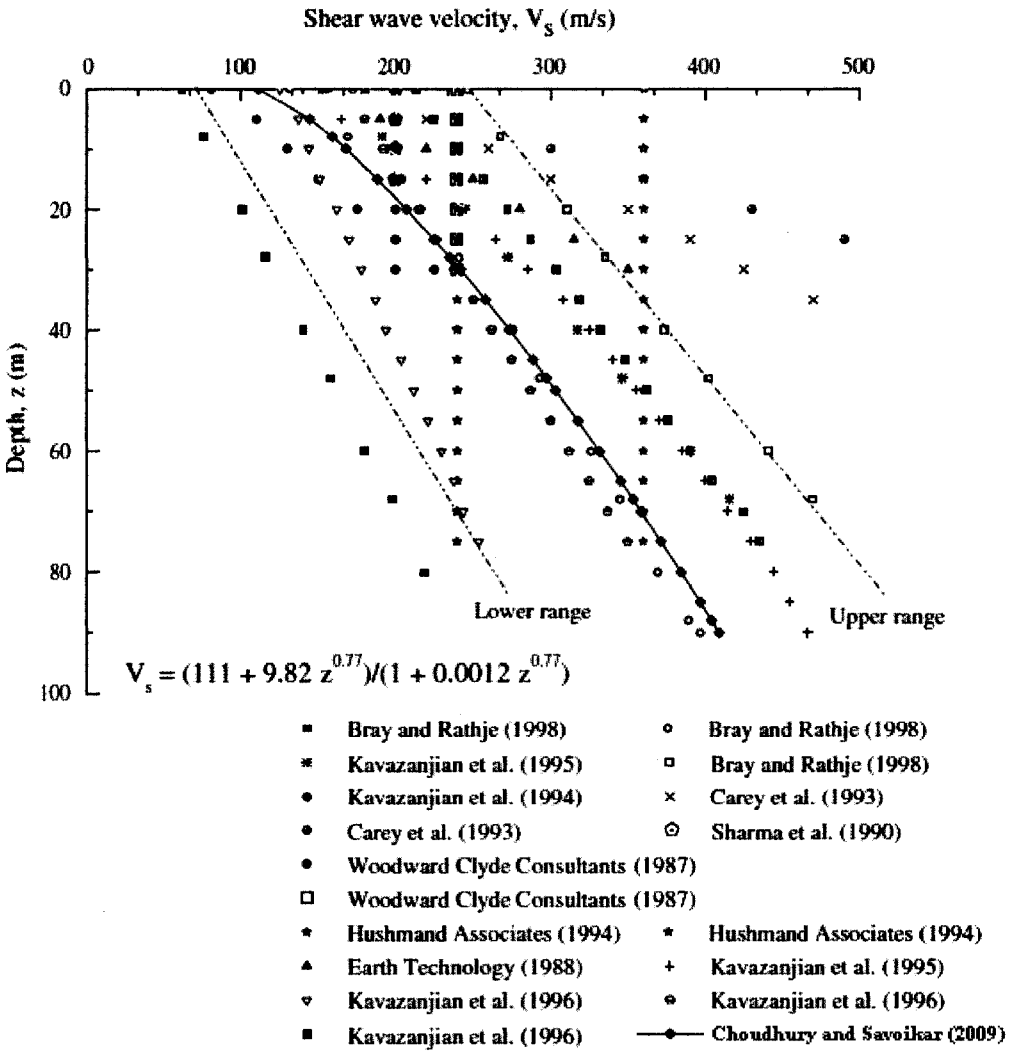

Figure 2.4: S-wave velocity vs. depth profiles in various solid waste sites (Choudhury and Savoikar, 2009).

Table 2.1: Summary of published P-wave and S-wave velocities.

Source	Location	Depth Range (m)	P-wave Velocity (m/s)	S-wave Velocity (m/s)
Cardarelli and Di Filippo (2004)	Caprarola, Italy	10	280	-
Cardarelli and Di Filippo (2004)	Rome, Italy	5-15	300-600 (Increasing with depth)	-
Lanz (1998)	Switzerland	10	<1000	-
Kavazanjian et al. (1996)	Los Angeles, California	0-60	-	150-400 (Increasing with depth)
Bouazza and Kavazanjian (2000)	Melbourne, Australia	0-30	-	60-250 (Increasing with depth)
Sharma et al. (1990)	Richmond, California	0-15	717	198
Catley et al. (2006)	Ste.Sophie, Quebec	0-30	275-400	-

In addition to the S-wave velocity vs. depth profiles, unit weight vs. depth profiles were also obtained for the same cross-sections. Choudhury and Savoikar (2009) provide unit weight vs. depth profiles in Figure 2.5. Most of the profiles illustrated in Figure 2.5 were taken from Kavazanjian et al. (1996). Choudhury and Savoikar (2009) were able to use curve fitting techniques to then relate S-wave velocity to unit weight.

First, data from Figure 2.4 were used to develop Equation 2-9 to relate the S-wave velocity with depth in a landfill:

$$V_s = \frac{111 + 9.82z^{0.77}}{1 + 0.0012z^{0.77}} \qquad (2\text{-}9)$$

Next, data from Figure 2.5 was used to develop Equation 2-10 to relate the unit weight of waste to depth in a landfill:

$$\gamma_{waste} = \frac{14.46}{(1+e^{6.06-0.207z})^{0.064}} \quad (2\text{-}10)$$

where:

γ_{waste} = unit weight of waste (kN/m^3)

z = depth (m)

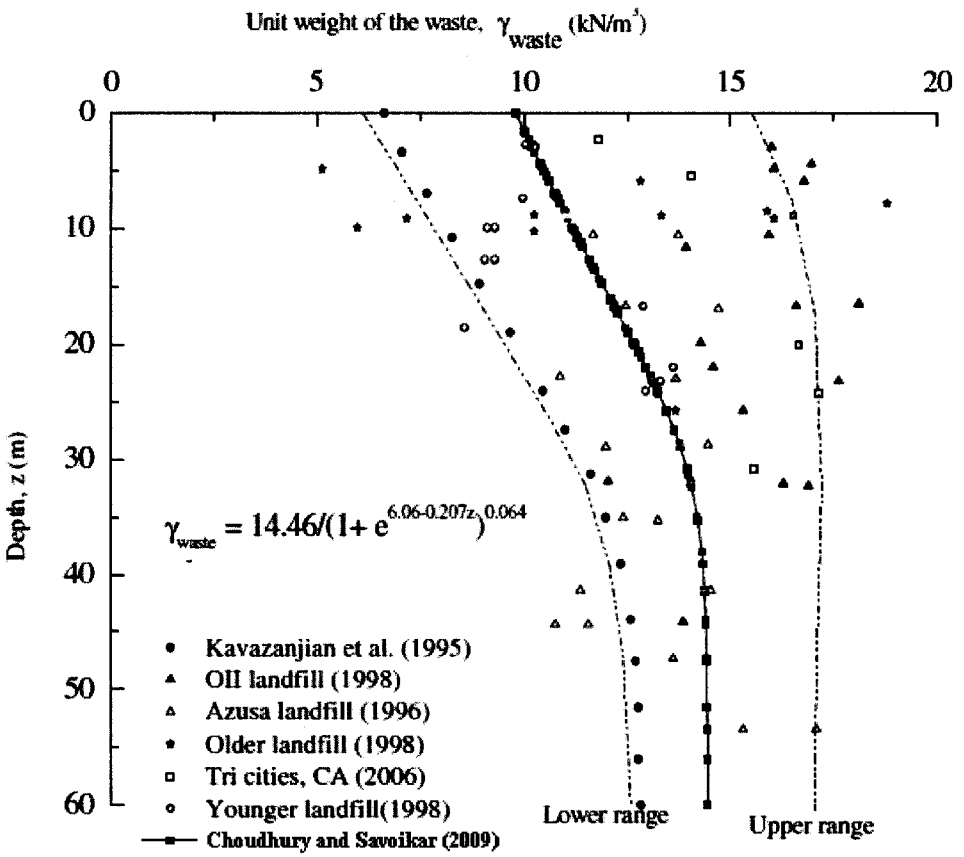

Figure 2.5: Unit weight vs. depth profiles in various solid waste sites (Choudhury and Savoikar, 2009).

Finally, Figure 2.6 can be generated by combining the curves given by Equations 2-9 and 2-10. Again, curve fitting techniques were employed to relate S-wave velocity to the unit weight of the waste in Equation 2-11.

$$Vs = \frac{1}{0.0174 - 0.000978\gamma_{waste}} \tag{2-11}$$

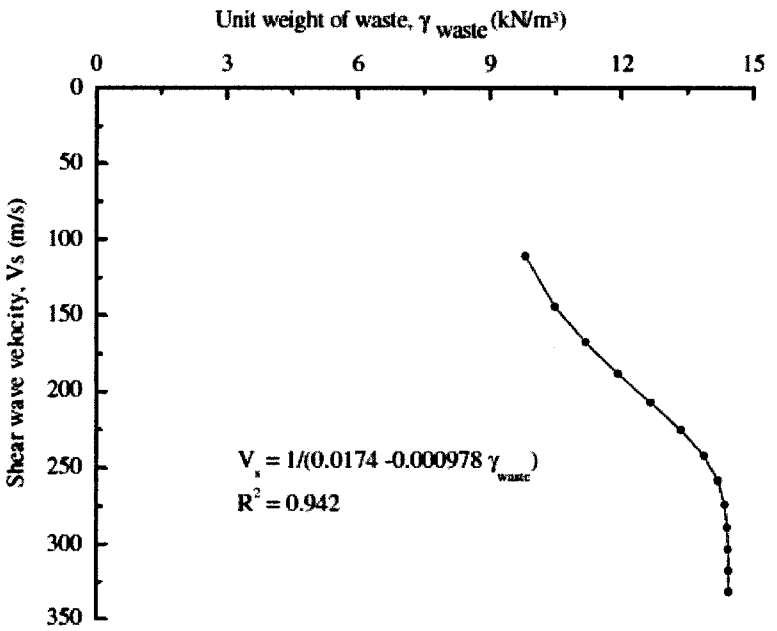

Figure 2.6: Plot of unit weight of waste as a function of shear wave velocity (Choudhury and Savoikar, 2009).

2.4 Attenuation of Seismic Waves

When a seismic wave is generated from a point source in an infinite homogeneous elastic medium, the wave energy travels outward in a spherical fashion over the area given by $4\pi r^2$. This area increases with the square of the distance, r, and therefore the energy per unit area is reduced by $1/r^2$. The amplitude, A, decreases as 1/r with increasing r as described in Equation 2-12:

$$A = \frac{A_o e^{\alpha r}}{r} \tag{2-12}$$

where:

A = amplitude at distance r

A_0 = initial amplitude

r = distance from point source

α = attenuation coefficient

In addition to wavefront spreading, attenuation also occurs by means of absorption into the material as heat. Scattering is also another cause for attenuation in heterogeneous materials. In this case, some of the wave energy will deviate from a straight trajectory when passing through a local non-uniformity. Experimental studies indicate that over a given distance, higher-frequency waves will attenuate quicker than lower-frequency waves (Sharma, 1997). As a result, a sharp wavefront will degenerate into a long wavetrain as the distance of travel increases.

2.5 Seismic Equipment

2.5.1 Sources

A number of factors must be considered when choosing an appropriate seismic source such as strength, frequency content, repeatability, portability, cost, time between shots, environmental damage and safety requirements (Miller et al., 1986).

The frequency spectrum of the source determines the level of resolution of subsurface structures (Schuck and Lange, 2007). The frequency content of the source signal is dependant on both the primary energy and the ground coupling. Coupling to a soft material results in low frequencies with large amplitudes, where as coupling to a hard material would yield high frequencies with small amplitudes (Schuck and Lange, 2007). A source polarized vertically with respect to the earth's surface can generate P-waves and SV-waves. A source polarized horizontally with respect to the earth's surface can generate P-waves, SV-waves and SH-waves. Figure 2.7, illustrates the direction of propagation of the waves generated by the different sources.

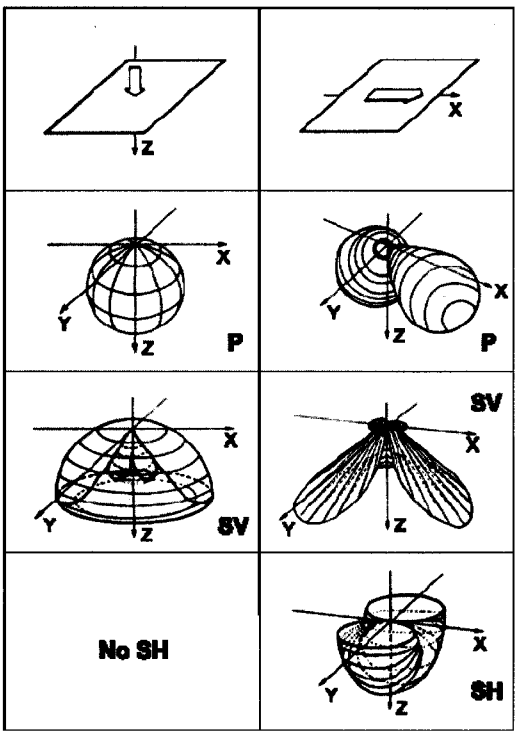

Figure 2.7: Direction of wave propagation with a vertical source (left) and a horizontal source (right) (Schuck and Lange, 2007).

Vertical Surface Sources

For wave generation from the surface, the seismic hammer, the seismic gun and the weight-drop are all commonly used vertical seismic sources.

Seismic hammer - An inexpensive option for shallow seismic work is a sledge hammer striking a metal plate on the ground. The signal generated has a fairly broad frequency spectrum and therefore provides a high subsurface resolution (Schuck and Lange, 2007). The hammer does not generate a large amount of energy and often, many consecutive strikes have to be summed, or "stacked", in the specialized terminology of exploration seismology in order to increase the signal over noise ratio. The seismic hammer is considered a suitable source for surveys down to depths of up to 100 m in rock (Schuck and Lange, 2007).

Seismic or Buffalo gun –The gun, which consists of a chamber fitted with a barrel housing a 12-gauge blank shotgun shell, can be used to generate a P-wave signal from the surface. It has been shown to generate a more powerful signal than the seismic hammer (Miller et al., 1986). For good coupling, the gun must be fired into a water filled auger hole approximately 0.5 m deep. Problems with signal repeatability arise when using the same auger hole a number of times. During the first few shots, much of the energy is lost due to the cavity enlarging. After a few more shots, the integrity of the hole is greatly diminished making it difficult to use.

Weight drops - Large weights ranging from 10-250 kg are lifted a few metres off the surface by a hydraulic system and dropped onto a metal plate. They generate a more powerful signal than a hammer or gun. The weight drop is considered a suitable source for depths down to 1000 m (Schuck and Lange, 2007).

Horizontal Surface Sources

Recall that S-waves can travel both as SH-waves and SV-waves. Even though some vertical sources are able to generate SV waves, the P-wave generated from the same source can obscure the signal, and therefore SH-waves are often preferred for site investigations (Schuck and Lange, 2007). In addition, SH-waves do not convert to P-waves or SV-waves during transmission or reflection (Schuck and Lange, 2007). S-waves tend to have a lower frequency content than P-waves generated from the same source (Schuck and Lange, 2007). SH-waves can be generated by striking a buried metal i-beam or board in a horizontal, sideways fashion.

Borehole Sources

For wave generation in boreholes, impulsive borehole sources such as sparkers, mechanical hammers and explosives (blasting caps) are used (Gibson and Peng, 1994).

Piezoelectric Sparkers - The sparker uses a high voltage electrical discharge to generate a high frequency seismic signal. It is possible to generate both P-wave and S-wave signals. It is considered ideal for tomographic surveys because of signal repeatability, high frequency content and reliability (Baria et al., 1989).

Mechanical Hammers – Mechanical hammers can be used to generate both P-waves and S-waves. The hammer is attached to a cylinder which is coupled to the borehole wall using an inflatable balloon or an arched metallic arm. A cable connected to a hammer is pulled and then released in order to strike the side of the borehole.

Explosives - Commonly used as an uncased borehole source, explosives can generate only a P-wave signal. The signal is not as repeatable due to the large cavity created by the blast. Special permission needs to be obtained to store and transport explosives. Hazardous and waste disposal sites often generate large amounts of gas and explosives are not a desired source option.

2.5.2 Geophones

Geophones are motion-sensitive transducers that convert ground velocity into an electrical voltage. The moving-coil geophone (Figure 2.8), contains a coil suspended with springs inside the magnetic field of a permanent magnet. A seismic wave causes a relative movement between the magnetic field and the coil. A voltage is then generated in the coil by induction. The signal generated from the geophone corresponds to a seismic trace recorded on a single channel of a device called a seismograph.

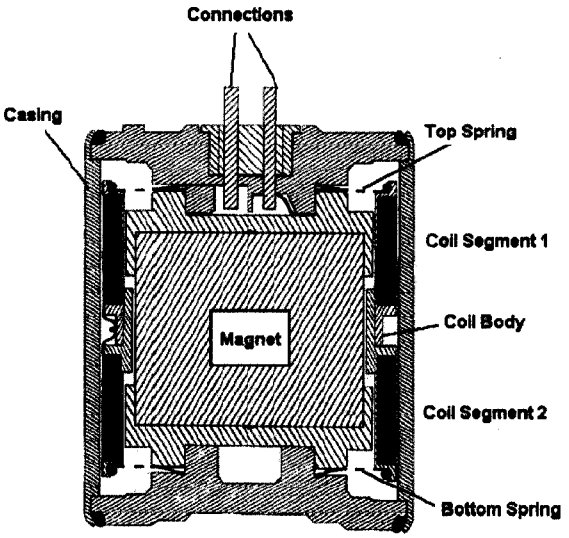

Figure 2.8: Moving-coil geophone (Schuck and Lange, 2007).

Three-component geophones consist of three individual geophones oriented orthogonally in three different planes. The vertical geophone is designed to record up-and-down ground motion (mostly associated with P-waves) and the two horizontal geophones are designed to record side-to-side ground motion (mostly associated with SH-waves SV-waves).

Borehole geophones are coupled to the borehole casing using a mechanical spring. Some borehole geophones are also equipped with an orienting mechanism that ensures consistent alignment of one of the two horizontal components in the magnetic north-south direction, and the other in the magnetic east-west direction.

2.6 Seismic Borehole Methods

Boreholes allow the design of seismic experiments with different geometries: vertical seismic profiling and crosshole seismic surveys.

Figure 2.8 (left) illustrates the typical raypaths used during a vertical seismic profiling survey: a source signal is generated from the ground surface and recorded by the borehole geophone in the form of a direct wave and a reflected wave if the seismic energy encounters an impedance contrast. In our case, the base of the landfill could potentially correspond to an interface for reflection events. Both the source and geophone can have variable positions. The horizontal distance between the source and the borehole is referred to as the "offset". The distance the wave travel between the source and receiver is referred to as the "raypath distance".

Crosshole seismic surveys use two boreholes to record waves propagating along a dense network of raypaths. The source is placed in one borehole and the geophone in the other borehole. The objective is to create a geometry as shown in Figure 2.9 (right).

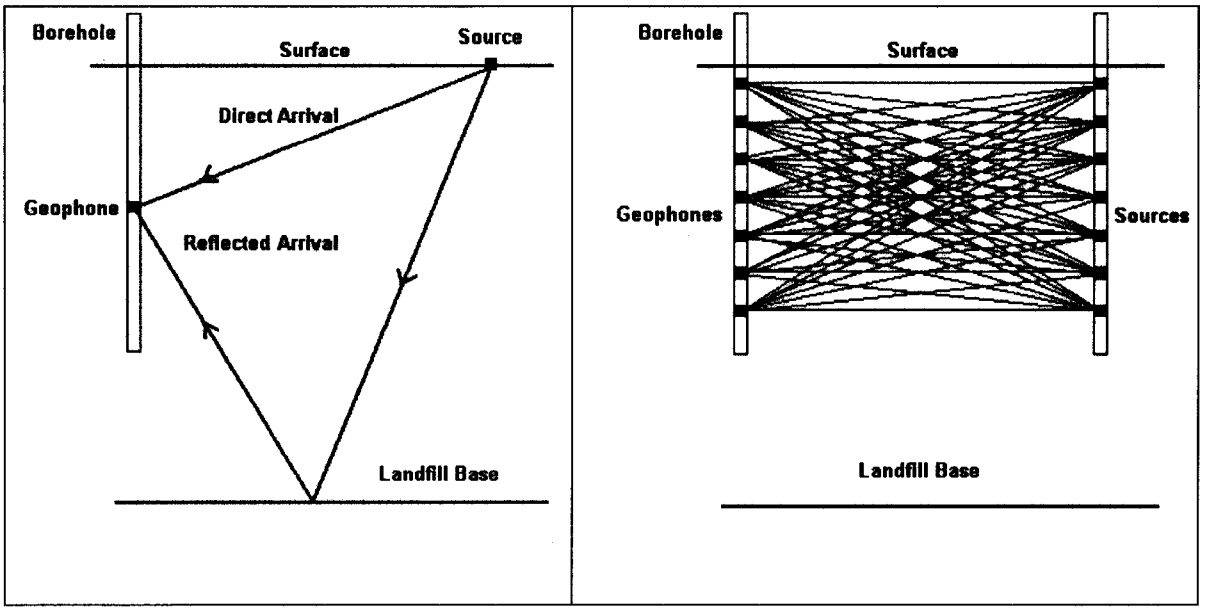

Figure 2.9: Typical raypaths for a VSP survey (left) and crosshole survey (left).

2.7 The Tomography Approach

If the medium through which seismic waves are traveling is homogeneous, it would a simple process to use traveltimes to obtain velocity since the distance between the source and geophone is known. However, in real world situations, velocity variations usually exist in both vertical and horizontal directions. Using the measured traveltime and known source-receiver distance, only the average velocity along the raypath can be determined, not the actual velocity distribution.

Seismic tomography is essentially an inverse problem: from the integrals of a function, find the function, in this case, velocity. The method uses traveltimes along multiple raypaths, as shown in Figure 2.8 (right), to estimate the velocity distribution. The Simultaneous Iterative Reconstruction Technique is commonly used for engineering applications. Goulty (1993) briefly describes the approach. The cross-section to be

imaged is broken down in a number of small two-dimensional cells. An initial velocity is assigned to each cell by the interpreter. Then, knowing the geometry between each source-receiver pair, the traveltime can be calculated by summing the propagation time within each cell along the raypath.

The difference between the calculated traveltime and the observed traveltime is distributed as a correction to the velocity in all cells along that raypath. This process is done for all raypaths simultaneously. Since most cells are intersected by more than one raypath, the velocity correction is simply the average velocity correction from every raypath traveling through that cell. This leads an updated velocity distribution and the process is repeated in an iterative fashion. Iterations continue until the difference between the calculated and observed traveltimes is below a specified threshold.

2.8 Data Processing

Since seismic borehole methods rely on the traveltimes of direct waves between the sources and geophones to obtain velocity, first breaks, that is, the arrival times of the direct waves, have to be picked which is in most cases a manual, subjective process done by an interpreter.

Noise on the seismic record can make it difficult to accurately pick the first breaks. A few steps can be taken to aid in picking first arrivals. The grouping of seismic traces from different geophone depths originating from a single source location into a common source point gather helps to visualize the direct arrival event. As the geophone is moved

to a deeper location, the wave will have to travel further, and the direct arrival will show up slightly later on the seismic record. Figure 2.10 is an example of a gather of traces for a single source location. The dashed lines indicate the picked first breaks. An additional option to improve picking is to filter out noise from frequencies known to have not originated from the source. The method for designing an appropriate filter is discussed in detail in Chapter 4. Figure 2.11 is the same gather shown in Figure 2.10 with a filter applied. It is easier to pick first breaks on the filtered gather.

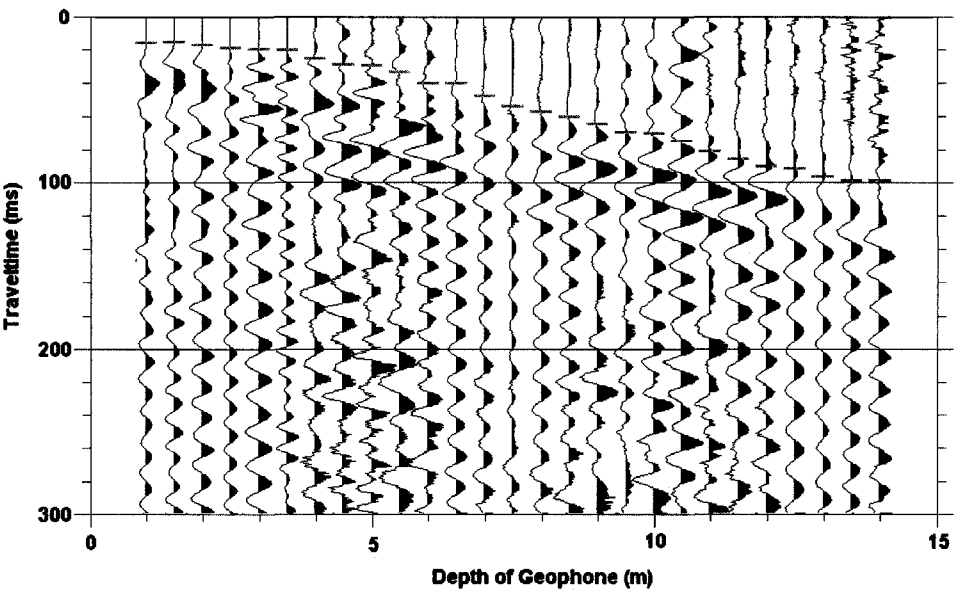

Figure 2.10: Common source point using a 5 m offset. Automatic gain control 5% scaling has been applied.

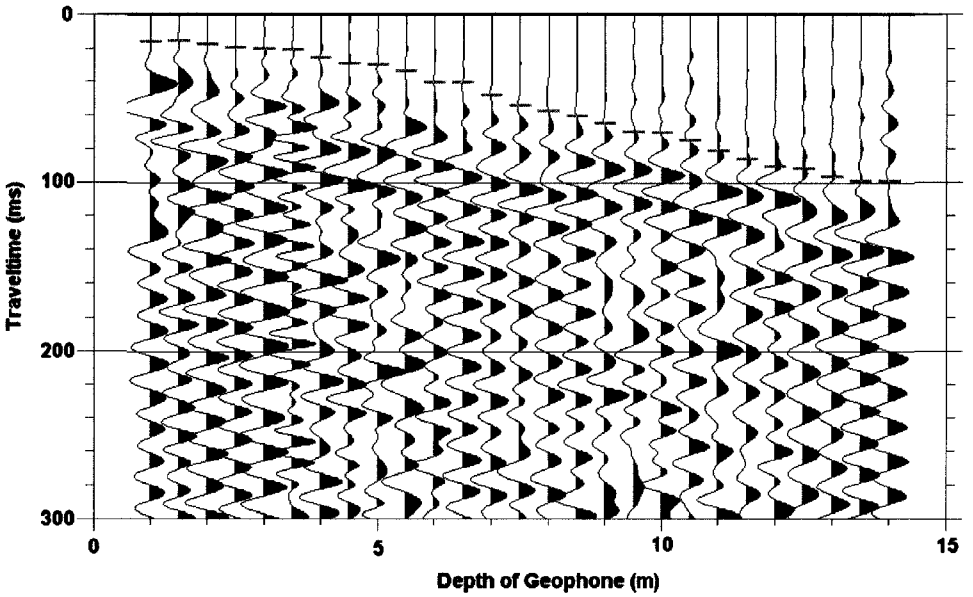

Figure 2.11: Common source point gather using a 5 m offset. Automatic gain control 5% scaling has been applied. Data has been filtered between 0/0 – 80/100 Hz.

Initial Velocity Model

Tomography requires an initial velocity model to be specified. Essentially, the user needs to have an idea about what the velocity distribution is, before tomography can be used to accurately determine it.

The easiest approach is to determine the average velocity along the raypath by dividing the raypath length by the recorded traveltime. This gives at least a crude estimate of the range of velocities present. A more sophisticated approach is to use the difference in direct arrival traveltimes over selected geophone depth intervals to determine the velocity. Basically, plots of first breaks versus raypath distance are created. Lines of best fit are computed over intervals that appear linear. The inverse of the slope of the line of best fit yields the velocity over that interval. Choosing how many intervals, and therefore

velocity layers, exist is a somewhat subjective process. The layered model determined from this process can then be used as an initial velocity model for the tomographic inversion.

2.9 Tomography Software

The seismic tomography software package selected for this projet is GeoCT-II developed by GeoTomo LLC (www.geotomo.com). It is a 2D seismic modelling and imaging package designed for engineering applications. It includes an advanced model builder; finite-difference full wavefield calculation for acoustic, elastic, and anisotropic media; raytracing and tomography for refraction, reflection, crosshole and VSP geometry.

Sheen et al. (2005) have done a review of different tomography software packages including GeoCT-II. They noted that the default parameters in GeoCT-II do not work that well. For near-surface work, the default smoothing parameters are about 10 times too large. An advantage to GeoCT-II, however, is that the algorithms are relatively fast and therefore obtaining optimal parameters by empirical experimentation is not difficult.

Carpenter et al. (2004) have also assessed the GeoCT-II package using a number of different models. Essentially, synthetic cross-sections were generated with a known velocity structure. Raytracing through the model from known source and receiver points was performed to calculate traveltimes. These calculated travel times were then inverted using a variety of different initial models to obtain the velocity structure. The inverted velocity structure was compared to the original velocity structure in order to assess the

reliability of the program. The inversions were found to be very sensitive to the initial model and had the most success with gradient models. Default tomography parameters for x/y smoothing ratio and smoothing control were not very reliable. The x/y smoothing ratio controls the relative smoothing between the x and z dimensions. Increasing the parameter will tend to generate bedding-like structures. Increasing the smoothing control will lead to a decrease in data misfit and a smoother velocity model. Conversley, decreasing the smoothing control will lead to an increase in data misfit and a rougher velocity model. Using an x/y smoothing ratio of 1 to 2 and using a smoothing control of 0.1 to 0.5 proved more effective. The grid spacing used should be less than half of the geophone spacing. Very large numbers of shot and receiver locations were required to detect fractures and sinkholes. In real-world applications, data acquisition efforts would be very high.

2.10 Methods to Determine Moisture Content in Waste

A number of different geophysical methods, listed in no particular order, including gravity, electromagnetic and electrical methods, tensiometry, and seismology, have been utilized in attempts to measure the moisture content of waste. Catley (2006) discusses in detail both the principles and limitations of these methods to determine moisture content in waste. An overview is provided below.

2.10.1 Gravity

Waste samples must be collected through the destructive means of either drilling or excavation. Samples are weighed, dried, and then weighed again to determine moisture

content. The limitation is that only point measurements can be made, and they may not be representative of the surrounding waste. Many samples must be obtained which is quite time consuming and therefore quite costly (Yuen et al., 2000).

2.10.2 Electromagnetic Methods (EM)

EM methods are commonly used to measure moisture content in sands. The bulk dielectric constant of the medium, including air, water and sand particles, is measured and then calibration relationships are used to determine moisture content. The dielectric constant of water is much larger than that of air or solids and small changes in moisture content can significantly change the bulk dielectric constant. Landfills tend to have high dielectric constants from metals and salinity. It would be difficult to distinguish between changes in moisture content or changes due to other conductive materials (Yuen et al., 2000). EM instruments used on landfills include TDR probes, capacitance probes and ground penetrating radar, which was attempted during this project.

Time Domain Reflectometry (TDR) - TDR probes are used to find the volumetric moisture content of a medium by using the relationship between the traveltime of an EM wave along the probe cable and the dielectric constant of the medium. The difficulty with using TDR probes in a landfill arises from the heterogeneity of both the waste and leachate (Li and Zeiss, 2001). TDR provides only point measurements and therefore determining the moisture distribution throughout the landfill would be quite time consuming. In addition, the highly conductive leachate results in severe signal

attenuation. Li and Zeiss (1999) found they were unable to determine volumetric water contents higher then 30% in a landfill due to signal attenuation.

Ground Penetrating Radar (GPR) - GPR is a high resolution time-domain pulsed electromagnetic (EM) method utilizing waves in the frequency band of 10-1000 MHz, which are considered radar. Pulses of EM energy are sent into the ground and when the wave encounters a contrast in the dielectric constant of the material, some of the energy is reflected back and recorded. Figure 2.12(a) illustrates the principle of GPR reflection profiling and Figure 2.12 (b) shows the radar record – or "radargram" – of the cross-section shown Figure 2.12(a).

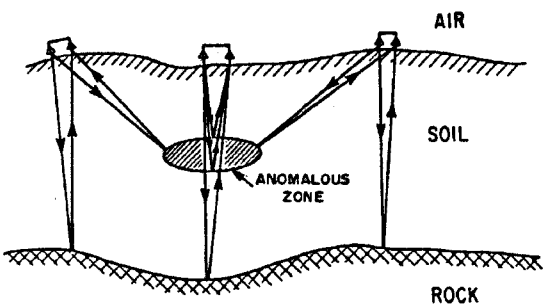

Figure 2.12(a): GPR Reflection Profiling (Davis, 1988).

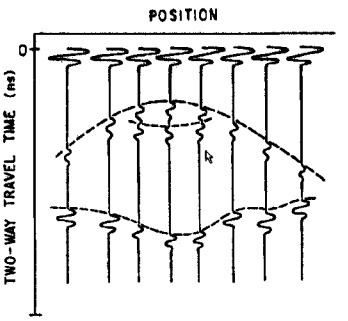

Figure 2.12(b): Radargram for Fig. 2.11(a) (Davis, 1988).

The optimal subsurface for this method contains materials with low attenuation coefficients, which in the case of GPR, consists of resistive materials with such as ice, sand, crude oil, bedrock and fresh water. Under these conditions, GPR has been known to penetrate at depths down to 50 m. In contrast, GPR is not well suited for highly conductive materials such as wet clay or silt or salt water. In this case, the range of GPR decreases to just a few metres (Davis, 1988). The highly conductive nature of landfills results in difficulty using this method. Green et al. (1999) were able to outline the lateral

boundaries of an old landfill site by the attenuation of the GPR signal. Porsani et al. (2004) conducted a GPR survey to delineate a contaminant plume at a landfill site. The upper limit of the contaminant plume was easily identifiable within the landfill by weak signals or the absence of reflectors. These weak returns were due to the highly conductive nature of the contaminant zones which did not allow deep penetration of the radar waves. The penetration depth varied from 4 m to 20 m. Figure 2.13 shows the radargram for one of the profiles within the landfill.

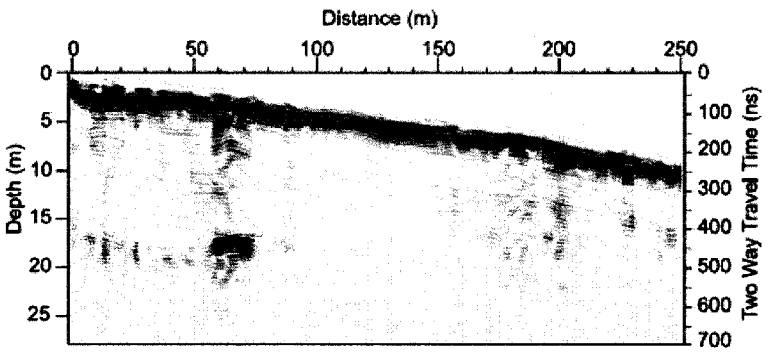

Figure 2.13: Radargram from a GPR profile within a landfill site (Ponsari et al., 2004).

2.10.3 Resistivity Soundings

Determination of moisture content using resistivity soundings rely on the relationship between electrical conductivity and its strong dependence on moisture content (Gawande et al., 2003). In addition to moisture content, electrical conductivity measured in a landfill will also have a strong dependence on temperature and water mineralization (Guerin et al., 2004). Electrical current is injected by two current electrodes which creates a potential difference in the medium. The potential difference is measured using two potential electrodes and electrical resistivity can be determined using the measured potential difference and survey geometry. Heterogeneity of waste prevents electric

current from flowing uniformly through the waste and therefore leads to inaccurate results (Yuen et al., 2000). Leachate in landfills can have very high conductivity which can mask variations due to actual moisture content (Yuen et al., 2000).

Gawande et al. (2003) conducted laboratory studies to relate electrical conductivity and moisture content in solid waste. It was only possible to develop calibration relationships above 35% moisture content. Cardarelli and Di Filippo (2004) conducted resistivity surveys at a landfill site in which low values of resistivity were measured along leachate drains. This is the area most likely to contain the more saturated waste. Guerin et al. (2004) conducted a study on three different landfill sites in France to assess the feasibility of using electrical conductivity to determine changes in moisture content. Electrical 2D soundings conducted at the first site resulted in high conductivity measurements along the sloped edge of the landfill that corresponded to visible water seepage on the surface. At a second site, on a cold day, leachate was injected into the waste via a perforated vertical borehole. 2D soundings were able to measure an increase in resistivity in a zone of influence about 3.6 m wide and 5 m deep. There was an increase in resistivity because the temperature of the leachate was approximately 15°C, much lower than that of the surrounding waste at more than 40°C. Moisture content had less of an effect on resistivity than temperature. At a third site, on a hot day, leachate injected via a perforated vertical borehole yielded a decrease in resistivity in the cone of influence. In this case, the effect of temperature on resistivity was small compared to the addition of moisture. In summary, Guerin et al. (2004) concluded that there is no systematic way to determine if

the decrease in waste temperature or the increase in moisture content will have a stronger effect on the resistivity.

2.10.4 Tensiometry

Tensiometry relates moisture content in a porous media to pore-water suction measurements via the soil-water characteristic curve. The heterogeneity of the waste makes it difficult to select an appropriate soil-water characteristic curve (Yuen et al., 2000). Tensiometers are only able to make point measurements, have a small effective sampling area, and can experience contact problems with the waste (Yuen et al., 2000). Korfiatis et al. (1984) experimented with tensiometers in solid waste and were not able to effectively measure moisture content between field capacity and saturation.

2.10.5 Seismic Methods

Seismic methods in landfills offer several advantages over the methods discussed above. Seismic surveying is non-destructive, data can be recorded without having to excavate into the waste. It is possible to record data over large areas as opposed to obtaining point measurements. The seismic signal is unaffected by leachate strength unlike EM or resistivity methods. A previous surface seismic survey was conducted at the Ste. Sophie bioreactor by Catley et al. (2006). P-wave reflections from the base of the landfill were recorded at the surface. A two-day reflection survey was carried out to identify changes in P-wave velocity before and after the addition of leachate. The survey was conducted in an identical fashion on both days; however, leachate was injected to the waste at the

beginning of the second day. Using two trenches oriented perpendicular to the survey line, approximately 1 m^3 of leachate was injected per metre length of trench.

The common midpoint (CMP) method was used to visually enhance the continuity of reflections. Within each CMP gather, the midpoint was sampled at 12 different shot-receiver distances ranging from 39m to 73m. The differences in P-wave velocity due to the addition of leachate were estimated using the hyperbolic curvature of the landfill bottom reflection in each CMP gather. The results from two different interpreters are shown in Figure 2.14. There was an injection trench at 40 m from the origin of the survey line. At distances between 31 m and 45 m along the survey line, that is within 5-9 metres from the injection trench, the velocities after the leachate injection are on average 22m/s faster than before the leachate injection. Paired t-test indicated that there is a 95% probability that the velocities between the two days are significantly different. At distances greater than 45m along the survey line, that is beyond the zone of influence of the injection trench, the paired t-test indicated that the velocities between the two days are not significantly different at the 95% confidence level.

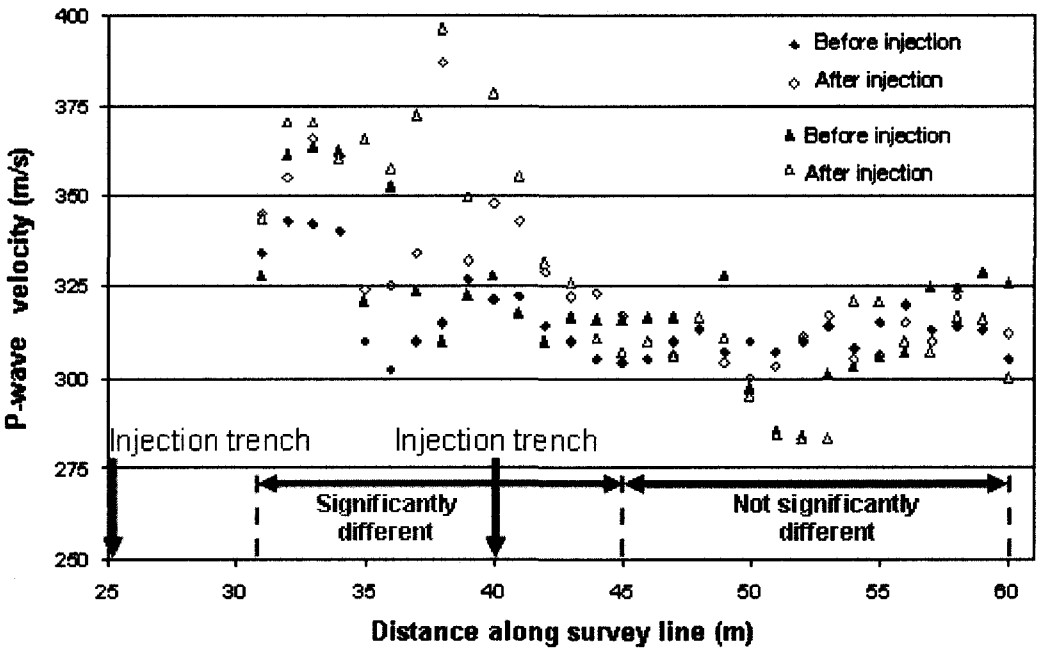

Figure 2.14: Seismic velocities of the landfill bottom reflection measured using hyperbolic curvature by two different interpreters (red and blue symbols) before and after leachate injection (Catley et al., 2006).

The surface seismic study demonstrated that it was possible to detect changes in P-wave velocity with the addition of moisture. The limitation to surface reflection surveys, however, is that the observed velocity is only an average velocity over the entire thickness of the waste column. It is possible to record changes in velocity horizontally across the landfill but not vertically through the landfill using reflection velocities directly. A seismic reflection tomography approach would allow for the detection of P-wave velocity changes in both the vertical and horizontal directions. A crosshole tomography approach would allow for greater resolution of different velocity features within the waste.

3.0 Survey Overview

3.1 Pre-Survey Installation of Vertical Boreholes

In order to conduct a seismic tomography survey there needs to be a method to place geophones within the waste. Access via vertical boreholes was the easiest way to accomplish that and, in November of 2007, two vertical boreholes were drilled on the top of the landfill. The boreholes were constructed of 3 inch inside diameter PVC. They were grouted with bentonite and capped at the bottom. They were drilled to a depth of 15 m. This depth limit was imposed because the third series of the leachate/biogas collection trenches had already failed (Figure 1.1). In order to maintain the integrity of the second series trench, installed at a depth of approximately 20 m, drilling was only permitted to a depth of 15 m by landfill management.

It was also necessary to add water to the waste between the boreholes. To accomplish this, boreholes were installed on either side of a fourth series biogas collection trench and were separated by a distance of 10 m. It was initially presumed that the most efficient method to inject water between the boreholes would be the gravel trench. The trench would take the water easily and then it could infiltrate downward into the waste. If the water was injected into the waste directly, there would be the risk of materials such as plastic bags blocking the bottom of the water injection which would impede the flow. It would simply take too long to inject water and create unreasonable survey times.

3.2 Survey 1

3.2.1 Objectives and Methodology

Survey 1 was a 2-day survey conducted in November 2007. The main objective was to record both P-wave and S-wave direct arrivals, generated by P-wave and S-wave boreholes sources, using a borehole under both wet and dry conditions. On day 1 both P-wave and S-wave direct arrivals were recorded under relatively dry conditions. On the morning of day 2, water was injected between the boreholes and an identical survey to that of day 1 was conducted in order to note changes in P-wave velocity with the addition of water. Recall that only the P-wave direct arrivals should change with the addition of water. The S-wave direct arrivals are not effected by changes in saturation, and are being recorded to identify density differences based on the solid structure alone. A transient test was also conducted during the addition of water. In this case, direct arrivals along a single raypath were recorded multiple times at small time intervals in order to detect changes with increasing saturation.

3.2.2 Equipment

A 10 Hz, 3-component geophone was used during the survey. The 3 components consist of 1 vertical component, best suited for detecting P-waves and SV-waves and 2 orthogonal horizontal components, best suited for detecting SH-waves. The geophone, shown in Figure 3.1, was coupled to the borehole wall with a mechanical spring. The seismograph, shown in Figure 3.2, was a Geometrics Geode. The borehole source used was a small hammer activated by a weight drop mechanism. The hammer is struck against the side of the borehole in a direction that is parallel to direction of wave

propagation. The surface source was a 5.4 kg seismic hammer struck against a flat metal plate, which produces mainly P-waves. Images showing the sources used are provided in Figure 3.3.

Figure 3.1: A 10 Hz 3-component borehole geophone

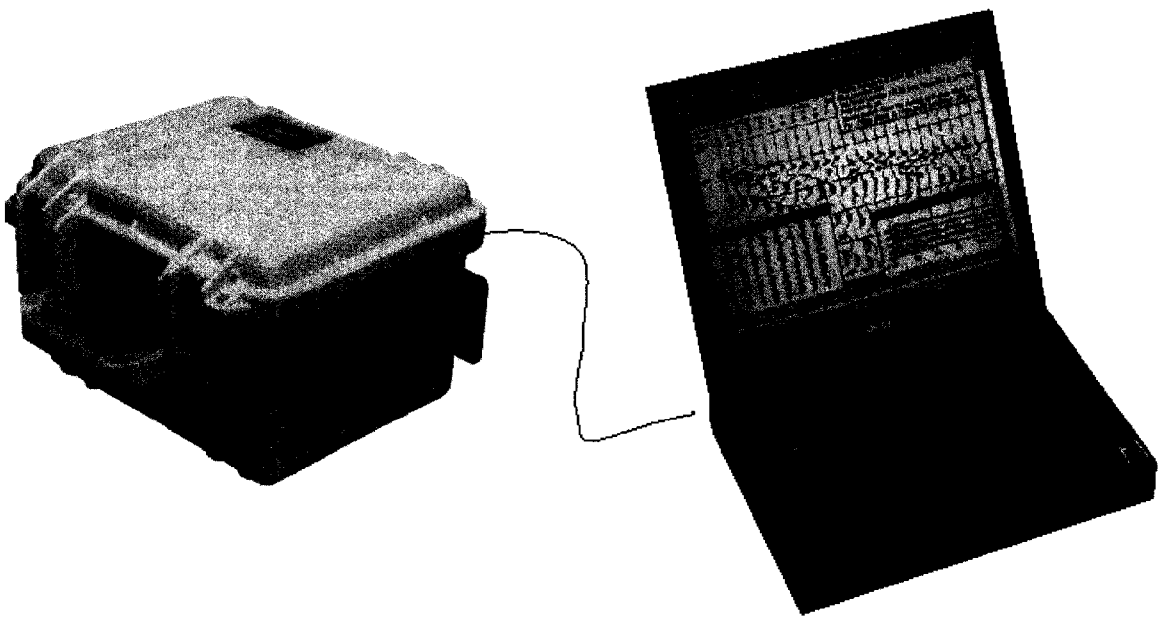

Figure 3.2: Geometrics Geode Seismograph (Geometrics)

Figure 3.3: A borehole P-wave source (left). Seismic hammer (right).

3.2.3 Data Acquisition

On day 1, to obtain a crosshole data set, a geophone was placed at a depth 15 m from the surface and the P-wave source in the opposite borehole at a depth of 15 m. A shot, or release of seismic energy, is made by the source. Stacking is a technique where multiple shots are taken and the seismic traces recorded from each shot are summed. Constructive Interference enhances the signal to noise ratio. In this case 10 traces are stacked for each shot-geophone location. The geophone was then moved up the borehole in steps of 1 m and the next stacked trace was recorded. This process was repeated until the geophone reached the surface of the landfill. The geophone was then moved back down the borehole to a depth of 15 m and the source location was moved up by a distance of 1 m. Again, the process was repeated for all geophone locations. It was the intention that the source be moved in 1 m steps until it reached the surface of the landfill. This would have provided the dense raypath coverage shown in Figure 3.4.

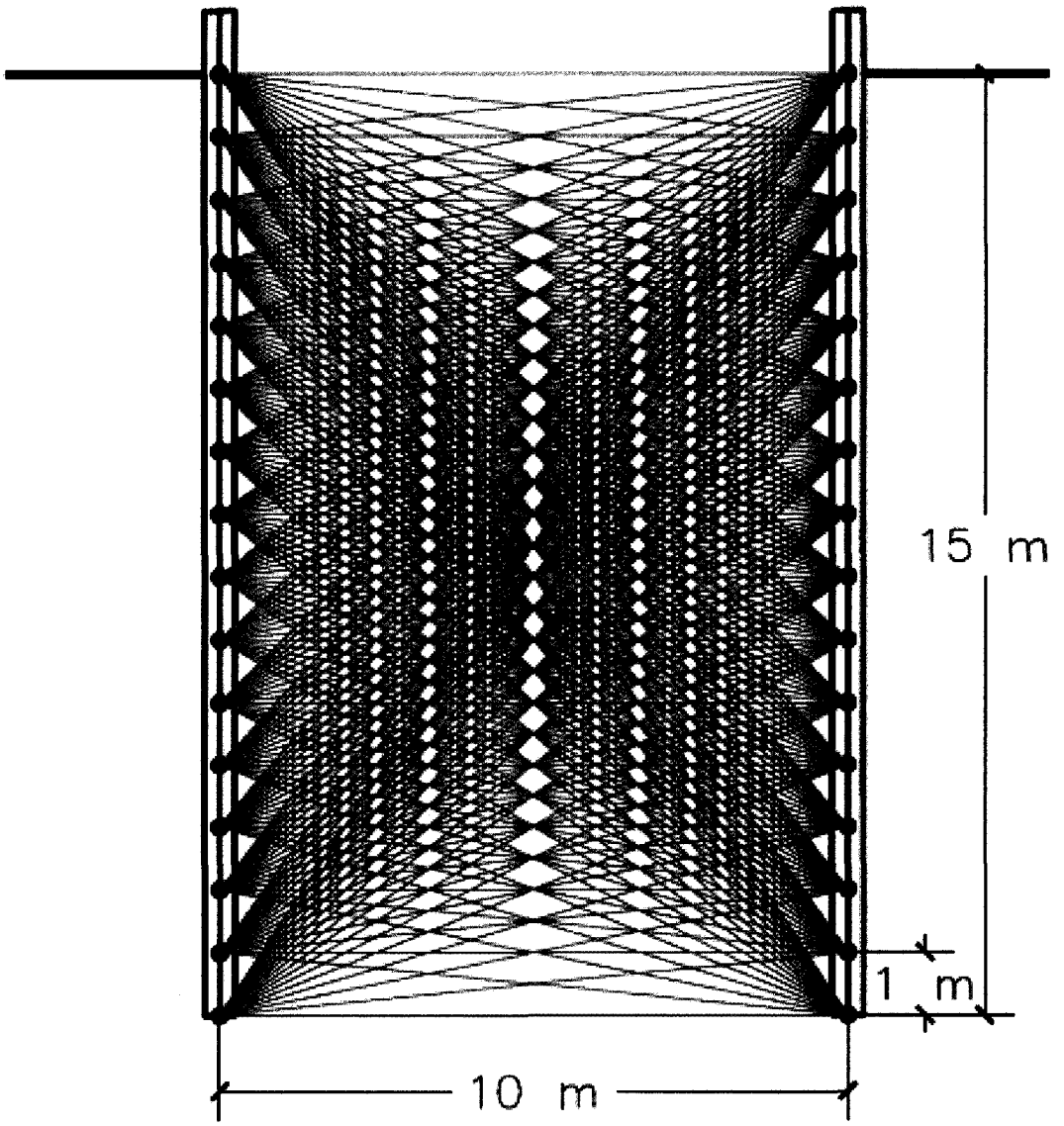

Figure 3.4: Raypath coverage initially planned.

However, it was quickly realized that no signal was being recorded at the geophones. The signal generated by the borehole P-wave source was simply not strong enough to be recorded at the geophone in the opposite borehole even for the shortest raypath of 10 m. Since the borehole S-wave source is known to produce an even weaker signal than the P-

wave source (C. Phillips, personal communication), the plan of using the borehole S-wave source was abandoned.

The only alternative left was to use a surface 5.4 kg hammer source striking a flat steel plate and conduct a vertical seismic profiling (VSP) survey. The geophones were again placed at a depth of 15 m in one borehole and the hammer source adjacent to the other borehole 1 m perpendicular to the plane between the boreholes. Stacked seismic traces were recorded in the manner described above. The VSP geometry imposes a severe limitation in terms of raypath coverage. A large shadow zone exists between the boreholes at depths of approximately 8-15 m, with limited or no raypath coverage as seen in Figure 3.5. The crosshole survey consists of 75 unique raypaths, whereas the VSP survey consists of only 30. Unfortunately much of the shadow zone coincides with the area where the largest changes in P-wave velocity were anticipated.

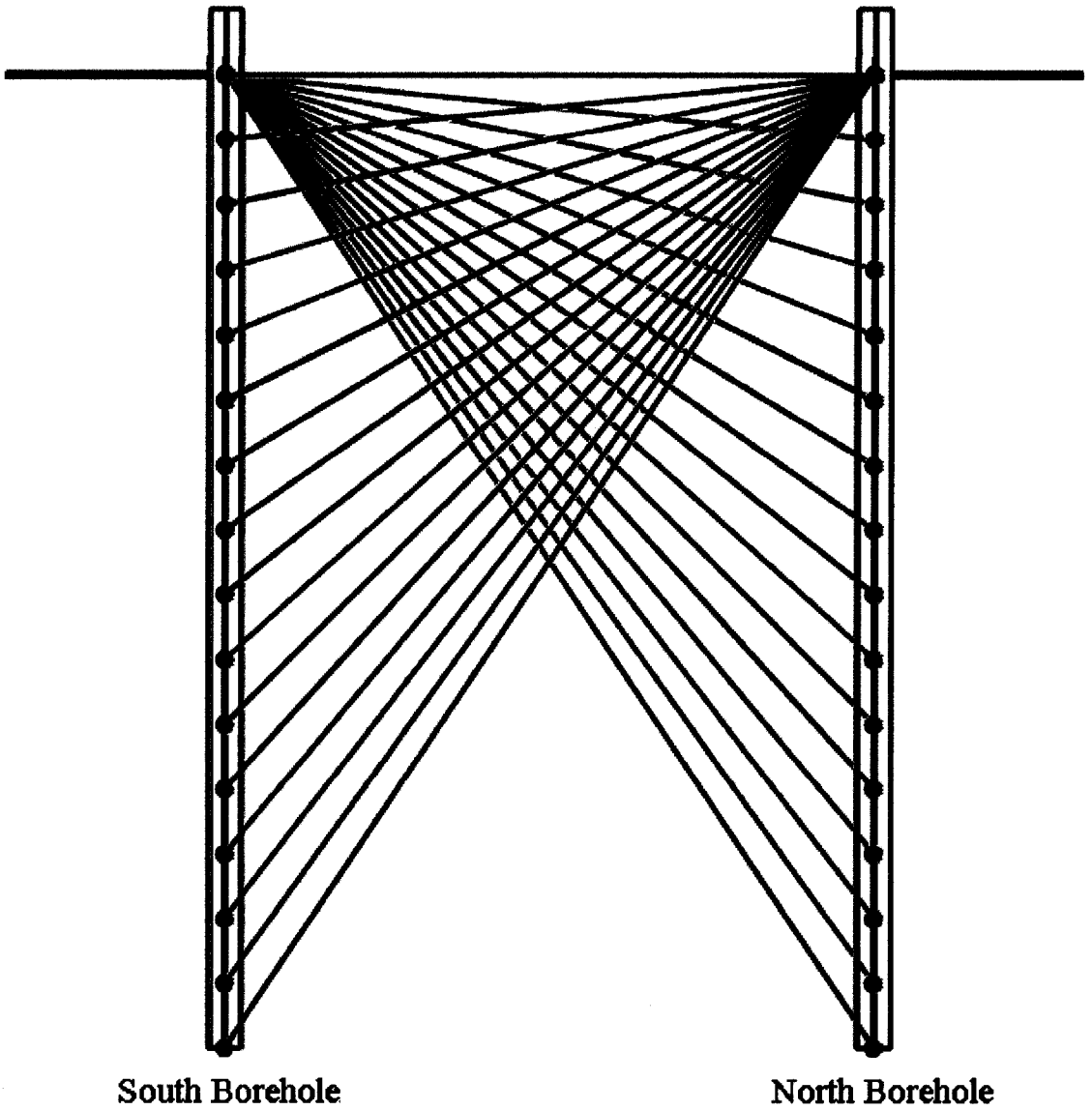

Figure 3.5: Limited raypath coverage using a surface source

On day 1, a P-wave vertical seismic profile (VSP) was obtained for each borehole. Recall, a VSP is simply a gather of seismic traces for variable geophone depths generated from a single offset. Recall that offset refers to the horizontal distance between the surface source and the borehole. We were only able to collect a P-wave VSP because at the time of this survey only a flat metal plate was available.

On the morning of day 2 approximately 5000 L of water was injected between the boreholes to greater water contents compared to the day before. Since a clay cover had placed over the waste, a 3 m deep, 3.3 m wide excavation was dug between the two boreholes in order to ensure water would be able to infiltrate into the waste. The excavation along with the different layers of the cover can be seen in Figure 3.6. It was situated directly on top of a biogas collection trench which is about 1 m in width and 1.5 m in depth. Figure 3.7 illustrates the size and location of this excavation.

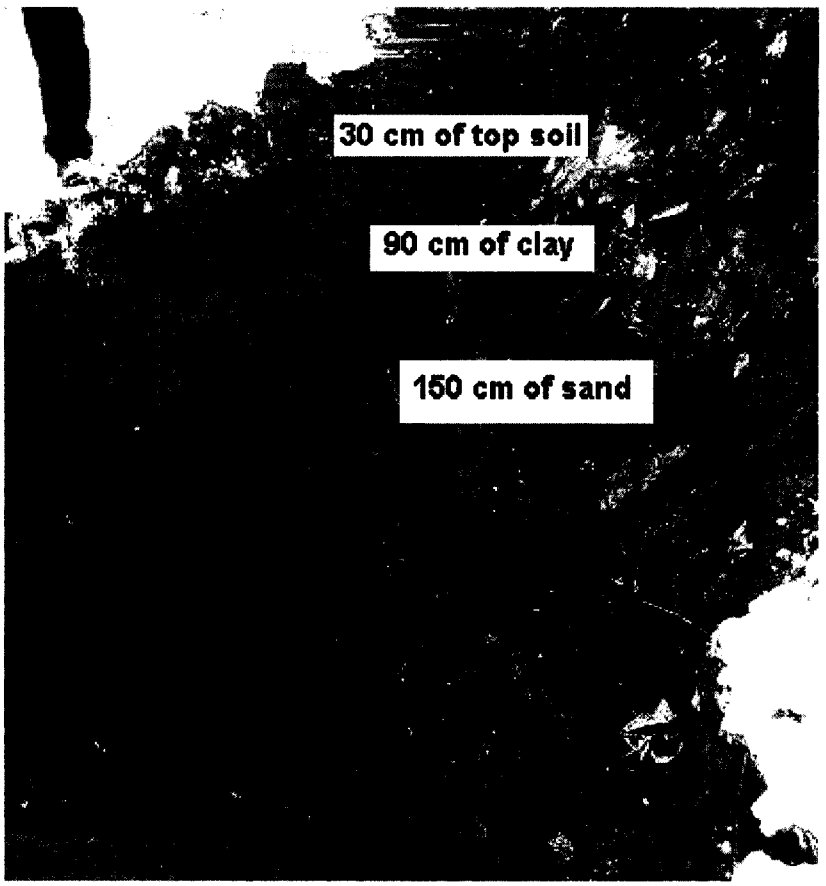

Figure 3.6: The excavation with a side wall showing the different layers of the cover.

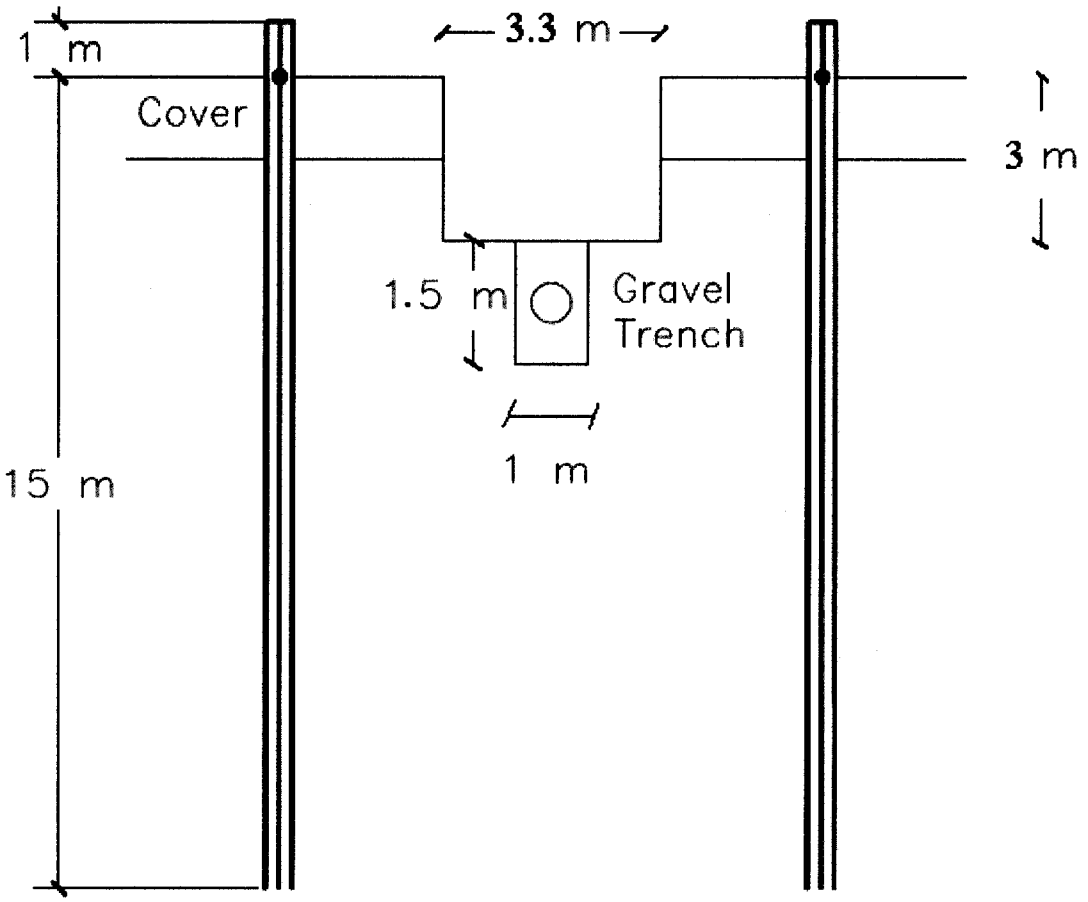

Figure 3.7: Cross-section showing the excavation between the boreholes

Water was added via a truck carrying a 1000 L reservoir as can be seen in the photos shown in Figure 3.8. The truck was required to make 5 trips, which took about 2 hours. The amount of water added was limited mainly by the time left to complete the survey. During the addition of water, a transient test was conducted to assess any changes in the seismic recordings over time. A geophone was placed in each borehole at a depth of 12 m from the surface as illustrated in Figure 3.9. Approximately every 10 minutes shots were taken from both shot locations, and recorded in the opposite borehole. Ponding occurred during the addition of water and persisted for almost an hour after the final truck load had

been added. After all of the water had infiltrated the waste, a P-wave VSP survey identical to that of day 1 was conducted in order to detect changes due to water addition.

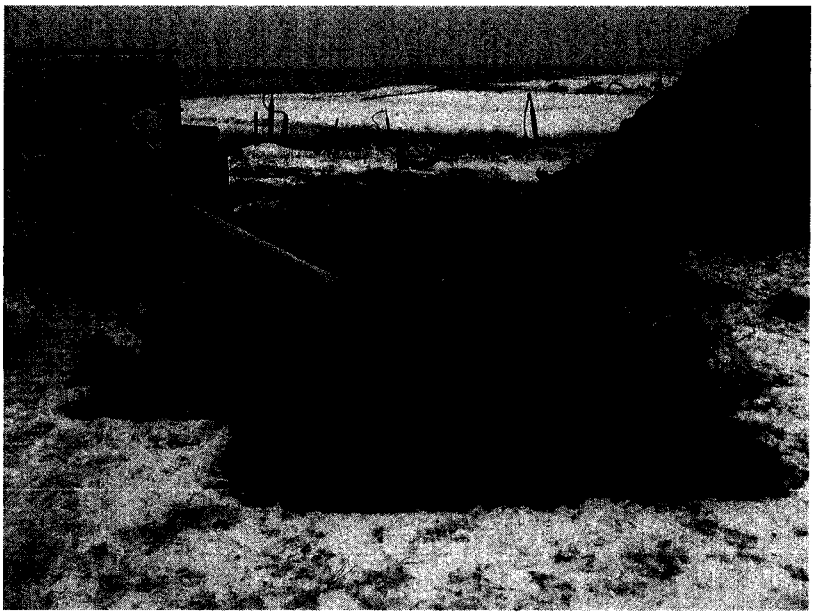

Figure 3.8: The addition of water into the excavation via the water truck.

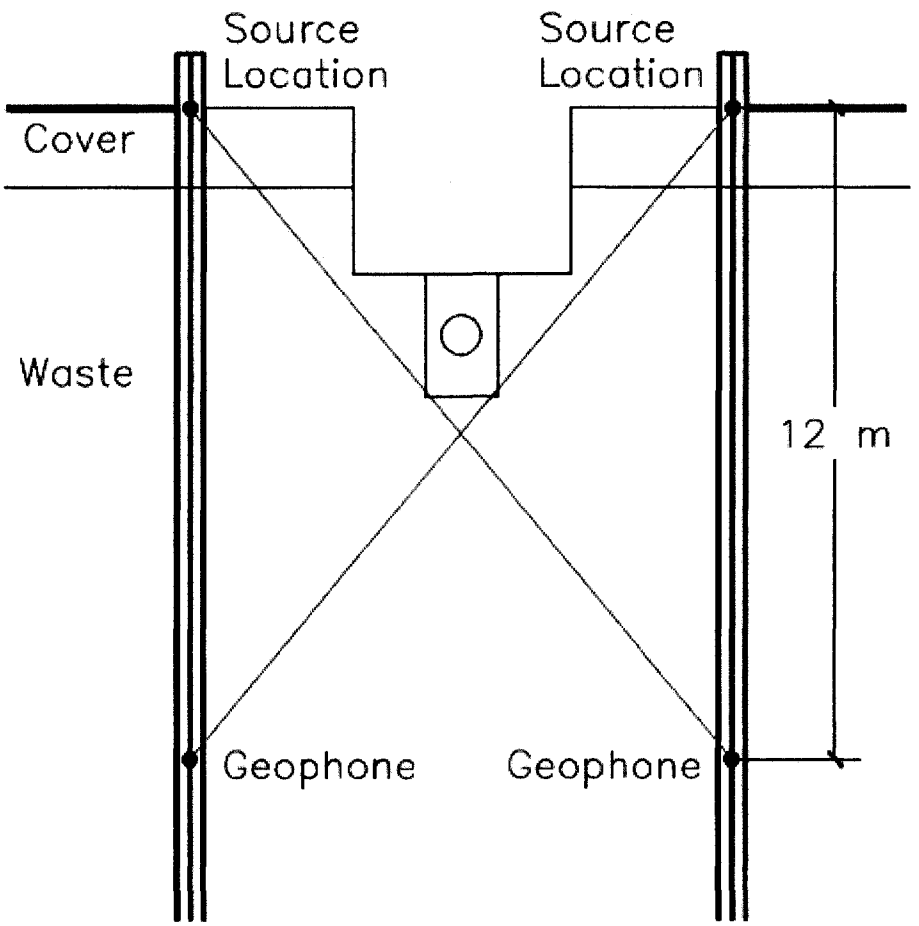

Figure 3.9: Survey geometry and raypaths for the transient survey

Table 3.1: Data Acquisition Parameters for Survey 1

Date	November 19-20, 2007
Seismograph	Geometrics Geode
Sources	Borehole P-wave, 5.4 kg seismic hammer with flat plate
Receivers	R.T. Clark 10 Hz 3-component borehole geophone
No. of Channels	3 (Vertical, Horizontal 1, Horizontal 2)
Geophone Spacing	1 m
Offset	10 m
Sampling interval	0.0625 ms
Record length	1.024 s

3.3 Survey 2

3.3.1 Objectives and Methodology

Survey 2 was a 2-day survey conducted in June of 2008. The objective was to characterize the waste in terms of seismic wave propagation, in particular P-wave and S-wave velocity. In addition to using the seismic hammer, the seismic gun source was tested for this application. The gun is primarily a P-wave source and is known to produce a stronger signal than the hammer (Miller et al., 1986). The stronger signal was required for two reasons. Firstly, because the hammer data collected at a 10 m offset from Survey 1 was noisy and therefore difficult to pick the first arrivals against the background noise. Secondly, because the surface source provides limited raypath coverage as shown in Figure 3.5. Moving the source to larger offsets would extend the depth of possible raypath coverage, improving the chance to detect changes in P-wave velocity. This is illustrated in Figure 3.10. The higher frequency of the seismic gun source was desired in order to obtain a sharper wave front and therefore be able to detect smaller time shifts in the direct arrivals. The reason for the need of a higher frequency signal is further explained in Chapter 6.

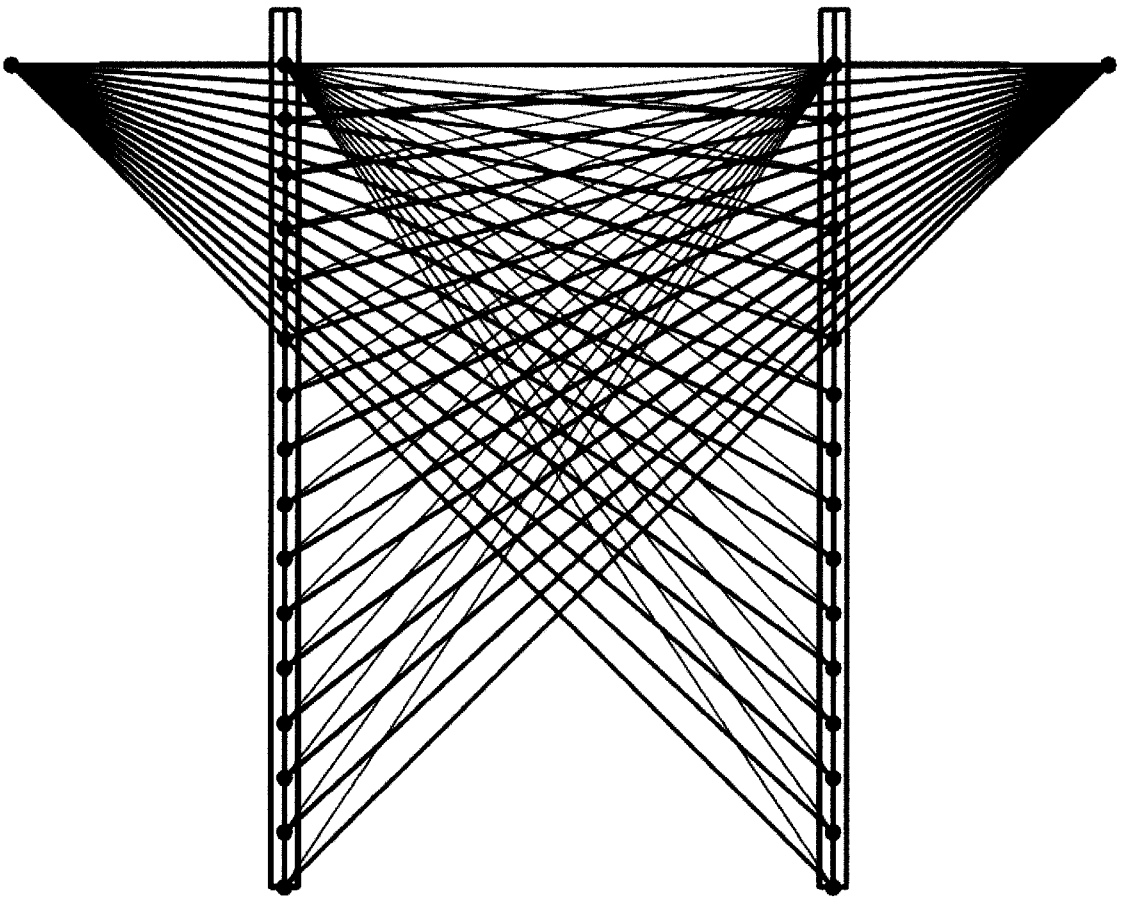

Figure 3.10: Extending the source offset extends the depth of raypath coverage as shown by the blue raypath lines.

3.3.2 Equipment

Similar to Survey 1, the seismograph used was a Geometrics Geode. The geophone used was the Geostuff BH3 3-component borehole geophone with orienting capability. The orienting capability allows the horizontal components to be oriented towards magnetic north-south and east-west after being moved in order to ensure angular consistency at each recording location. Velocities of horizontally polarized S-waves can vary with azimuth and maintaining orientation for every source-geophone location for the entire borehole can allow for better identification of S-waves (Geostuff, 2009).

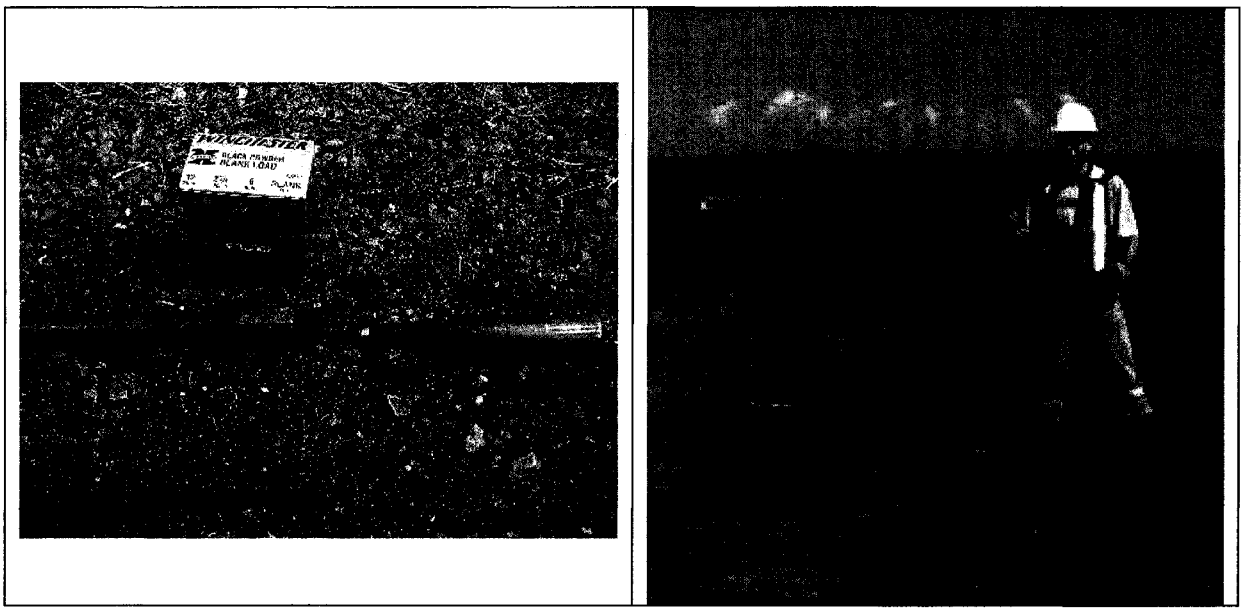

Figure 3.11: The seismic gun (left) (Catley, 2006). Preparing to fire the seismic gun (right) (Catley, 2006).

The seismic gun, sometimes called a Buffalo gun (Miller et al., 1986), consists of a chamber fitted with a barrel housing a 12-gauge blank shotgun shell as seen in Figure 3.11. In order to fire the gun, a 0.5 m deep hole is augured and filled with water. The chamber is then placed into the water-filled hole and the firing rod is dropped into the chamber to fire the blank shell.

The seismic hammer was also used as both a P-wave and S-wave source. When using the hammer, P-waves are generated from hitting a flat plate, and S-waves are generated from hitting the side of an I-beam with the other side dug into the ground. The positioning of the I-beam, with the flat side face perpendicular to the survey line, can be seen in Figure 3.12. During Survey 2, the I-beam was hit in both north and south directions. In other words, one side is hit, and then the I-beam is repositioned to that it can be hit in the opposite direction. The purpose of generating S-waves from either direction with the I-

beam is to be able to test if they are polarized. This is explained in more detail in Chapter 5.

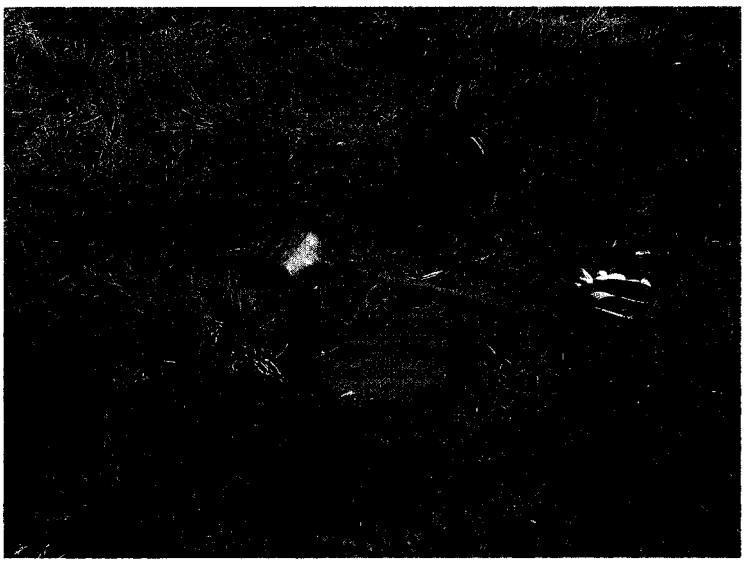

Figure 3.12: The flat plate, I-beam and seismic hammer

3.3.3 Data Acquisition

For this survey, only the north borehole was used to collect data. VSP data were acquired at offsets increasing in a northerly direction from the north borehole so that there would be no interference from the gravel trench. The seismic hammer was used collect both P-wave and S-wave VSP data at offsets of 5 m and 10 m from the north borehole. The geophone spacing was decreased to 0.5 m intervals in order to obtain a denser data set and better identify events. Three shots were taken at each offset location, a vertical hit on the flat plate to generate P-waves, and 2 hits on either side of the I-beam to generate S-waves. Each shot had a variable number of stacks ranging from 5 to 10. The number of stacks was determined by a visual inspection during acquisition. When there appeared to be no visible improvement of the signal to noise ratio, no further data were summed. The

seismic gun was used to collect VSP data at 10 m, 15 m and 20 m offsets. The geophone spacing was maintained at 0.5 m. A new hole was augured every 5-10 shots.

Table 3.2: Data Acquisition Parameters for Survey 2

Date	June 16-17, 2008
Seismograph	Geometrics Geode
Sources	Seismic Gun, 5.4 kg Seismic Hammer with flat plate and I-beam
Receivers	Geostuff 10 Hz 3-component borehole geophone
No. of Channels	3 (Vertical, Horizontal 1, Horizontal 2)
Geophone Spacing	0.5 m
Offset	5 m, 10 m, 15 m, 20 m
Sampling interval	0.125 ms
Record length	2 s

3.4 Survey 3

3.4.1 Objectives and Methodology

Survey 3 was a 2-day survey conducted in November of 2008. The main objectives were to: 1) detect changes in P-wave velocity under variable moisture conditions, and 2) further characterize the waste in terms of attenuation versus distance. To help gather a more complete data set, VSP data were collected using a seismic hammer at 15 m offset. Recall, VSP data were obtained in Survey 2 with the seismic gun at 10 m, 15 m and 20 m offset. It would now be possible to compare VSP data from gun and hammer sources at 10 m and 15 m offsets. In addition to seismic surveying, a crosshole Ground Penetrating Radar (GPR) survey was also conducted to attempt to detect changes with moisture content. An overview of the GPR technique is discussed in Chapter 2. It was intended to complement the seismic data set. A GPR survey was conducted because the equipment was made available at the time by a research group at INRS. It was not preferentially selected over other geophysics methods.

On day 1, both P-wave and S-wave direct arrivals were recorded under dry conditions. On the morning of day 2, water was injected between the boreholes and an identical survey from the day before was conducted in order to note changes with the addition of water. The GPR survey was conducted in a similar fashion. After completion of Survey 1, a large pipe had been installed vertically into the gravel biogas collection trench at the bottom of the excavation. The pipe was installed about 2 m west of the plane of the two boreholes as seen in Figure 3.13. This pipe was used to inject water between the boreholes. The injection pipe was connected to the biogas collection trench. The boreholes and injection pipe can be seen in Figure 3.14.

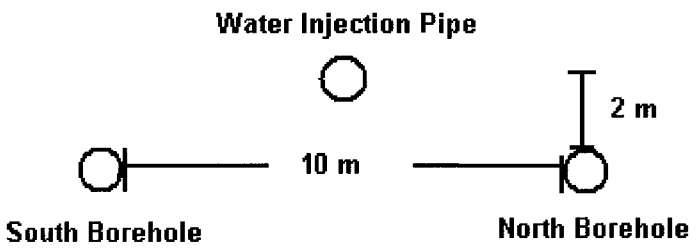

Figure 3.13: Location of the water injection pipe relative to the north and south boreholes.

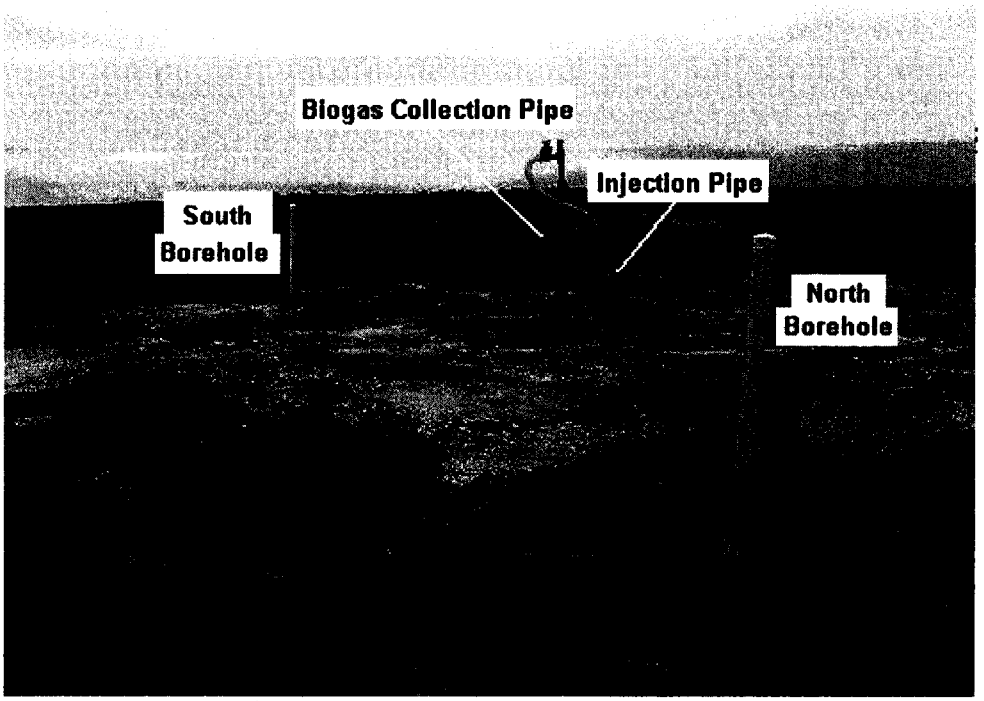

Figure 3.14: Experimental Set-up showing the two boreholes and the injection

3.4.2 Equipment

Due to problems with the seismic gun, further explained in Chapter 5, only the seismic hammer source was used. A flat steel plate, and an I-beam were used to generate P-waves and S-waves respectively. A Geometrics Geode seismograph was used with a 10 Hz BH3 Geostuff 3-component borehole geophone. For the GPR survey, a borehole source and receiver system was used with 100 MHz antennas.

3.4.3 Data Acquisition

Part 1

In a similar fashion to Survey 1, three-component VSP data were collected at 10 m offsets from both boreholes, as shown in Figure 3.5. On this occasion, only one side of the I-beam was used to generate S-waves in order to reduce data acquisition time. Each shot was stacked 10 times. On day 1, VSP data under dry conditions were obtained. On

the morning of day 2, approximately 7000 L of water was injected between the boreholes. Since the 5000 L of water injected during Survey 1 did not appear to affect P-wave velocity, more water was added. The chosen amount of 7000 L of water was a balance between increased water content and the time needed to collect data on day 2. Data collection began 0.5 hours after the 7000 L of water was added. VSP data were then collected in identical fashion to day 1 to obtain P-wave velocity under wet conditions. During the addition of water, a transient survey was conducted. Two geophones were placed in the north borehole at 5 m and 12 m, as shown in Figure 3.15, and maintained at this depth for the duration of the survey. P-wave and S-wave shots were taken at a 10 m offset 1 m west of the south borehole every 10 minutes for 2 hours during water injection and for 0.5 hours after the injection. Each shot was stacked 10 times.

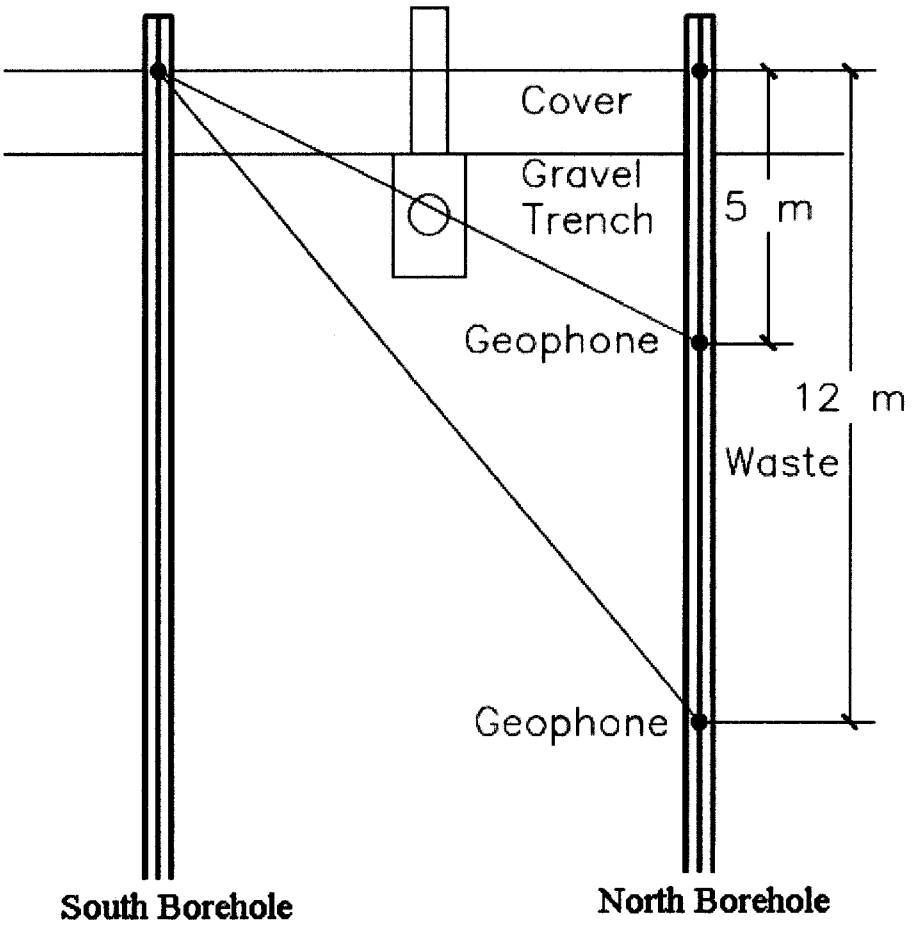

Figure 3.15: Transient survey geometry

A crosshole GPR survey was conducted using 100 MHz antennas. Unfortunately, it was not possible to record a radar signal at the borehole separation of 10 m. The waste material is simply too conductive and the GPR signal is largely attenuated. The technique was abandoned and the survey was not conducted on day 2.

Part 2

For the characterization survey, only the north borehole was used. Shots were taken in a northerly direction from the north borehole to avoid interference from the gravel trench.

The seismic hammer was used to collect P-wave and S-wave VSP data every 1 at offsets ranging from 1 m to 25 m. Two geophones were held constant at depths of 2.5 m and 10 m. The S-waves were generated striking only one side of the I-beam. Each shot was stacked 10 times. VSP data with a constant offset of 15 m and geophone spacing of 0.5 m were also obtained so that it could be compared with the 15 m offset seismic gun VSP. Each shot was stacked 10 times. A summary of data acquisition parameters for Parts 1 and 2 can be found in Table 3.3. A summary of the VSP data collected is presented in Table 3.4. A summary of all three surveys is outlined in Table 3.5.

Table 3.3: Data Acquisition Parameters for Survey 3

Date	November 19-20, 2008
Seismograph	Geometrics Geode
Sources	5.4 kg Seismic Hammer with flat plate and I-beam
Receivers	2 Geostuff 10 Hz 3-component borehole geophone
No. of Channels	3 (Vertical, Horizontal 1, Horizontal 2)
Geophone Spacing	0.5 m for constant offset surveys
Shot offset	Variable for each survey
Sampling interval	0.125 ms
Record length	2 s

Table 3.4: Summary of VSP data collected

	Source		
Offset (m)	Hammer - Vertical Shot	Hammer - Horizontal Shot	Seismic Gun
5	yes	yes	no
10	yes	yes	yes
15	yes	yes	yes
20	no	no	yes

Table 3.5: Summary of Survey 1, Survey 2, and Survey 3.

	Survey 1	Survey 2	Survey 3
Objectives	Test Equipment	Test Equipment	Detect P-wave velocity changes
	Detect P-wave velocity changes	Improve understanding of seismic velocities	Create a more complete data set
Sources Used	Borehole P-wave	Seismic Gun	Surface Hammer
	Surface Hammer	Surface Hammer	
Hit Types Used	P-wave	P-wave	P-wave
		S-wave	S-wave
Geophone Spacing	1 m	0.5 m	0.5 m

4.0 Seismic Characterization of Solid Waste

This chapter is an overview of the properties of seismic waves that that propagate through solid waste. The following topics are discussed: filtering of seismic data, comparison of seismic sources, wave type identification, quality of data versus offset and tomography.

4.1 Filtering of Seismic Data

Picking first breaks is a crucial initial step for several analyses, tomography, for instance. In order to help identify first breaks a frequency filter can be applied to seismic traces. The filter is used to eliminate frequencies known to fall outside the expected signal band. Figure 4.1 illustrates the frequency content of vertical geophone data for a hammer source at a 5 m offset with no filter applied. The majority of the signal is being generated between 0-200 Hz. The spikes between 1000-4000 Hz are simply noise and can be filtered out. If a 0-200/250 Hz filter is applied, the remaining signal is more likely to have been generated from the seismic source, as shown in Figure 4.2.

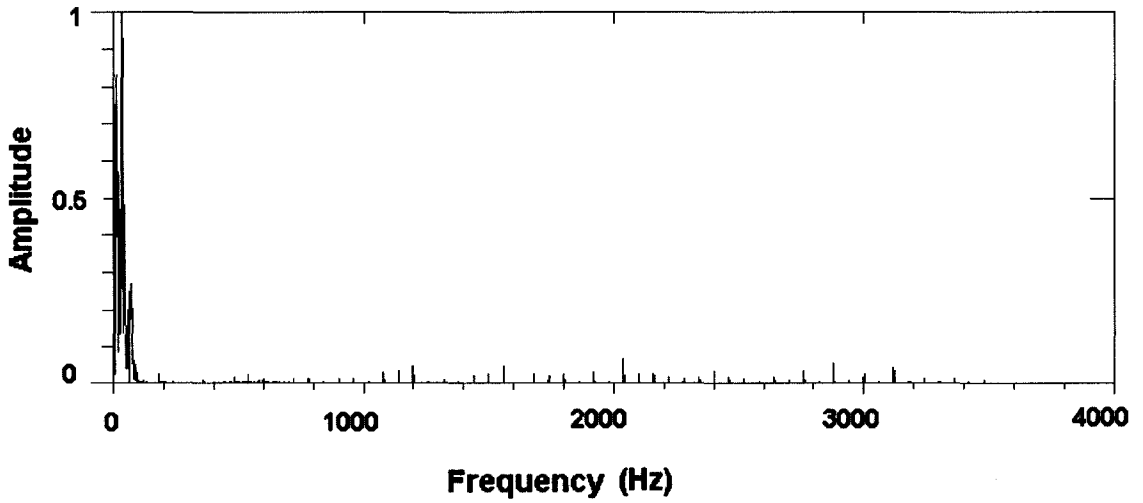

Figure 4.1: Frequency response for vertical geophone data for a hammer source at a 5 m offset with no filter applied. Trace length = 2 s. Sampling interval = 0.125 ms.

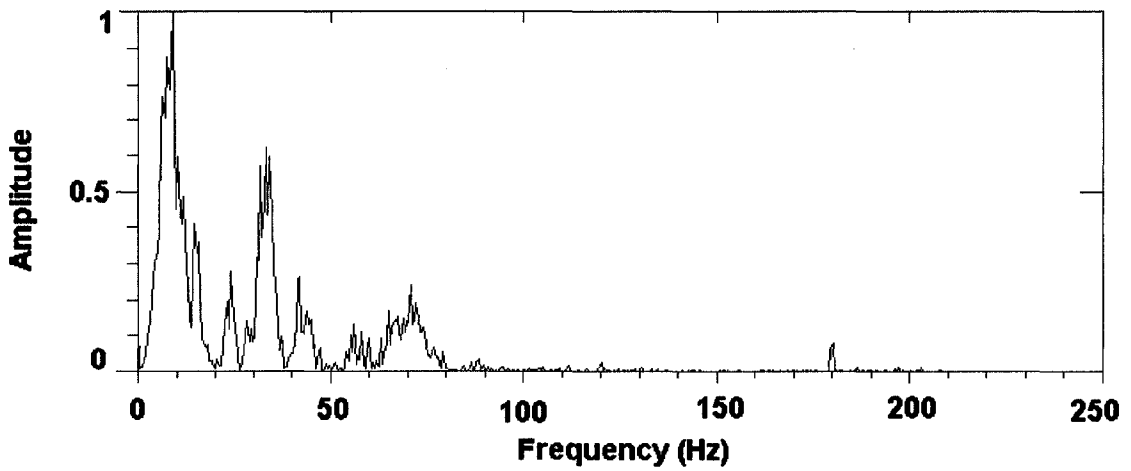

Figure 4.2: Frequency response for the data presented in Figure 4.1 with at 0-200/250 Hz low-pass filter applied.

4.2 Comparison of Seismic Sources

Three different seismic sources were used during this study, a borehole P-wave source, and two surface sources, a 5.4 kg seismic hammer and a seismic gun. The borehole source was abandoned early during the first survey because its signal was weaker that the background noise and therefore undetectable. The seismic gun was tested during the second survey because it is generally known to provide a stronger signal than the hammer (Millar et al., 1986).

Unfortunately, there was a triggering issue with the gun. The time-zero recorded by the system was not consistent from shot to shot. The Interprex seismic picking software displays multiple seismic traces and indicates the first breaks picked by the user by dashed lines. Figure 4.3 shows the VSP data obtained using the seismic gun at a 10 m offset. Figure 4.4 shows the VSP data obtained using the seismic hammer for the exact same geometry and same trace scaling. Both figures have been plotted using the

maximum of each trace as a scaling factor for that particular trace. As a result, each trace appears to have a similar signal strength. A few of the picks on the seismic gun VSP data, most notably for depths of 3.5 m, 4.5 m and 10.5-12.5 m, appear to be time shifted. Malfunction of the triggering system was most likely the cause for this issue.

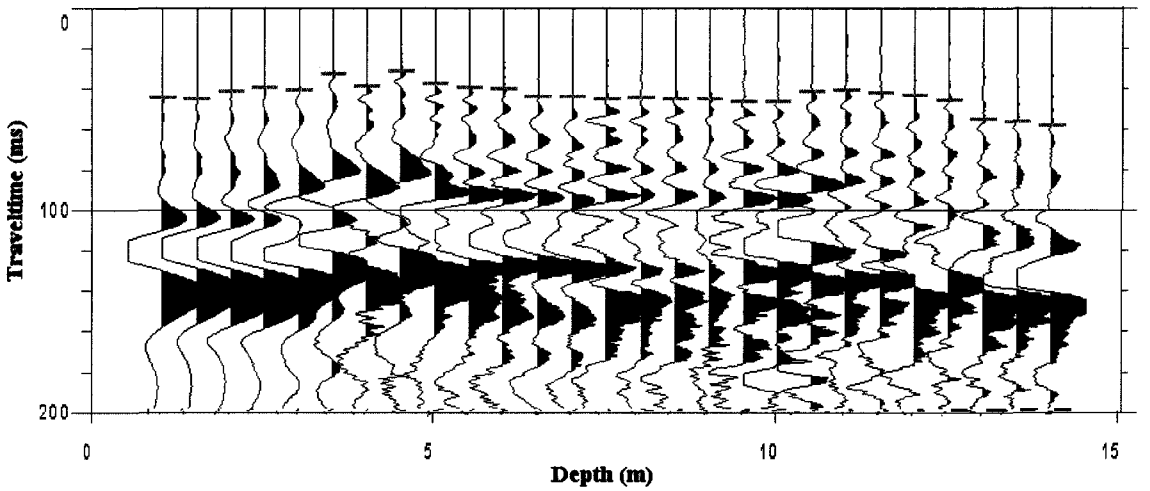

Figure 4.3: Vertical-component geophone VSP data obtained at a 10 m offset using the seismic gun. A 0-200/250 Hz filter has been applied and a trace maximum scaling has been applied.

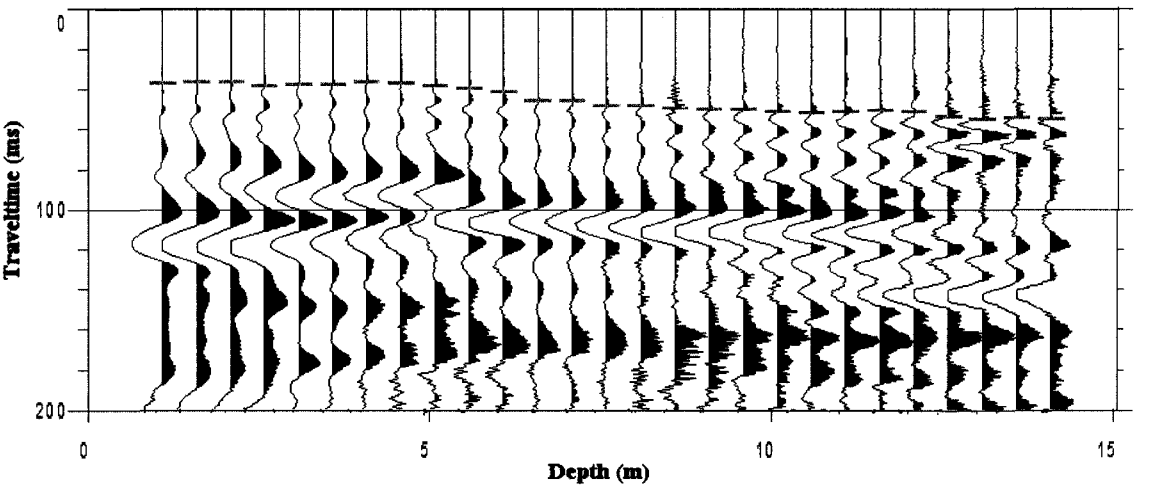

Figure 4.4: Vertical-component geophone VSP data obtained at a 10 m offset using the seismic hammer. A 0-200/250 Hz filter has been applied and a trace maximum scaling has been applied.

Another problem with the gun signal is its lack of repeatability. In order to fire a shot, the gun must be placed in an augured hole filled with water. During each shot, the explosion enlarges the hole. After about 10 shots, the cavity becomes too large and a new hole needs to be used. Changes in size and shape of the cavity results in different source signal signatures. Some of the signal energy is lost during the creation of these cavities.

It was initially assumed that the seismic gun would provide a stronger signal and the source could be moved to larger offsets in order to survey the landfill at greater depths. In order to investigate which source had the stronger signal in this particular application, both the seismic hammer and the seismic gun vertical-component VSP data were plotted directly over top of each other. This was done in Matlab using the CREWES (Margrave, 2005) software package. In Figure 4.5, the seismic hammer traces are shown in blue and the seismic hammer traces are shown in red. No scaling has been applied to the traces in order to accurately compare wave amplitudes, and therefore signal strength between traces. Somewhat surprisingly, the seismic hammer gives a stronger signal than the seismic gun through the entire depth range. This might be related to the different frequency content of the hammer and the gun signals.

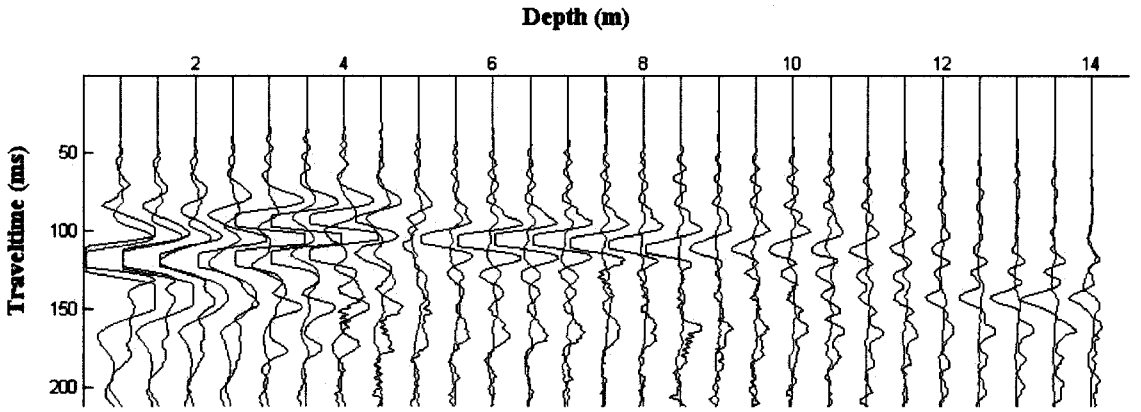

Figure 4.5: The hammer VSP (blue) data plotted over the gun VSP (red) data. A 0-200/250 Hz filter has been applied and a global maximum scaling has been applied.

The seismic gun is generally thought to generate data with a higher frequency than the seismic hammer (S. Pullan, personal communication). In order to validate this assumption, the frequency spectra of data generated by the gun and the hammer and recorded using the same vertical-component geophone (mostly P-waves) are plotted in Figures 4.6 and 4.7, respectively. The dominant frequency of the observed signal is taken from the middle of the largest peak. The dominant frequency of the seismic gun data is approximately 16 Hz, slightly higher than the dominant frequency of the seismic hammer at approximately 10 Hz. The frequency spectrum of hammer data recorded by a horizontal-component geophone (mostly S-waves) is shown in Figure 4.8. These data have a higher dominant frequency of approximately 45 Hz and the spectrum is more erratic than that of the vertical-component data shown in Figure 4.7. Highly attenuating material, such as solid waste, attenuates higher-frequency signal over shorter distances than lower-frequency signal. This might explain why the signal generated by the gun (dominant frequency $\approx$ 16 Hz) is generally weaker than that of the hammer (dominant frequency $\approx$ 10 Hz).

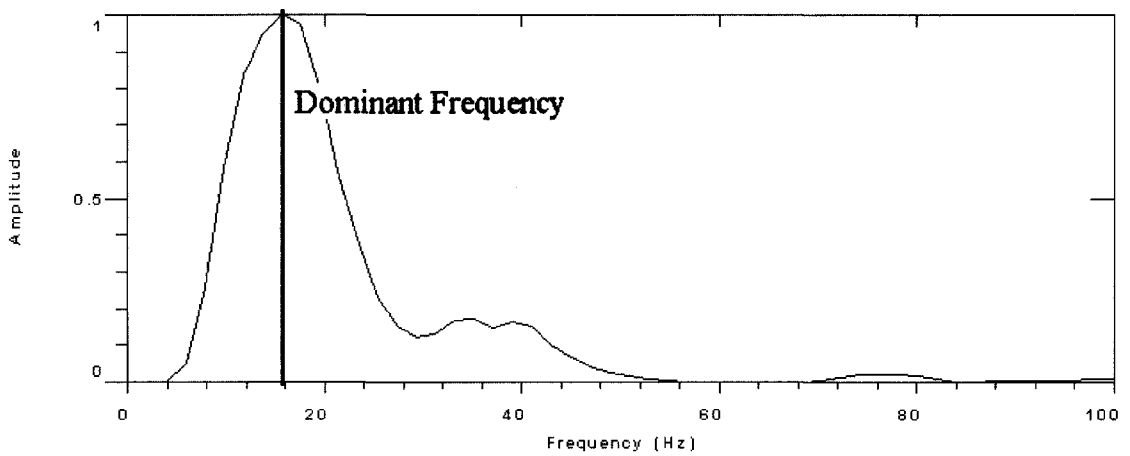

Figure 4.6: Frequency spectrum for seismic gun data recorded by the vertical-component geophone at a 10 m offset.

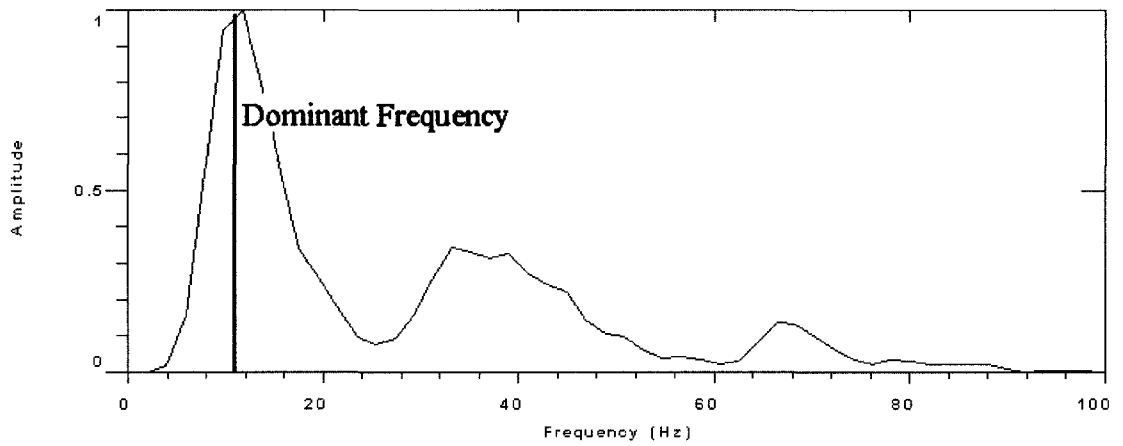

Figure 4.7: Frequency spectrum for seismic hammer data recorded by the vertical-component geophone at a 10 m offset.

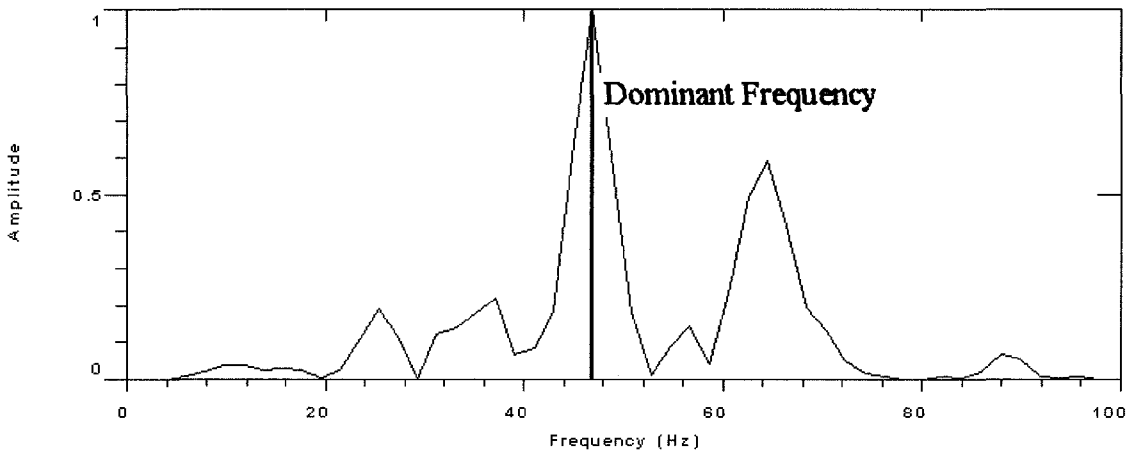

Figure 4.8: Frequency spectrum for the seismic hammer data generated from a positive horizontal hit and recorded by a horizontal-component geophone channel at a 10 m offset.

In summary, the use of the seismic gun was abandoned after Survey 2 in favour of the seismic hammer for three reasons:

1. The hammer has a reliable time-zero reference.
2. The source signature of the hammer is more repeatable than that of the gun.
3. The hammer generates a stronger signal than the gun for this application.

4.3 Spatial Resolution

The resolution of different velocity structures within the subsurface is dependant on the wavelength of the signal being generated. Wavelengths can be computed by dividing wave velocity by the dominant frequency. Section 4.2 illustrates that the dominant frequency of P-waves and S-wave is approximately 10 Hz and 45 Hz respectively. A discussion of seismic velocity is presented in Section 4.6. It is assumed that P-waves have an average velocity of about 400 m/s and S-waves have an average velocity of 160 m/s over the depth of the boreholes. This would translate to wavelengths of 40 m and 3.5 m

for P-waves and S-wave respectively. The distances between the source and geophone fall within the range of 5 m – 20 m, much less than a single wavelength for P-waves and a few wavelengths for S-waves. Waves travelling at this distance from the source are considered to be in the "near-field". The corresponding resolution, particularly for P-waves, is rather low. Using a higher frequency source would reduce the wavelength and increase resolution. However, higher frequency sources tend to attenuate over shorter distances and given the attenuating nature of the waste, difficulties in signal detection would arise.

Resolution of velocity images is also dependant on the aperture of the observational array, in other words, the multi-angular coverage provided by the crossing rays. Since in this case it was only possible to generate a detectable signal from the surface, the multi-angular coverage through the waste was limited.

4.4 Wave Type Identification

Clearly identifying distinct P-wave and S-wave modes in the near-field can be challenging. However, during the course of this project, it was possible to generate and record both P-waves and S-waves propagating through the waste.

A vertical hit with the seismic hammer will generate mostly P-waves, therefore most of the energy is recorded by the vertical-component geophone. A horizontal hit, struck towards (positive) or away (negative) from the geophone, can generate both P-waves

(mostly captured by the vertical-component geophone) and S-waves (mostly captured by the two horizontal-component geophones.

Figure 4.9 shows all hit types (vertical, positive and negative) recorded by the vertical component geophone. The positive horizontal hit appears to be generating the strongest signal, possibly a mix of P-waves and SV-waves, that is, shear waves polarized in the vertical direction. Figure 4.10 shows all hit types (vertical, positive and negative) on the horizontal channel. All hits seem to provide an equal amount of energy on the horizontal 1 channel. The same is true for the horizontal 2 channel shown in Figure 4.11.

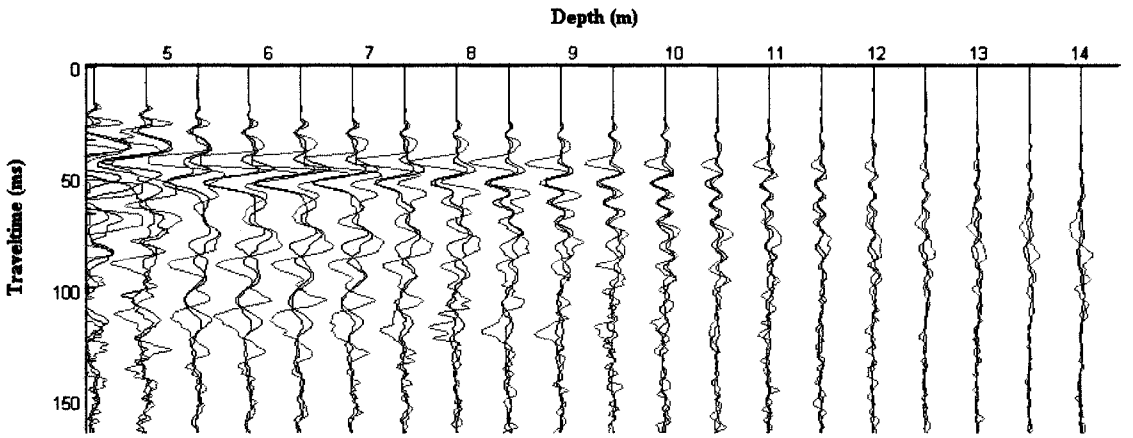

Figure 4.9: Vertical hit (blue), positive horizontal hit (green) and negative horizontal hit (red), recorded on the vertical channel using a seismic hammer at a 5 m offset. A 0-200/250 Hz filter has been applied.

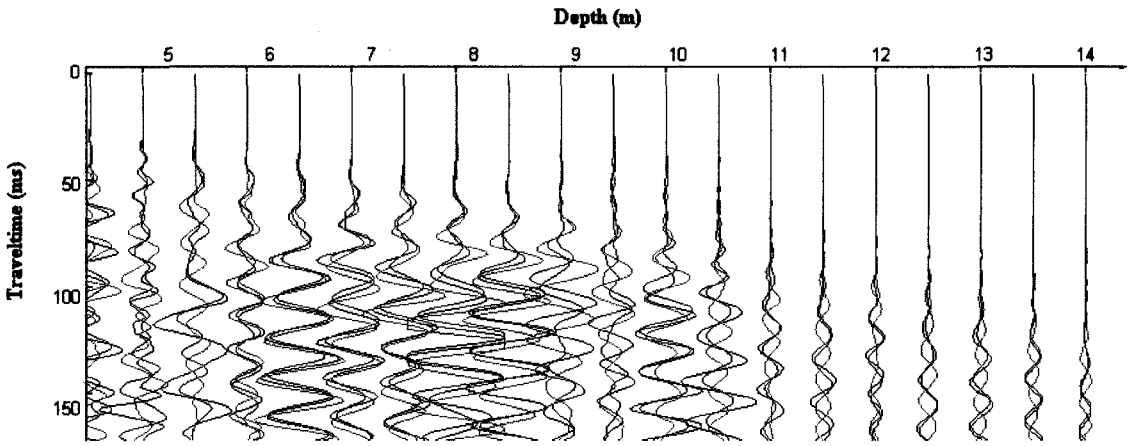

Figure 4.10: Vertical hit (blue), positive horizontal hit (green) and negative horizontal hit (red), recorded on the horizontal 1 channel using a seismic hammer at a 5 m offset. A 0-200/250 Hz filter has been applied.

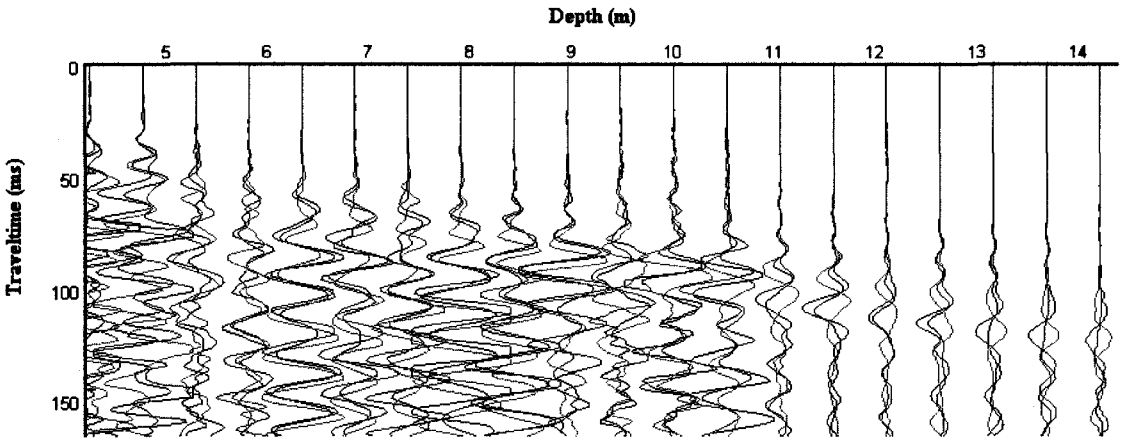

Figure 4.11: Vertical hit (blue), positive horizontal hit (green) and negative horizontal hit (red), recorded on the horizontal 2 channel using a seismic hammer at a 5 m offset. A 0-200/250 Hz filter has been applied.

An orienting geophone with 2 perpendicular horizontal components was used to collect S-wave data. The horizontal 1 component was always oriented towards magnetic north. The I-beam was in a NW direction so that there was a 45 degree angle between the I-beam and the horizontal-component geophones. This was done so that equal levels of

energy would reach both geophones. If it is the case, then positive and negative shots recorded on the same horizontal channel should have opposite polarity. This is a quick test to identify S-waves on the recordings. Figures 4.12 and 4.13 show positive and negative shots for the horizontal 1 and 2 channels, respectively. In both cases, most of the traces, notably between 10.5 m – 14 m depths, do in fact show reversed polarity. However, at other depths, notably between 6 m -10 m, there appears to be a slight phase shift and this behaviour is not as well developed. Again, this could be due the issue of waves propagating in the near-field.

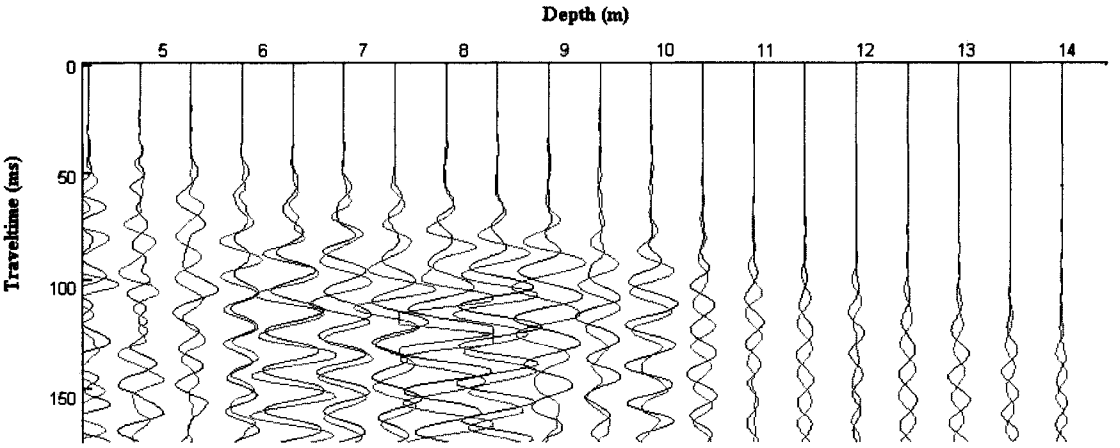

Figure 4.12: Positive horizontal hit (green) and negative horizontal hit (red), recorded on the horizontal 1 channel using a seismic hammer at a 5 m offset. A 0-200/250 Hz filter has been applied.

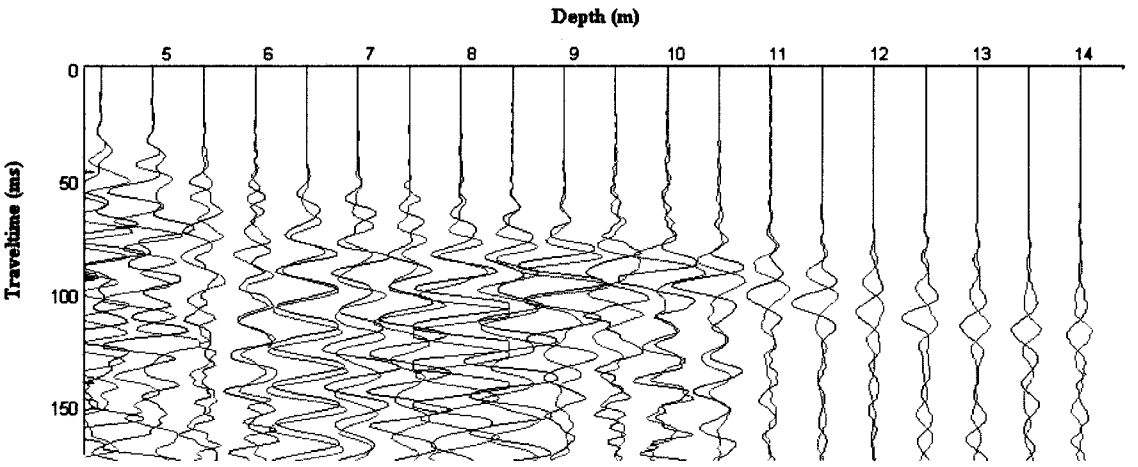

Figure 4.13: Positive horizontal hit (green) and negative horizontal hit (red), recorded on the horizontal 2 channel using a seismic hammer at a 5 m offset. A 0-200/250 Hz filter has been applied.

At this point, it is reasonable to assume that the vertical-component is mostly recording P-waves and the horizontal-component is mostly recording S-waves, as anticipated. Figure 4.14 is a typical P-wave VSP acquired using the seismic hammer striking vertically on the steel plate. This signal was recorded by the vertical-component geophone. The signal is consistent from trace to trace, and there is a noticeable change in the waveform at a depth of about 5 m. This is most likely due to the presence of the landfill cover. The near surface traces have travelled mostly through sand and clay cover, while the deeper traces have travelled mostly through the waste.

Figure 4.15 is a typical S-wave VSP acquired using the seismic hammer striking the side of the I-beam. The signal is less consistent from trace to trace. The slope of the first break picks through the waste is much larger than in Figure 4.14, reflecting the fact that S-waves have a slower velocity than P-waves. There is also a noticeable change in the slope

of the first break picks at depths less than 4 m. The smaller slope is due to the waves propagating at a having a faster velocity through the cover compared to the waste. At depths between 10 m and 14 m, the slope of the first arrivals appear fairly horizontal, indicating a positive velocity gradient with depth.

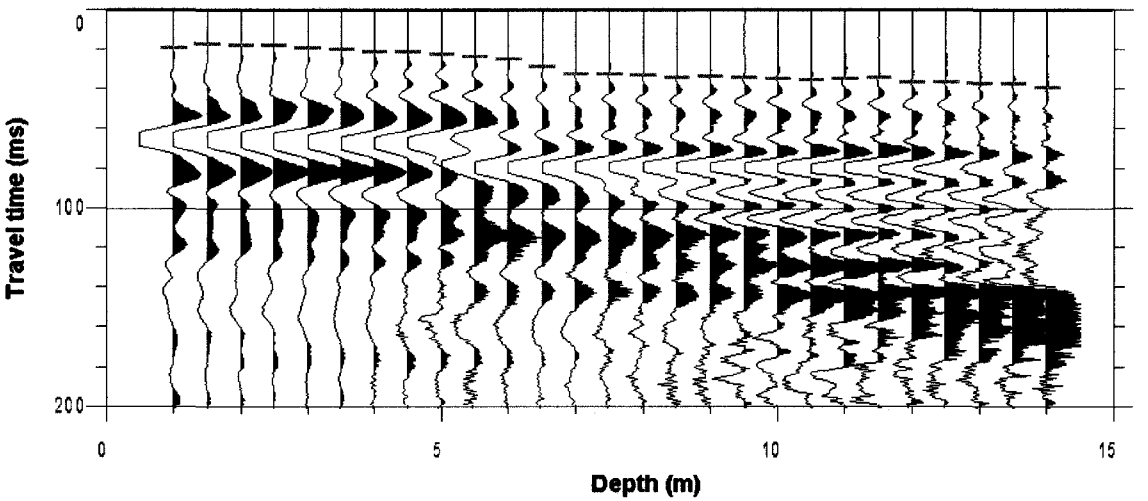

Figure 4.14: Vertical-component geophone VSP data recorded using vertical hit with seismic hammer at a 5 m offset. A filter of 0-200/250 Hz has been applied. A trace maximum scaling has been applied. First breaks indicated by the dashed lines.

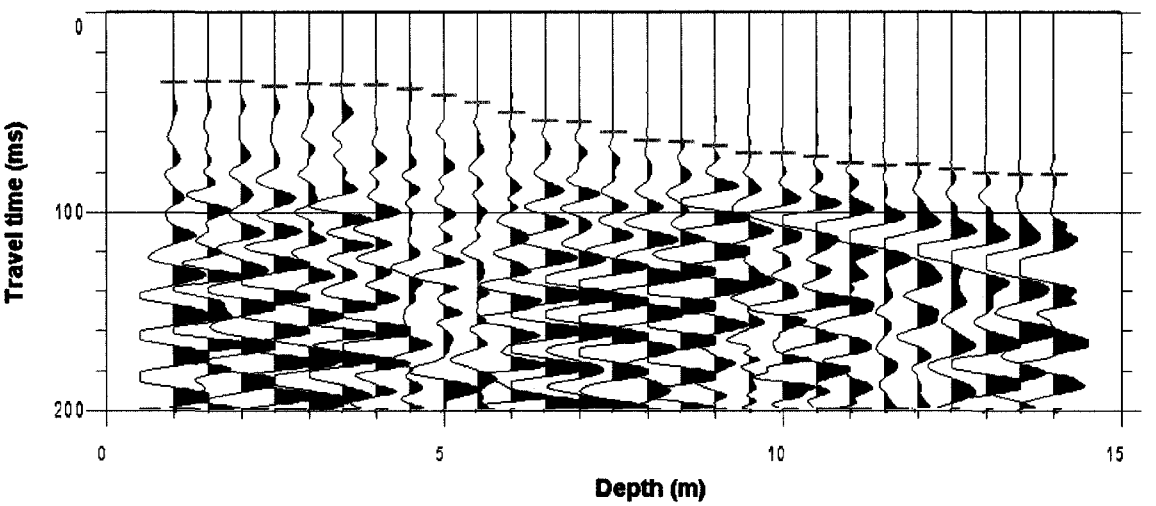

Figure 4.15: Horizontal-component geophone VSP data recorded using horizontal hit with seismic hammer at a 5 m offset. A filter of 0-200/250 Hz has been applied. A trace maximum scaling has been applied. First breaks indicated by the dash lines.

4.5 Quality of Data Versus Offset

The amplitude of a seismic wave attenuates over distance due to scattering and heat loss. Therefore, as the offset from the borehole increases, it becomes much more difficult to pick the first breaks over the background noise. Figure 4.16, Figure 4.17 and Figure 4.18 show VSP data recorded by the vertical-component geophone, and obtained using the seismic hammer at 5 m, 10 m, and 15 m offsets, respectively. At 5 m and 10 m offsets, the first breaks are easily picked for the entire depth range. At 15 m offset, a 0-80/100 Hz filter needed to be applied because of the large amount of noise. As a result, the first arrivals have a lower frequency content and therefore a broader waveform. In this case, it is more difficult to pick the first breaks accurately but the slope of the direct arrival event is still easy to follow. Figure 4.19, Figure 4.20 and Figure 4.21 show VSP data recorded by a horizontal-component geophone, and obtained using a seismic hammer at 5 m, 10 m and 15 m offsets, respectively. At a 5 m offset, picking the first breaks is a relatively easy task. At 10 m and 15 m offsets, it is difficult to pick the first breaks against the background noise. Figure 4.22, Figure 4.23 and Figure 4.24 show VSP data recorded by the vertical-component geophone, and obtained using a seismic gun at 10 m, 15 m and 20 m offsets, respectively. At a 5 m offset, picking the first breaks is a relatively easy task. At 10 m and 15 m offsets, it is difficult to pick the first breaks against the background noise.

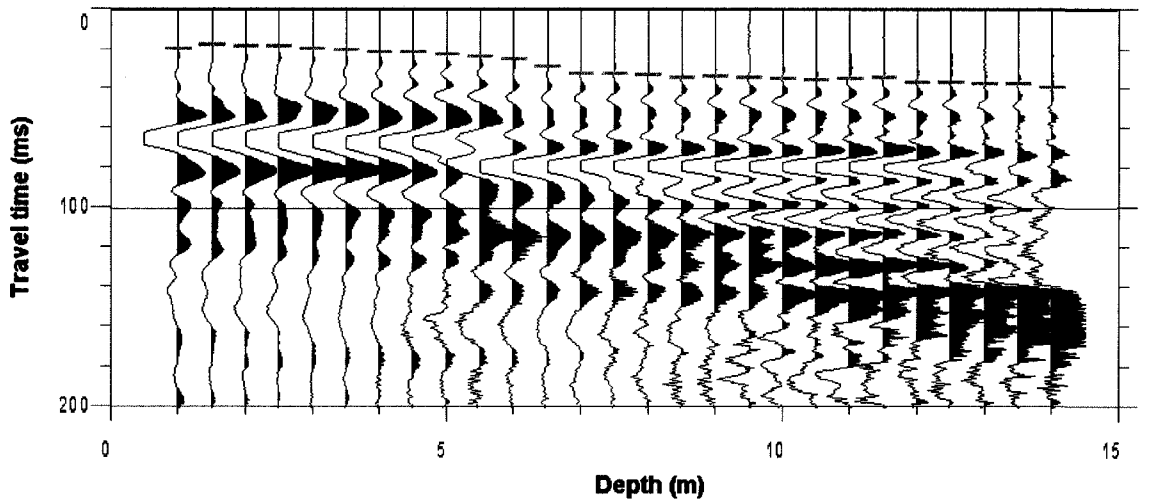

Figure 4.16: Vertical-component geophone VSP data recorded using the seismic hammer at 5 m offset. Filtered 0-200/250 Hz. Trace maximum scaling applied.

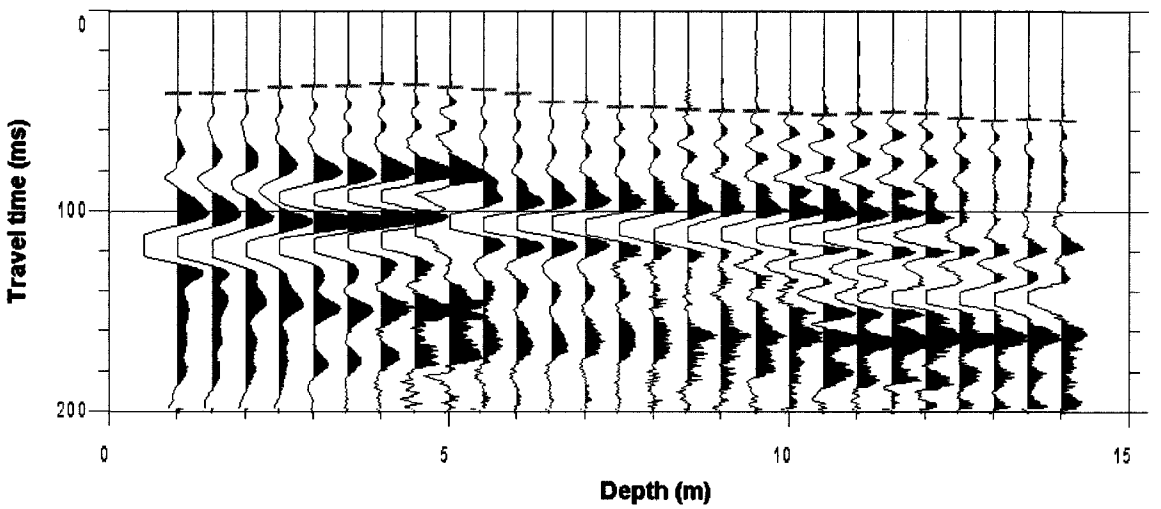

Figure 4.17: Vertical-component geophone VSP data recorded using the seismic hammer at 10 m offset. Filtered 0-200/250 Hz. Trace maximum scaling applied.

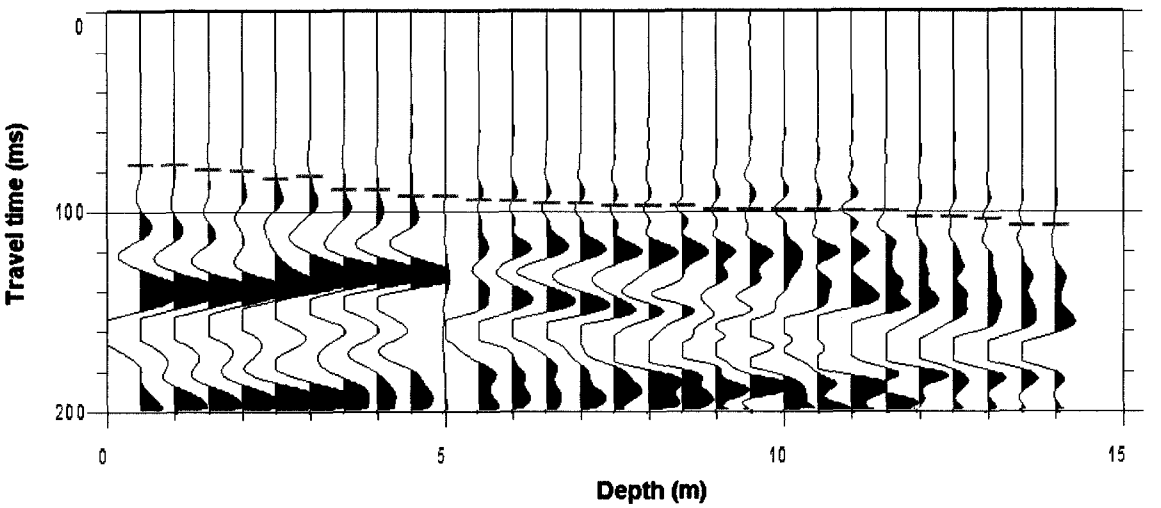

Figure 4.18: Vertical-component geophone VSP data recorded using the seismic hammer at 15 m offset. Filtered 0-200/250 Hz. Trace maximum scaling applied.

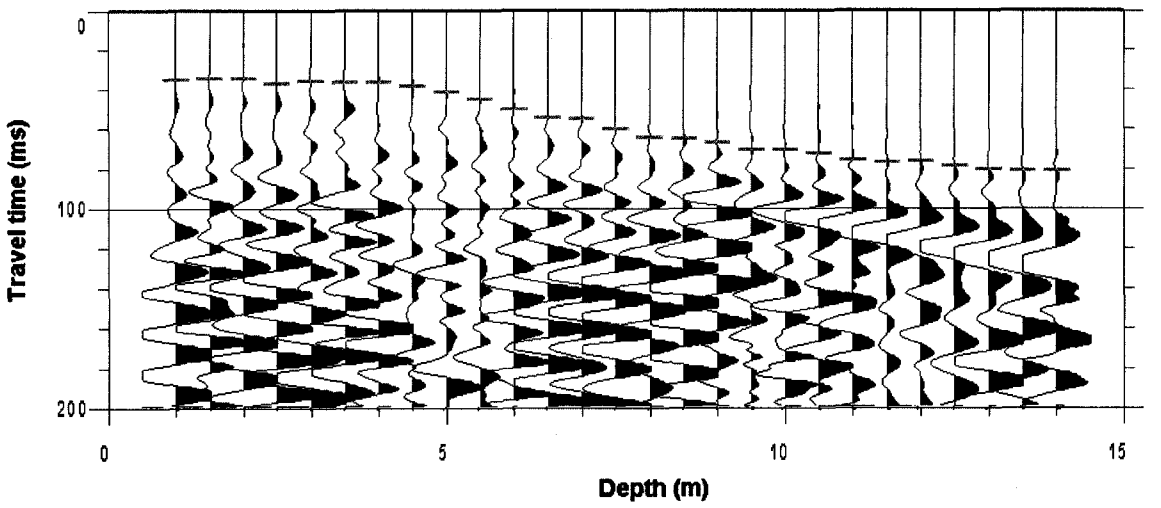

Figure 4.19: Horizontal-component geophone VSP data recorded using the seismic hammer at 5 m offset. Filtered 0-200/250 Hz. Trace maximum scaling applied.

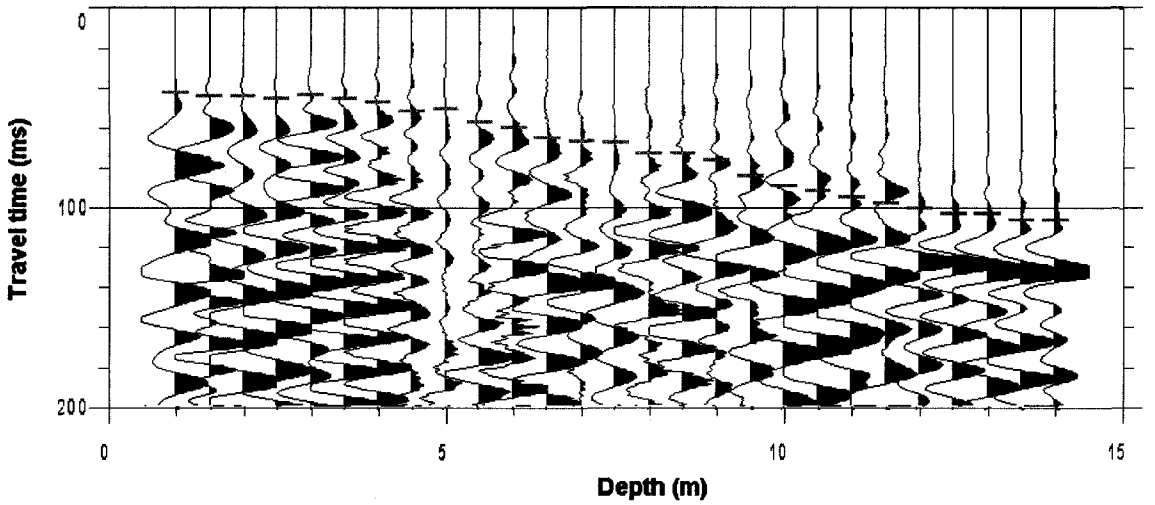

Figure 4.20: Horizontal-component geophone VSP data recorded using the seismic hammer at 10 m offset. Filtered 0-200/250 Hz. Trace maximum scaling applied.

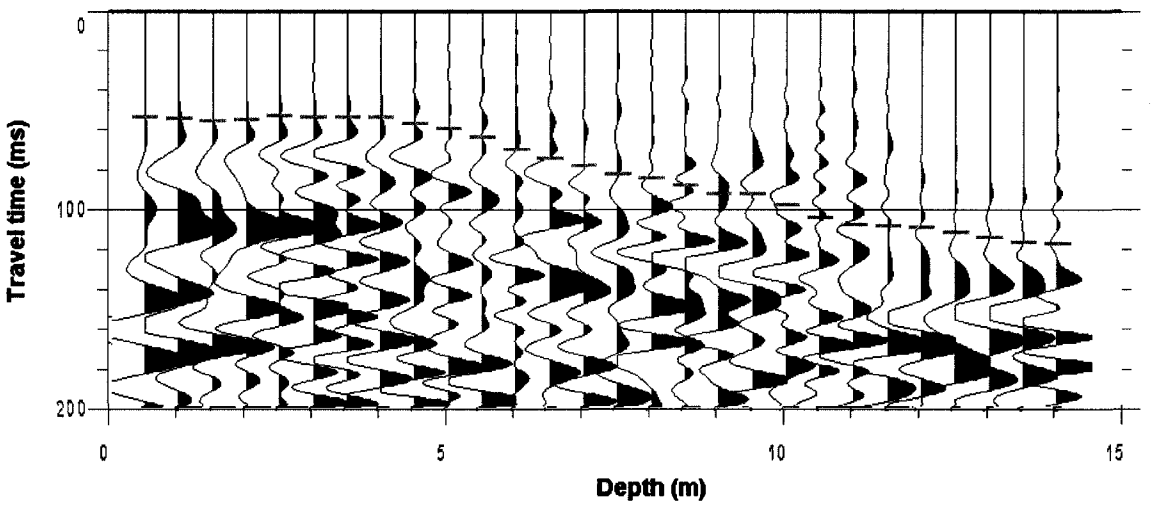

Figure 4.21: Horizontal-component geophone VSP data recorded using the seismic hammer at 15 m offset. Filtered 0-200/250 Hz. Trace maximum scaling applied.

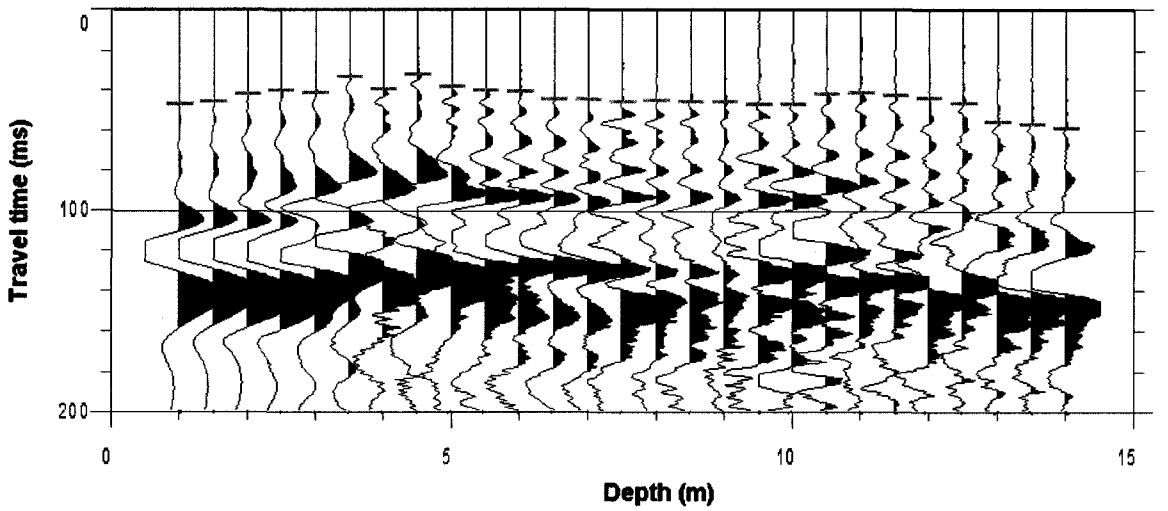

Figure 4.22: Vertical-component geophone VSP data recorded using the seismic gun at 10 m offset. Filtered 0-200/250 Hz. Trace maximum scaling applied.

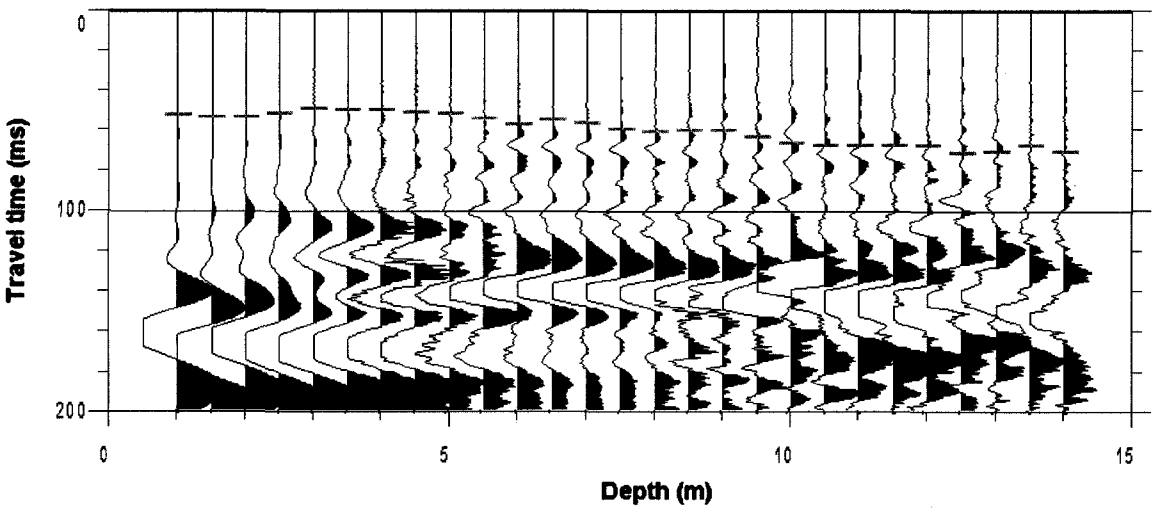

Figure 4.23: Vertical-component geophone VSP data recorded using the seismic gun at 15 m offset. Filtered 0-200/250 Hz. Trace maximum scaling applied.

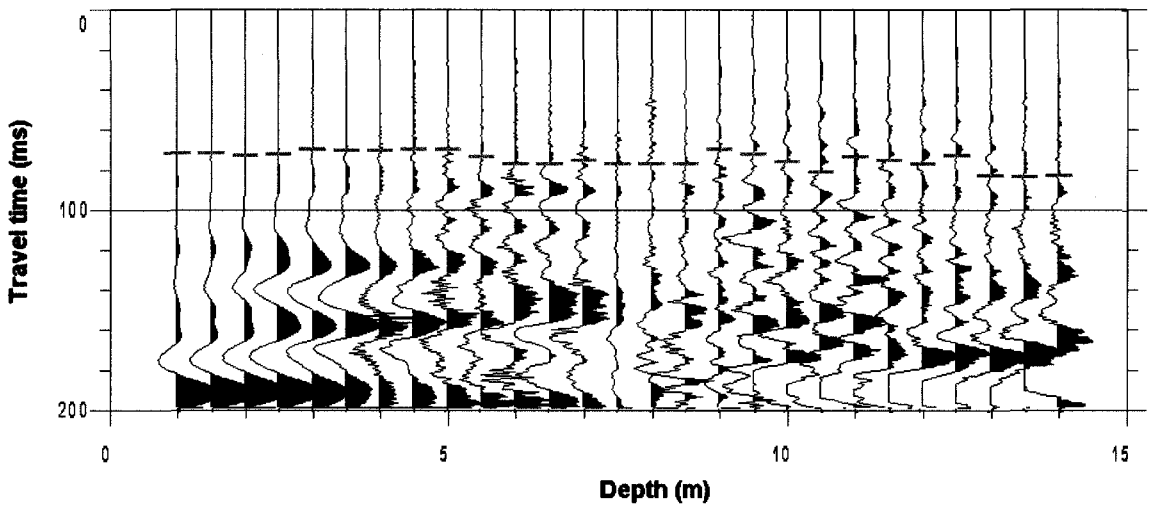

Figure 4.24: Vertical-component geophone VSP data recorded using the seismic gun at 20 m offset. Filtered 0-200/250 Hz. Trace maximum scaling applied.

The attenuation coefficient was estimated for both P-waves and S-waves using the seismic hammer at 5 m, 10 m and 15 m offsets. Each hammer hit has a slightly different energy level due to operator inconsistencies. Therefore, in order to accurately measure attenuation a reference geophone should have been placed in the borehole at the surface to record the exact wave amplitude for each shot. Unfortunately, a reference geophone was not employed when recording seismic data. The analysis therefore simply assumes that the seismic hammer has the same energy content in each shot, and that a rough estimate of the attenuation coefficient can be determined. It was not possible to use the seismic gun data to determine attenuation properties because of the highly variable energy content of each shot. The amplitude data oscillated with distance and it was not appropriate to fit an exponential function to the data set.

In order to find the value of the attenuation coefficient, Equation 2-12 was linearized to the form of $\ln(Ar) = \alpha r + \ln A_0$. Therefore, obtaining the slope for the line of best fit of

the ln(Ar) vs. r relationship would yield the attenuation coefficient α. The upper 3 m of data has been excluded because it corresponds to wave propagation mostly through the cover rather than through waste material. Figure 4.25 illustrates the P-wave attenuation with distance. The 5 m offset provided the closest fit to a linear function with a correlation coefficient (R^2) value of 0.90, giving an attenuation coefficient of -0.16 m^{-1}. The average P-wave attenuation coefficient is -0.126 m^{-1}.

S-wave amplitudes were much more erratic than P-wave amplitudes. Data do not seem to fit linear functions very well. This is probably because the amplitude data have not been corrected for individual A_O values, as no reference geophone was employed. The survey orientation was such that the seismic energy on both horizontal channels is approximately the same. Therefore, the maximum S-wave amplitudes for both horizontal channels were combined for the south hit in the analysis. Figure 4.26 illustrates the S-wave attenuation at 5 m, 10 m and 15 m offsets. The 15 m offset provided the closest fit to a linear function with an R^2 value of 0.52, giving an attenuation coefficient of -0.18 m^{-1}. The average S-wave attenuation coefficient is -0.263 m^{-1}, slightly higher than the P-wave attenuation. This is consistent with the fact that S-waves have a higher frequency content than P-waves (Figures 4.7 and 4.8) and therefore attenuate over shorter distances.

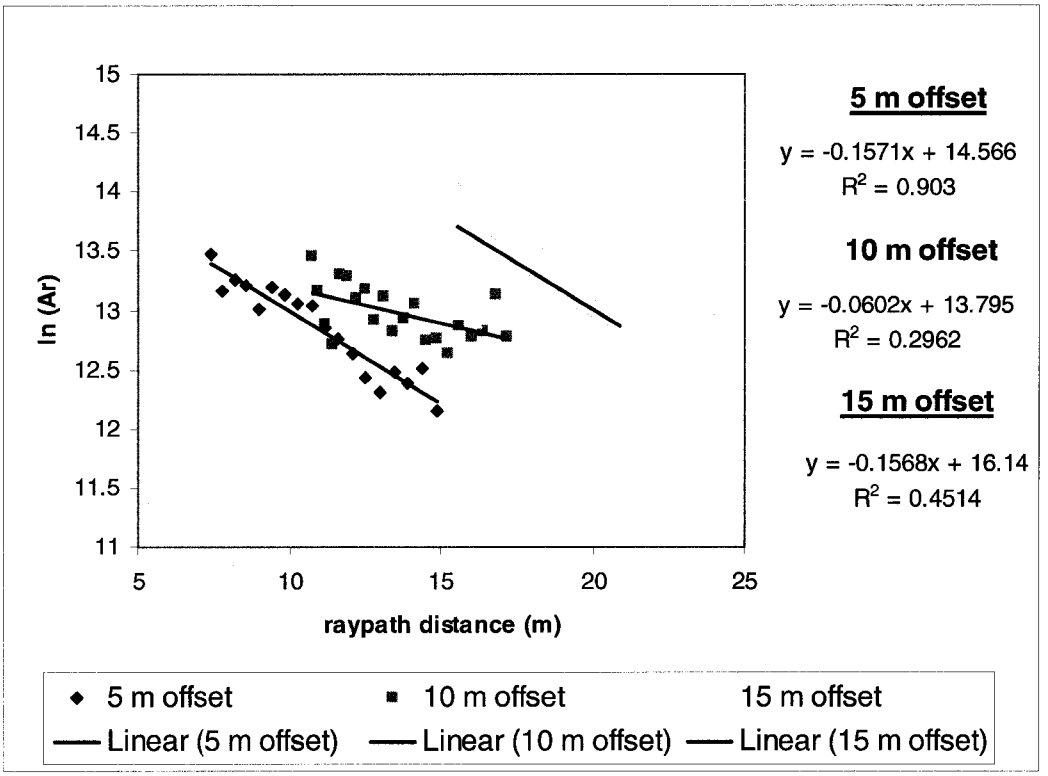

Figure 4.25: P-wave attenuation with raypath distance.

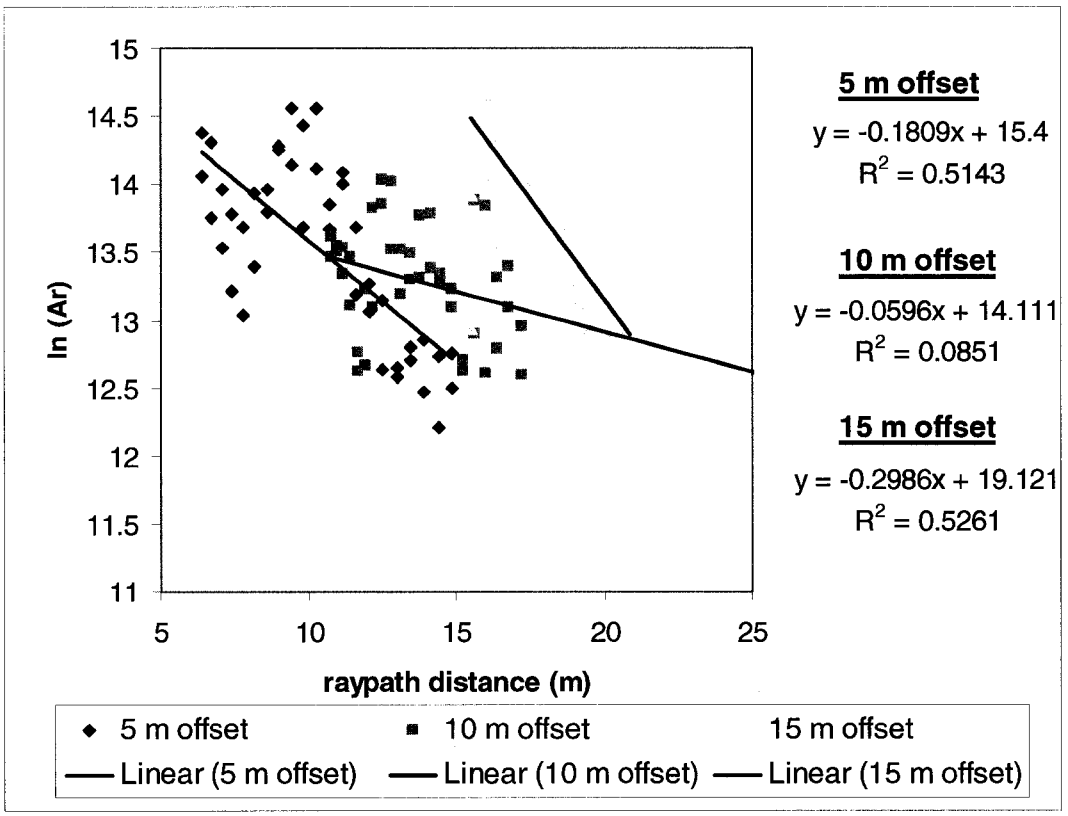

Figure 4.26: S-wave attenuation with raypath distance.

4.6 Tomography

Tomography is the mathematical inversion of traveltimes in order to obtain an image of the velocity structure. Tomography was performed using both P-waves and S-waves propagating within the waste column to help understand the potential of this technique to image velocity anomalies in a 2D plane. It should also be noted that for the case of P-waves, the area that is being inverted is smaller than a single wavelength. Therefore, the amount of detail that can be extracted using ray-based inversion methods is limited. Recall from Chapter 3 the limitations experienced from using only a surface source (Figure 3.5). The tomograms generated will provide velocity results for the entire rectangular plane in which data is available. However, only reliable results can be obtained for the area sampled by the raypaths; data for the rest of the plane have simply been extrapolated. This limited angular coverage with depth also contributes to poor resolution in the generated tomograms.

The GeoTomo GeoCTII tomography software package was used to invert the first breaks picked on VSP data into a tomogram. In order to generate a tomogram, the program must input the first breaks picked by the user, an initial velocity model, minimum and maximum velocity boundaries, the number of iterations to perform, a smoothing control parameter, and a x/y smoothing ratio parameter. The first break picking was completed using Interprex's IXSeg2Segy software. The selection of max/min velocity boundaries was based on a review of published values for seismic waves in solid waste (Table 2.1).

Determining an appropriate number of iterations and inversion parameters required the use of the GeoCTII software itself.

4.6.1 Layered Velocity Models

In order for tomography to work, there needs to be an initial velocity value placed in each cell. Since inversion solutions are not unique, the closer this initial value is to the actual velocity value, the more likely the tomographic algorithm will converge to a reasonable output. It was decided that a homogeneous two layer model was appropriate because the area between the boreholes is known to have a distinct cover layer and waste layer.

Consider S-waves recorded at a 5 m offset as shown in Figure 4.15. The associated first break picks were imported in Microsoft Excel and plotted against the raypath distance. Two lines of best fit were therefore computed, corresponding to the cover and the waste column. The reciprocal of the slope of each line of best fit gives the velocity over that interval. In the example shown in Figure 4.27, the S-wave velocity of 204 m/s through the cover and 136 m/s through the waste. The last few traces through the waste do not appear to arrive at the same time, indicating a positive velocity gradient. In this case, fitting lines over that interval is not appropriate because the velocity distribution is no longer homogeneous. A third layer was not added to the model because this behaviour represents had only been observed on a few traces.

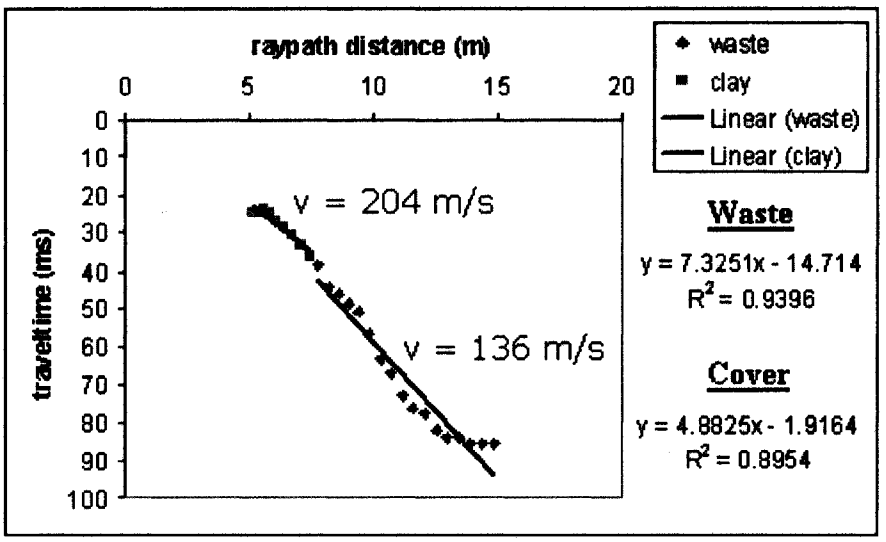

Figure 4.27: S-wave first break picks from Figure 4.15 plotted versus raypath distance.

4.6.2 Selection of the P-wave Initial Velocity Model

A number of different P-wave initial velocity models in Table 4.1 were created using GeoCTII's Build Model program. A smoothing control of 0.1 (Carpenter et al., 2004), recommended in literature, and a x/y smoothing ratio of 20, recommended in GeoCTII's user manual for VSP were used as input parameters.

Model Type	P-wave velocity at the surface (ms)	Gradient (m/s/m)
Homogeneous	200	0
	300	0
	400	0
	500	0
Velocity gradient increasing with depth	200	15
	300	15
	400	10

Table 4.1: P-wave initial velocity models created using *Build Model*

Figure 4.28 is the raytraced P-wave arrival times through the tomograms generated from each respective initial velocity model. To ensure a sufficient number of iterations were being used, the RMS error for each iteration was plotted in Figure 4.29. In most cases, after approximately 10 iterations, the RMS error remains constant, and iterating further will not improve results. However for the 200 m/s homogeneous initial model, most likely the least correct, it took almost 50 iterations for the RMS error to remain relatively constant. To be conservative, 50 iterations were performed for every inversion. All initial models give very similar results, however the 300 m/s surface velocity 15 m/s/m gradient model provided the lowest RMS error on the final iteration. This is the initial velocity model that will be used to determine inversion parameters and used to perform all P-wave inversions.

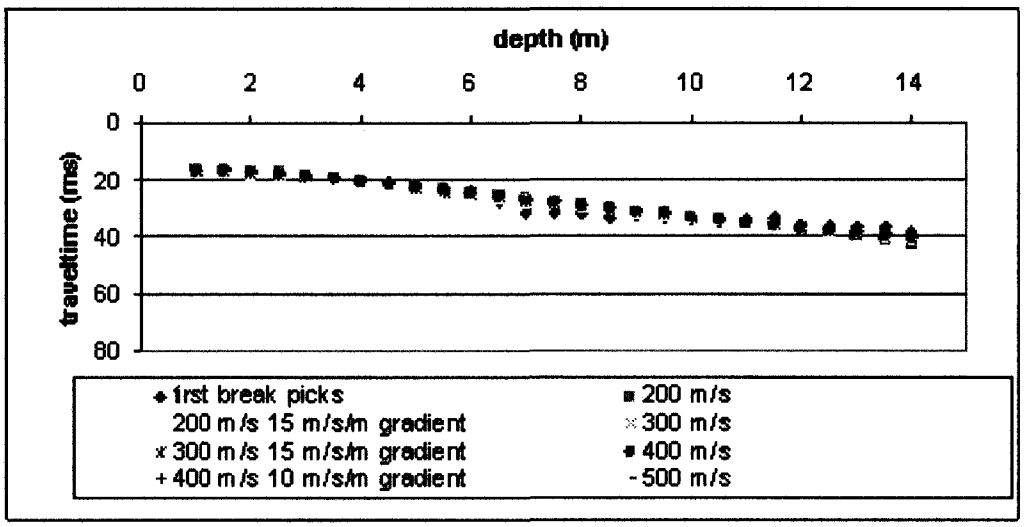

Figure 4.28: Observed and raytraced P-wave first breaks for inverted initial velocity models listed in Table 4.1.

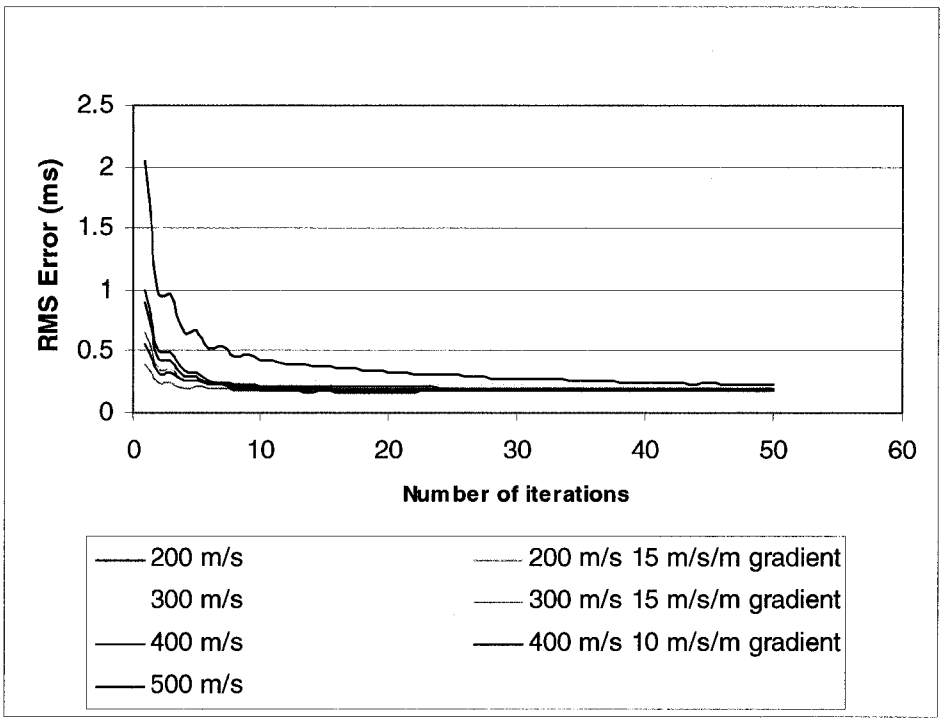

Figure 4.29: The RMS error (ms) between the raytraced and observed break for each iteration tomogram generated from the initial velocity models listed in Table 4.1.

4.6.3 Determining Inversion Parameters

In order to determine the most appropriate inversion parameters to use, only the initial P-wave model of 300 m/s surface velocity 15 m/s/m gradient was used.

Smoothing Control

The smoothing control parameter essentially determines the size of the velocity gradient between adjacent cells. A lower smoothing control value will allow for a larger velocity gradient between grid cells which will result in a lower data misfit, and rougher velocity model. In this case, the user is forcing the inversion to follow the picks very closely, which is not necessarily always the best approach due to the subjective nature of the picking procedure. Having a large velocity gradient between grid cells is probably not

realistic. A larger smoothing control value will provide a smoother velocity model, however, data misfit will probably increase.

Figure 4.30 shows the raytraced P-wave first arrivals through tomograms using different smoothing control values. A value of 0.1, recommended in the literature (Carpenter et al., 2004), for which the resulting tomogram is shown in Figure 4.31, was found to be a good compromise between following the first picks while ensuring a smooth velocity model. The plane shown in Figure 4.31 represents the total rectangular area in the waste in which all raypaths travel. The borehole is located at a horizontal distance of 0 m, and the shot point is located at a horizontal distance of 5 m.

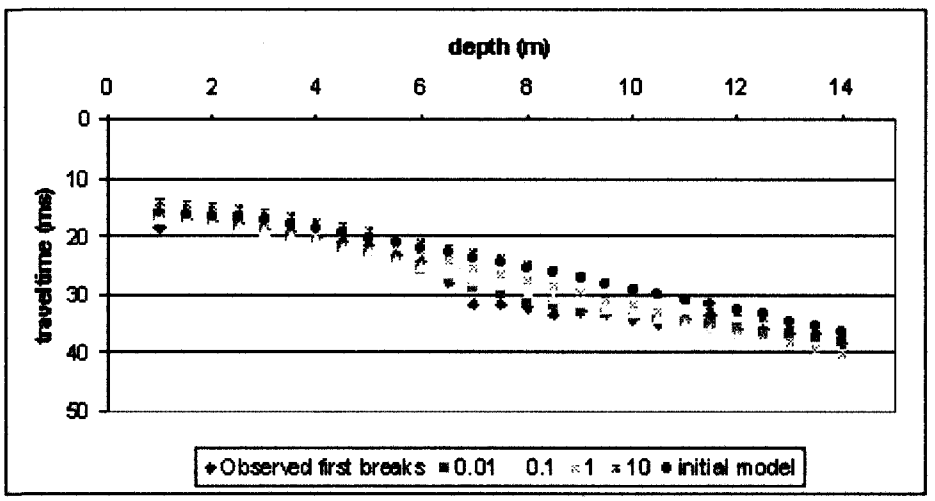

Figure 4.30: Observed and raytraced P-wave first breaks from tomograms using different smoothing control values.

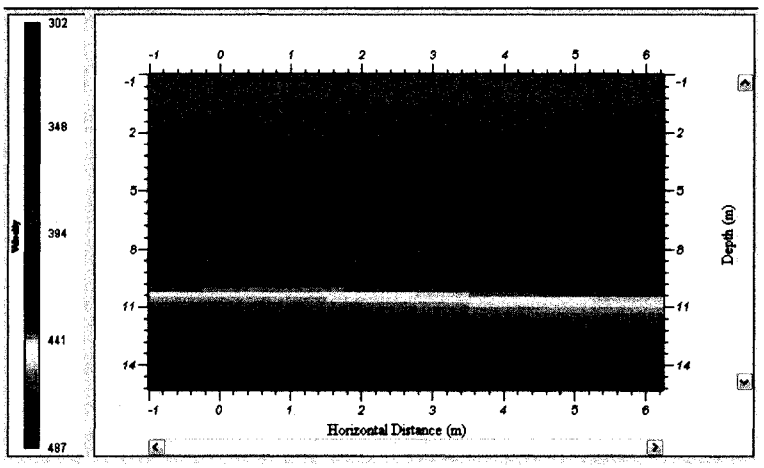

Figure 4.31: P-wave tomogram assuming an initial velocity model of 300 m/s surface velocity 15 m/s/m gradient, an x/y ratio of 20 and smoothing control of 0.1.

X/Y Ratio

The x/y ratio essentially determines how well the velocity should follow the grid cells to the left or right (i.e. lateral variations along the survey line), as opposed to the top or bottom (i.e. vertical variations versus depth). High x/y ratios will generate tomograms with more horizontal velocity layers. The GeoCTII user manual recommends values around 20 for VSP geometries. However, it should be noted that VSP surveys are traditionally used to determine the stratigraphy of overburden where the subsurface is highly layered and the velocity variations between layers can be quite high. Since this is not the case with solid waste, lower x/y ratios were tested. Figure 4.32 shows the observed and raytraced P-wave first breaks and using different x/y ratios. All x/y ratios give very similar results. Figure 4.33 and Figure 4.34 show the resultant tomograms for x/y ratios of 5 and 20 respectively. An x/y ratio of 5 does result in a little more vertical velocity variation in which the layers seem to dip slightly. The velocity variations are on the order of 10-20 m/s. The velocity distribution seems smoother for an x/y ratio of 20.

Since velocity variations are small between variable x/y ratios, it was decided that a value of 20 would be used in order to maintain horizontal layering.

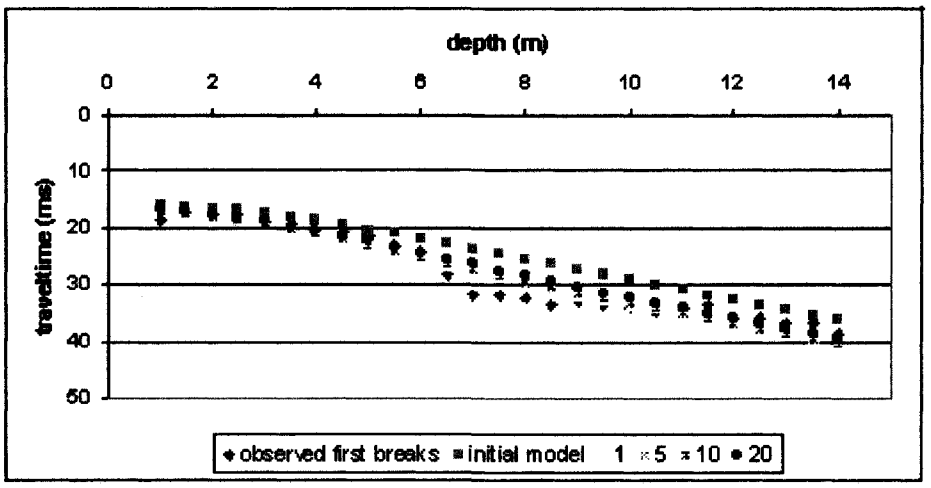

Figure 4.32: Observed and raytraced P-wave first breaks using variable x/y ratios.

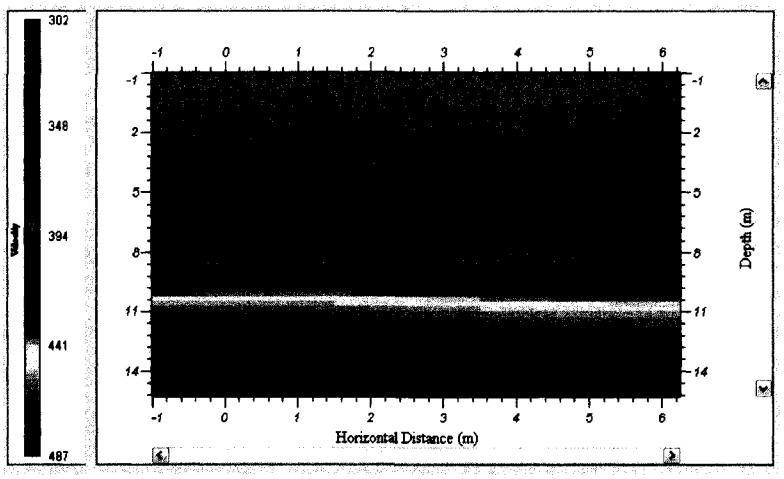

Figure 4.33: P-wave tomogram assuming an initial velocity model of 300 m/s surface velocity 15 m/s/m gradient, an x/y ratio of 5 and smoothing control of 0.1.

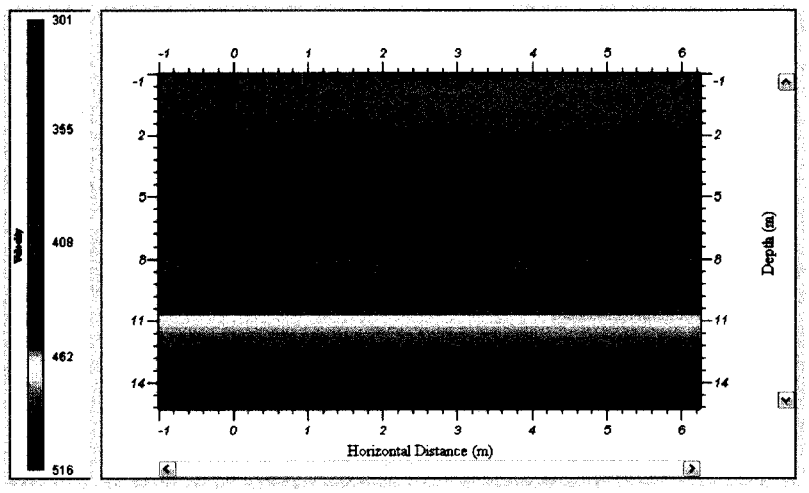

Figure 4.34: P-wave tomogram assuming an initial velocity model of 300 m/s surface velocity 15 m/s/m gradient, an x/y ratio of 20 and smoothing control of 0.1.

4.6.4 Selection of the S-wave Initial Velocity Model

In a similar fashion to the selection of an appropriate P-wave model, the different S-wave initial velocity models listed in Table 4.2 were tested. There seemed to be a large velocity difference between the cover and the waste in the S-wave profiles (Figure 4.27), therefore some of the initial velocity models contain a 2 m thick high-velocity cover layer above the waste column. The observed and raytraced first breaks for the inversions generated from the initial velocity models listed in table 4.2. The initial velocity model selected was the 200 m/s cover over 100 m/s waste with a 10 m/s/m gradient. A smoothing control of 0.1 was used. In this case, an x/y ratio of 5 gave much more reasonable results.

Model Type	S-wave velocity at the surface (ms)	Gradient (m/s/m)
Homogeneous	150	0
	200	0
	cover 200 waste 150	0
Velocity gradient increasing with depth	100	15
	150	15
	cover 200 waste 100	10

Table 4.2: S-wave initial velocity models created using *Build Model*

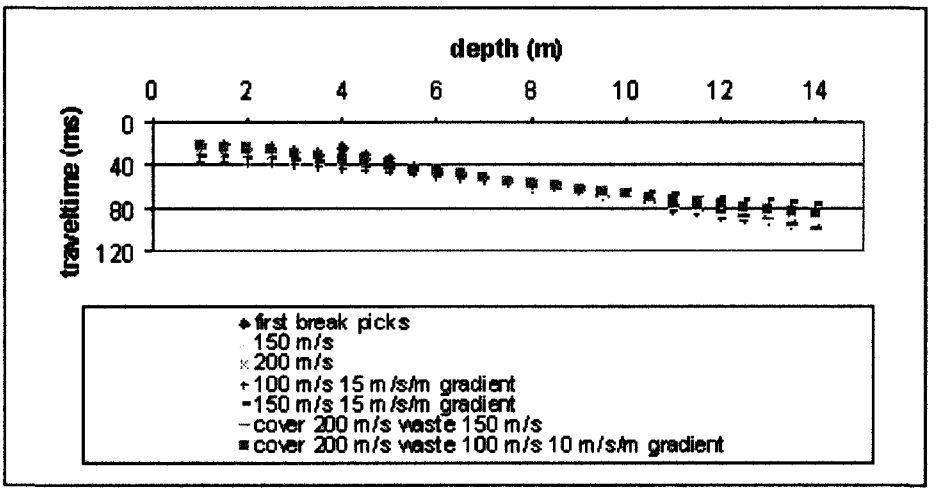

Figure 4.35: Observed and raytraced S-wave first breaks from tomograms generated by different initial velocity models

4.6.5 Resulting Tomograms

P-wave

Once an initial velocity model and appropriate inversion parameters have been determined, the tomography method can be applied. Figure 4.36, Figure 4.37 and Figure 4.38 are P-wave tomograms computed using the seismic hammer data acquired with 5 m, 10 m and 15 m offsets respectively. There is fairly good agreement between the 5 m and 10 m offset data, indicating that the first breaks were fairly accurately picked. The 15 m offset data exhibits a different velocity profile, indicating that the first breaks may not have been accurately picked. As the offset is extended, the area of waste sampled also changes. It could be possible that the variations are due to genuine lateral velocity changes. In all cases there is a positive velocity gradient up to up 500 m/s. These velocities agree well with published P-wave velocity values.

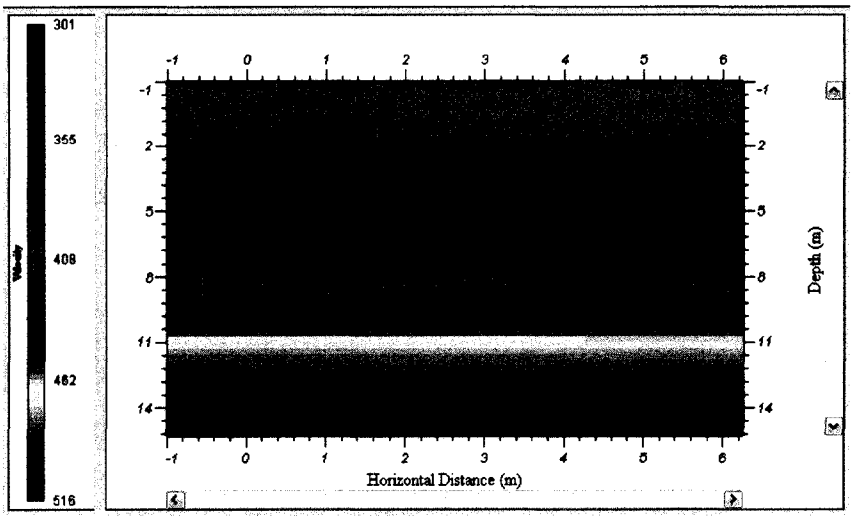

Figure 4.36: P-wave tomogram using the hammer (vertical channel, positive hit) at a 5 m offset

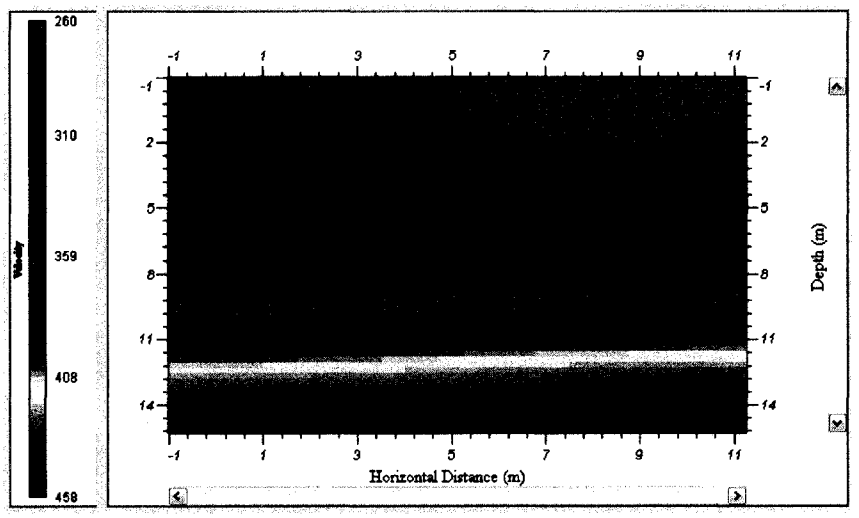

Figure 4.37: P-wave tomogram using the hammer (vertical channel, positive hit) at a 10 m offset

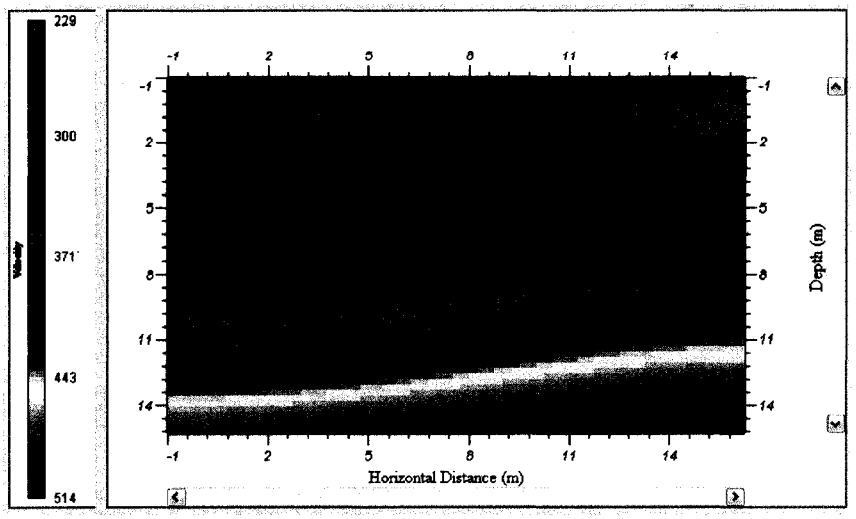

Figure 4.38: P-wave tomogram using the hammer (vertical channel, positive hit) at a 15 m offset

To improve the reliability of results, it is possible to combine the traveltimes from different offsets into one inversion. Figure 4.39 is the tomogram from between the boreholes using both north and south VSP data on Survey 1, day 1 combined. It was not possible to analyze the south borehole from day 1 and day 2 due to noise interference and the day 2 tomogram has been excluded. Figure 4.40 is the tomogram from combining both the 5 m and 10 m offsets in Survey 2. The 15 m offset was not included due to the unreliability of the first break picking. The data from Survey 3 was very noisy and difficult to pick the first breaks. It was not possible to generate accurate tomograms using the data from Survey 3.

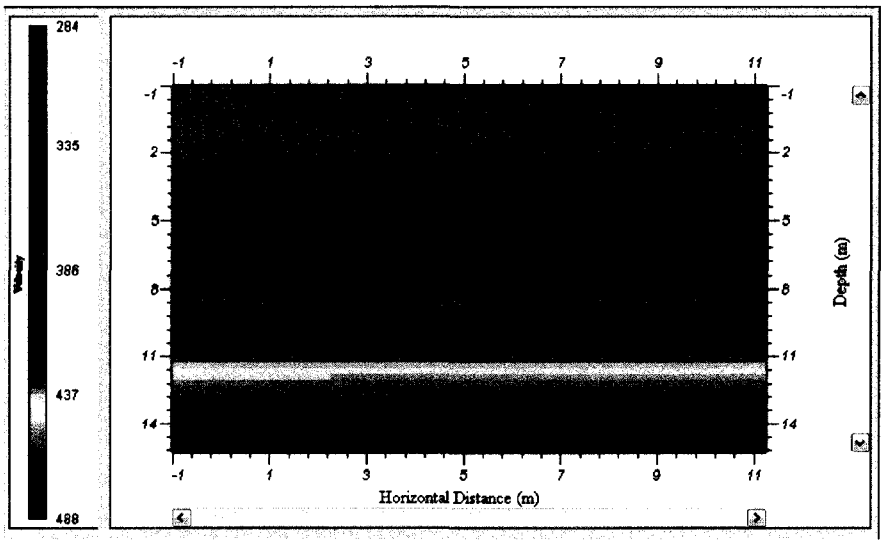

Figure 4.39: The combination of traveltimes into a single inversion from both boreholes on Day 1 during Survey 1.

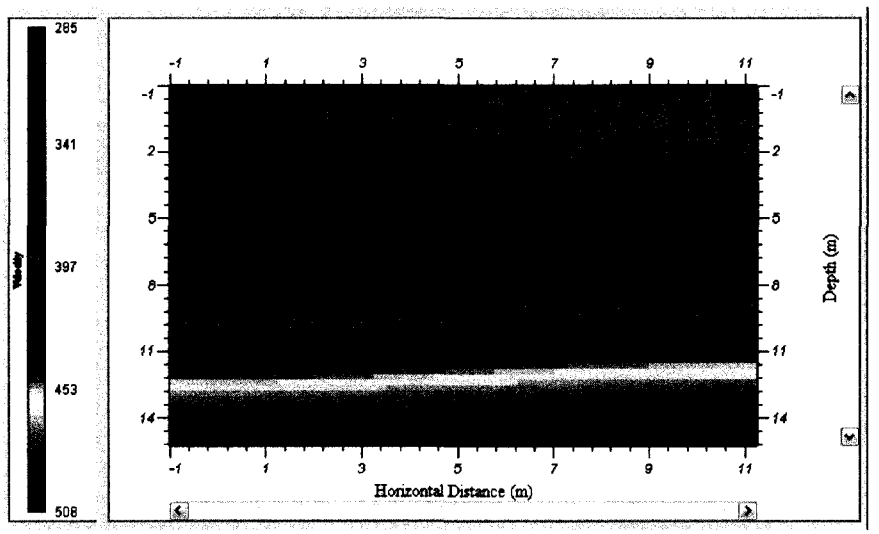

Figure 4.40: The combination of traveltimes into a single inversion from Figure 4.36 and Figure 4.37.

S-wave

Figure 4.41 and Figure 4.42 are the observed and raytraced S-wave first breaks acquired using the seismic hammer at a 5 m offset for horizontal channel 1 and horizontal channel 2 respectively. These should be essentially the same because the input data were recorded from the same shot and there is in fact excellent agreement between the velocity

distributions. In both cases, a higher velocity cover layer is visible with a velocity approximately 240 m/s. Beneath cover the velocity decreases to about 140 m/s and then increases again with depth to approximately 210 m/s. The S-wave velocity profile for a 10 m offset seemed to follow initial models too closely and is not considered to be very reliable. Many different models were attempted. As an example, Figure 4.43 is the resulting tomogram for a 200 m/s cover 150 m/s waste initial model. The S-wave wave data at 15 m was nearly impossible to pick and therefore not included. S-wave data was not collected during Survey 1 and the data acquired between the boreholes during Survey 3 was too noisy to accurately pick first breaks. As a result, it was not possible to combine different traveltimes from different data sets into a single inversion. The S-wave velocities shown in Figure 4.41 and Figure 4.42 fit well within the range of published S-wave velocities with depth by Choudhury and Savoikar (2009). It can therefore be assumed that Equation 2-9 is applicable for the Ste. Sophie bioreactor landfill. The Kavazanjian (1996) S-wave velocity profile from Figure 2.4 seemed to match the S-wave velocity profiles from this study the most closely. In this case, it could be assumed that the unit weight of the waste should fall in the range of 10-15 kN/m^3.

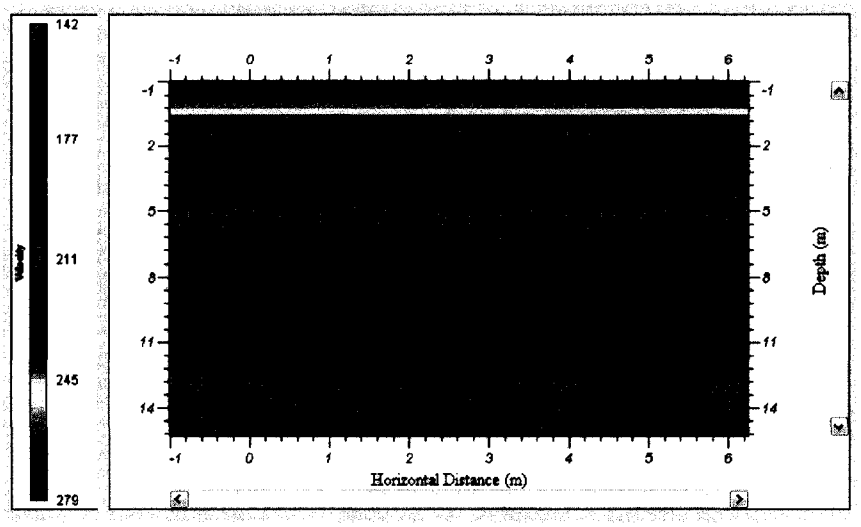

Figure 4.41: S-wave tomogram using the hammer (horizontal 1 component, south hit) at a 5 m offset.

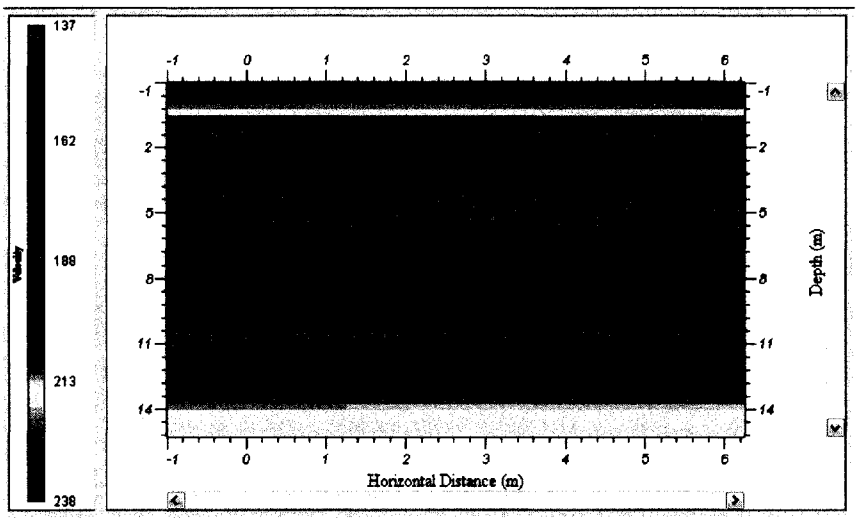

Figure 4.42: S-wave tomogram using the hammer (horizontal 2 component, south hit) at a 5 m offset

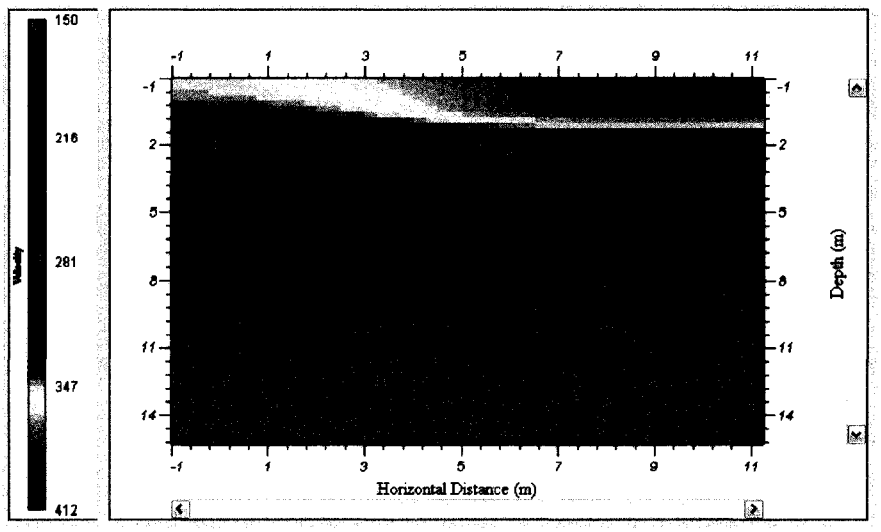

Figure 4.43: S-wave tomogram using the hammer (horizontal 2 component, south hit) at a 10 m offset

4.6.6 Comments on the Application of Tomography

There a few limitations in using a tomographic approach for this application. Firstly, the wavelengths are too large relative to the area being inverted to provide adequate resolution of different velocity structures. This issue is rather severe in terms of P-waves, due to the fact that the area being inverted does not represent even a single wavelength. The limited ray coverage provided by the surface source also reduces the level of resolution. In this case it would be difficult to know exactly where velocity anomalies are located in a horizontal direction.

It is essential in tomography to combine multi-offset VSP traveltimes into a single inversion. This was not possible for much of the data due to the inability to accurately pick first breaks. Single offset VSP tomograms are severely under-constrained and therefore the generated tomograms can not be heavily relied upon.

5.0 Seismic Velocity Under Variable Moisture Conditions

Recall that P-wave velocity is dependant on a number of different factors including saturation (see Section 2.2). This chapter analyzes P-wave velocity data collected from between the boreholes both before and after the injection of water. A discussion of the moisture distribution in the landfill as well as estimates for anticipated changes in saturation after the injection of water are also provided.

5.1 Moisture Content Variability in a Bioreactor Landfill

The optimal water content for biodegradation in solid waste falls with in the range of 40 to 70 % by weight on a wet basis (Reinhart and Townsend, 1998). Lower moisture contents reduce the degradation rate due to insufficient water to support the microbial mass. High moisture contents impede the flow of the landfill gas, reducing gas collection capabilities and therefore reducing the economic benefit. The field capacity of waste in landfills, which refers to the water content at which leachate will begin to drain out of the waste, falls within the lower end of this range. Field capacity is dependant on waste composition, age, density and porosity (Reinhart and Townsend, 1998). Incoming waste is usually below field capacity and the optimal range for biodegradation. Water can be added to the waste at the tipping face as the waste is placed in the landfill, through leachate recirculation pipes installed throughout the landfill and by infiltration due to precipitation. The Ste. Sophie bioreactor contains three series of horizontal leachate recirculation pipes that reintroduce leachate through the waste to increase the moisture content and therefore hence the biodegradation in the waste. The minimum water content

of the waste occurs at the time of placement. Over time the waste settles, reducing the pore space, and increasing the moisture content. Also, as the waste degrades, settlement increases and water is generated as a by-product, also increasing the moisture content.

Ideally, the entire landfill would be maintained at field capacity via continual leachate recirculation. However, moisture contents below field capacity are present due to preferential channelling of leachate. Despite the presence of a leachate collection system installed at the base of the landfill to collect the leachate that has percolated through the waste, saturated conditions can still occur. Microbial activity can cause clogging of the leachate collection pipe trenches (Rowe et al., 1997). Compaction and waste stabilization greatly reduce the permeability of the lower levels of waste thereby reducing vertical flow and therefore the volume of leachate collected. If the leachate collection system is unable to collect the excess leachate, mounding will occur and the lower levels of waste will begin to saturate. Localized mounds may also exist due to low permeability layers from daily and interim covers or certain waste types such as plastic (Reinhart and Townsend, 1998). Under saturated conditions, the flow of landfill gas and the biodegradation process is impeded (Reinhart and Townsend, 1998). It is difficult to control exactly where the leachate flows within the waste and therefore it is difficult to know the moisture distribution throughout the landfill.

5.2 Estimated Level of Saturation

In order to anticipate the sensitivity of P-wave velocity changes, the range of saturation at which the waste is maintained must be estimated. The Ste. Sophie bioreactor has been closed since 2005, so it is reasonable to assume that most of the waste has reached field capacity via leachate recirculation and infiltration. Yuen and Styles (2000) provide solid waste properties from a landfill in Melbourne, Australia that utilizes leachate recirculation. They have estimated an in-situ bulk density of 830 kg/m^3 with a corresponding porosity of 0.55, which they suggest represents well-compacted waste. Reinhart and Townsend (1998) suggest a field capacity of approximately 50% by wet weight for a similar density. Using these parameters, a saturation level of 0.75 was estimated. The waste located between the boreholes should have a water content at or lower than field capacity. This is because the functional leachate recirculation pipes are located at a level just below our boreholes and therefore leachate had not been recirculated through this portion of the waste. The moisture content in this area has only increased by means of infiltration, settlement and biodegradation.

P-wave velocities are not very sensitive to changes in moisture content for sand at saturation levels of 0.75 or lower (Yang, 2002). It is hoped that waste might exhibit a more sensitive behaviour at lower saturation levels.

5.3 Anticipated Changes with the Addition Of Water

There is no way of knowing what the actual initial moisture content is between the boreholes, however, as discussed above, it is most likely below field capacity. There is also no way of knowing how the added water distributes itself throughout the waste. Therefore it is difficult to evaluate the changes you would expect to see by adding a known volume of water. Recall, in Survey 1 about 5 m^3 of water and in Survey 3 about 7 m^3 of water was added between the boreholes. It is assumed that the initial saturation level is approximately 0.6, slightly below field capacity, and that the total volume of water added infiltrates a rectangular volume. The assumption of a rectangular volume is used because the excavation to which the water was added during Survey 1 was rectangular. It is then assumed that the water will simply infiltrate directly downwards from a 3 m by 3 m excavation. Three infiltration depths of 3 m, 5 m and 7 m are used. It is difficult to determine the actual depth of infiltration. Using saturated hydraulic conductivity values from Reinhart and Townsend (1998), it was found that water would reach a depth of almost 2 m over the 2 hour injection period. This can be considered the worst-case scenario because the waste between the boreholes is most likely not saturated. If we assume that the waste is below field capacity, then using the assumptions of the Green-Ampt model for infiltration, there exists a negative pressure, or suction, below the wetting front. In this case, water is actually drawn into the waste and would travel through the waste at a much faster rate than the saturated hydraulic conductivity. In a very simplistic approach, the estimated change in saturation is provided for a few different cases.

Case 1

Infiltration Volume of: 3 m* 3 m * 3 m = 18 m^3

Survey 1: Saturation increased from 0.60 to 1.0

Survey 3: Saturation increased from 0.60 to 1.0

Case 2

Infiltration Volume of: 3 m * 3 m * 5 m = 45 m^3

Survey 1: Saturation increased from 0.60 to 0.80

Survey 3: Saturation increased from 0.60 to 0.87

Case 3

Infiltration Volume of: 3 m * 3 m * 7 m = 63 m^3

Survey 1: Saturation increased from 0.60 to 0.75

Survey 3: Saturation increased from 0.60 to 0.80

In the above scenarios, depending on how large of an area the water infiltrates, it would be possible to obtain saturated conditions and therefore it would be possible to detect changes in P-wave velocity.

5.4 Changes in Velocity if Saturation Occurs for any Seismic Raypath

Although it might not be possible to obtain saturated conditions in the waste for long periods of time between the boreholes, it is quite possible to obtain saturated or near saturated conditions in some areas between the boreholes during the injection of water

and for a short period afterward. This is because the water has simply not had enough time to percolate downward through the waste. During Survey 1, water was added to the waste between the boreholes via a 3 m^3 excavation. Water was ponding at the surface for the majority of the water injection time. It can be reasonably assumed that some portion of the waste in the area under the excavation was close to saturated.

Consider the transient test during Survey 3 in which a geophone was maintained at a depth of 5 m during the addition of water. From Figure 3.11, approximately 10% of the raypath lays directly below the gravel trench in which the water is being added. If you assume that this portion of the raypath is saturated, the velocity of that wave should be significantly affected. Assuming an average waste P-wave initial velocity of 350 m/s, saturating about 10% of the raypath would result in a velocity of 465 m/s. The first breaks would then arrive approximately 8 ms earlier. An 8 ms traveltime difference would be easily noticeable on a VSP gather.

5.5 Survey 1 Results

During Survey 1, the north borehole vertical-component geophone VSP data, shown in Figure 5.1, was collected on Day 1. At the beginning of Day 2, 5 m^3 of water was added into the excavation between the boreholes. Then the north borehole vertical-component geophone VSP data, shown in Figure 5.2, was acquired in an identical fashion to Day 1. The first break time picks are indicated by the dashed lines. The time picks for both Day 1 and Day 2 are plotted together in Figure 5.3. The difference between the times for both days is very small. Day 2 time picks are not consistently less than those of Day 1 and

therefore any differences between the two are due to inaccuracies in the interpretation process. There also may be some inconsistencies in terms of the exact geophone placement in the borehole. Although, to provide an idea of how the waveforms appear relative to each other, Figure 5.4 shows both Day 1 and Day 2 VSP data plotted directly over top of each other. The waveforms for both days are quite consistent with each other. Although VSP data were also acquired from the south borehole on both days, the Day 2 VSP data recorded was only noise and it was not possible to compare them with Day 1 results. This could have been due to a coupling issue between the geophone and the borehole.

The results of the transient test are shown in Figure 5.5. In this case, a geophone was held at a constant depth of 12 m and a seismic trace was recorded every 10 minutes during the injection of water. The waveform over the 2 hour period is very consistent with no detectable increase in P-wave velocity.

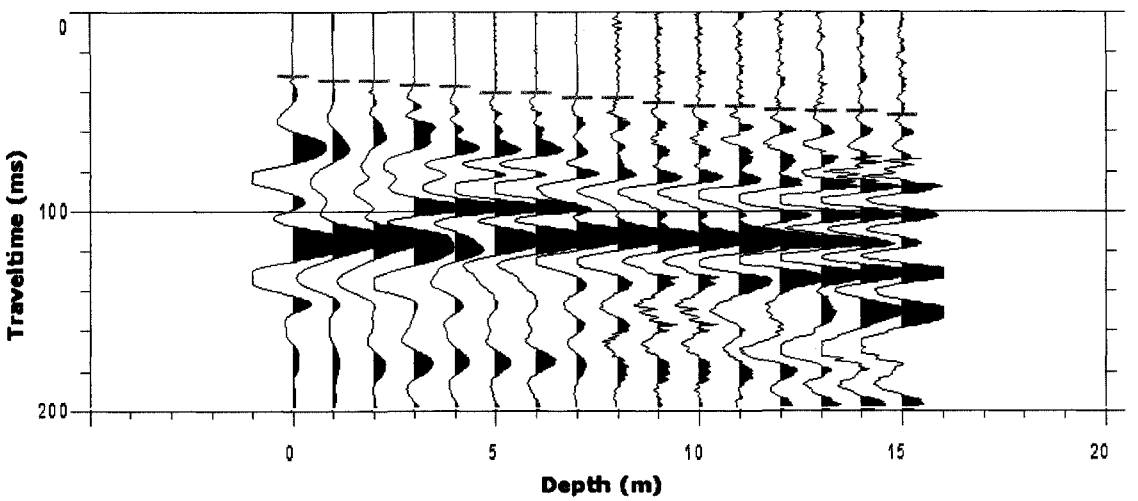

Figure 5.1: Survey 1. Vertical-component geophone VSP data and first break picks obtained from the north borehole on Day 1 at a 10 m offset. Maximum trace scaling. Filtered 0-200/250 Hz.

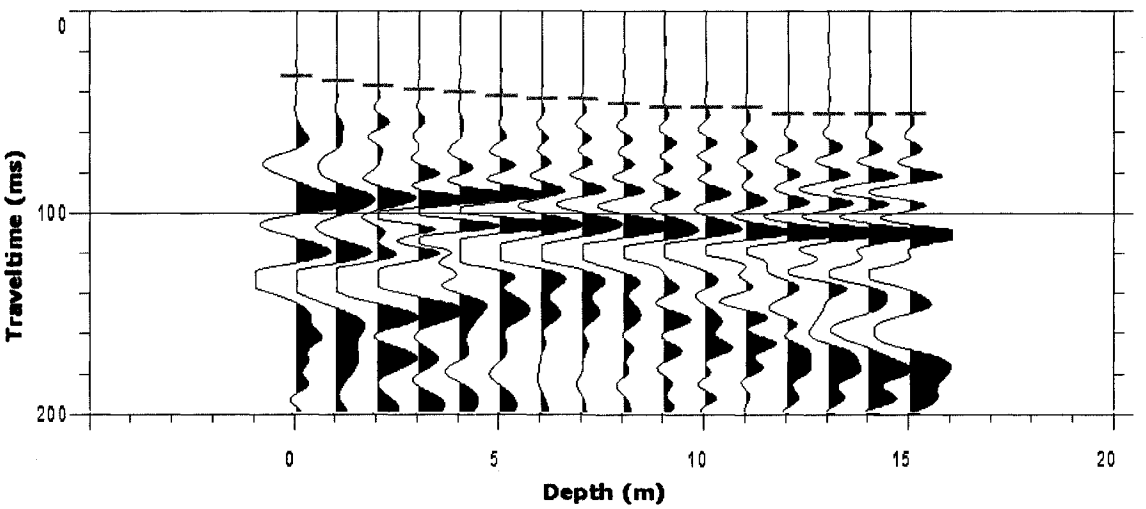

Figure 5.2: Survey 1. Vertical-component geophone VSP data and first break picks obtained from the north borehole on Day 2 at a 10 m offset. Maximum trace scaling. Filtered 0-200/250 Hz.

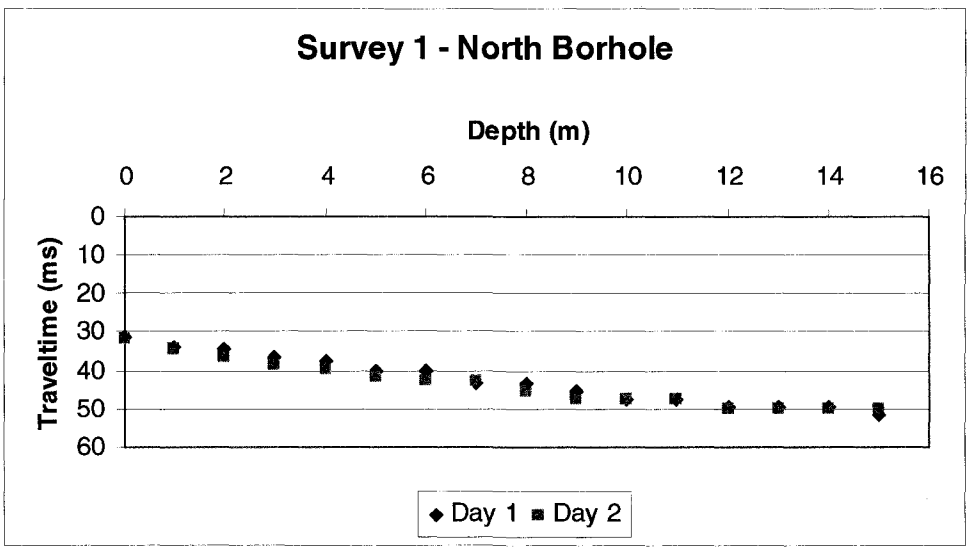

Figure 5.3: Survey 1 first break picks acquired using the north borehole from Day 1 and Day 2.

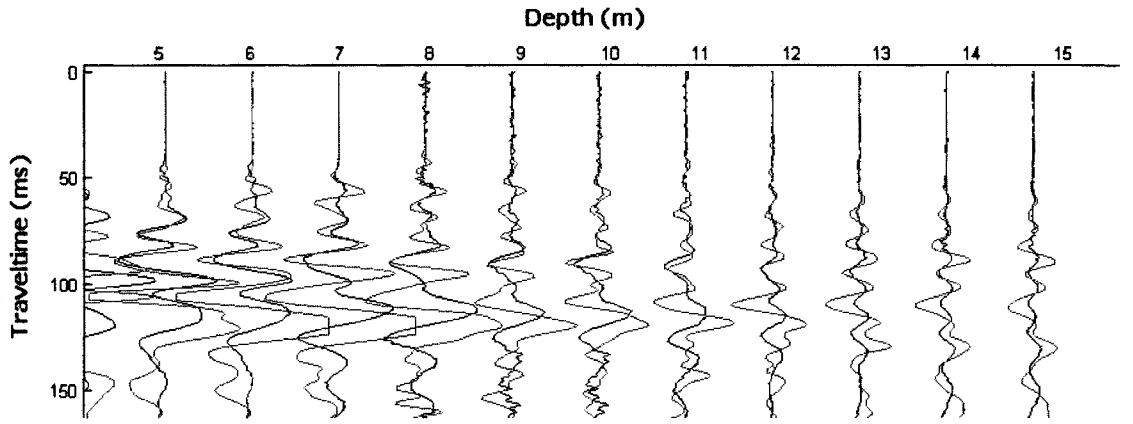

Figure 5.4: Survey 1. Vertical-component geophone VSP data from Day 1 (Blue) and from Day 2 (Green). Maximum global scaling. Filtered 0-200/250 Hz.

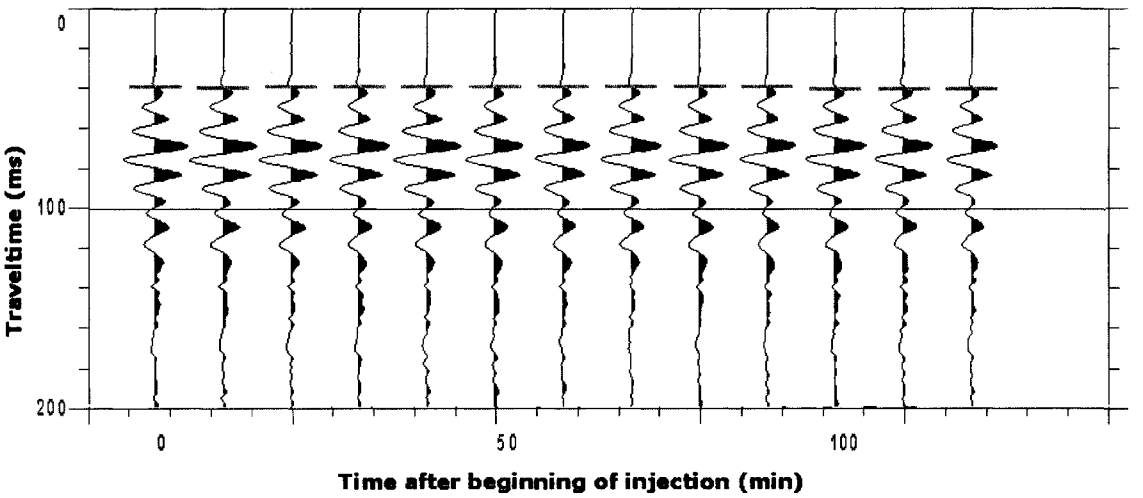

Figure 5.5: Survey 1. Vertical-component geophone seismic traces from a 12 m depth in the north borehole obtained every 10 minutes at a 10 m offset. Maximum global scaling. No Filter.

5.6 Survey 3 Results

Survey 3 was very similar to Survey 1 with a few minor changes. The geophone spacing was reduced to 0.5 m in order to better identify the first arrival event. The volume of water added was increased to 7 m^3 in order to increase the saturation level of the waste.

The water was added via a large PVC pipe installed into the gravel trench 2 m west from the plane of the two boreholes.

The vertical-component geophone VSP data for the north borehole for Day 1 and Day 2 are shown in Figure 5.6 and Figure 5.7, respectively. The vertical-component geophone VSP data for the south borehole for Day 1 and Day 2 are shown in Figure 5.10 and Figure 5.11, respectively. In both cases, the data are very noisy and it is very difficult to pick first arrivals against the background noise. A lower low pass filter was used due to the large amount of noise in the 100-200 Hz range. Instead of trying to pick the true first arrival, a larger amplitude portion of the waveform occurring in the window of 60-80 ms was picked instead. The waveforms were carefully examined for both days to ensure the same point on the wave was being picked.

The picked times for both days for the north and south boreholes are shown in Figure 5.8 and Figure 5.12 respectively. The picked times for the north borehole in Figure 5.12 are very similar. However in this case, Day 2 times have been consistently picked at earlier times than on Day 1. In this case, the reduction in traveltimes corresponds to a maximum velocity increase for all raypaths of about 10 m/s. The picked times for the south borehole in Figure 5.8 are very similar. Day 2 times are not consistently faster the Day 1 times. Because both VSP data do not consistently have faster picked times, it is still inconclusive as to whether or not there is an actual increase in P-wave velocity. Also, it seems unreasonable that the first arrival would increase by the same amount for the entire

depth range. Since the data is quite noisy, a point slightly earlier on the wave is being consistently picked.

To compare the waveforms, VSP data for Day 1 and Day 2 have been plotted directly over top of each other in Figure 5.9 and Figure 5.13 for the north and south boreholes respectively. In both cases, the waveforms are quite consistent with each other. There is quite a bit more noise on the south borehole VSP data. There is no obvious reason for this, however it could be due to a small crack in the borehole which would allow landfill gas to flow up the borehole and therefore generate noise. Also, the integrity of the grouting around the borehole might have diminished over the last year.

Similar to Survey 1, a transient test was conducted during the injection of water. Two geophones were maintained at constant depths of 5 m and 12 m and seismic traces were recorded every 10 minutes. Figure 5.14 shows the seismic traces since the start of the injection of water for a geophones depth of 5 m. Figure 5.15 shows the seismic traces since the start of the injection of water for a geophones depth of 12 m. Again, the first breaks were easily picked against the background noise and a later portion of the wave is picked to evaluate for relative changes. In both cases, the results over the 2 hour and 20 minute period are very stable, there is no detectable change in P-wave velocity during the injection of water.

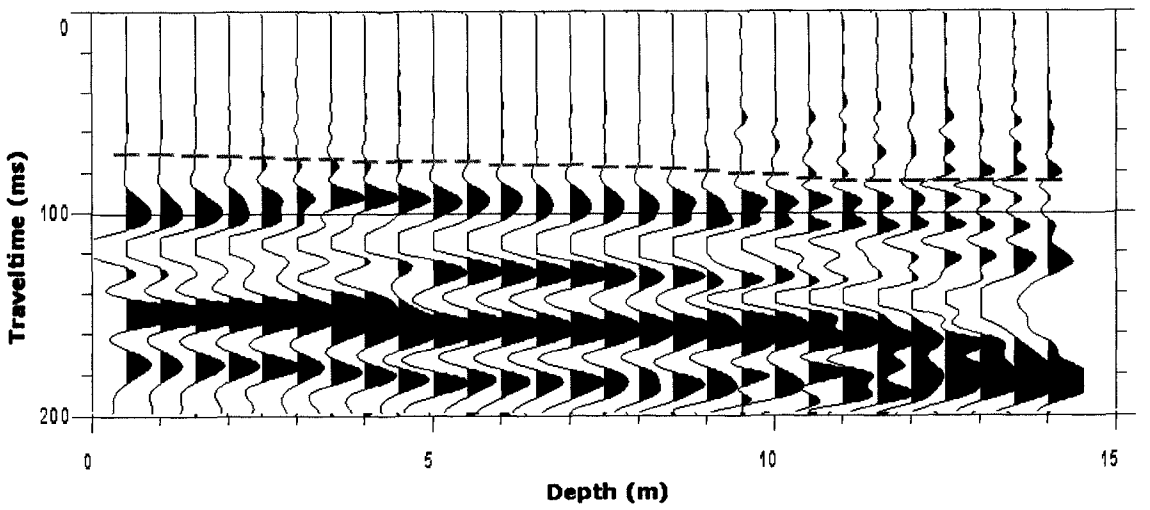

Figure 5.6: Survey 3. Vertical-component VSP data and first break picks obtained from the north borehole on Day 1 at a 10 m offset. Maximum trace scaling. Filtered 0-80/100 Hz.

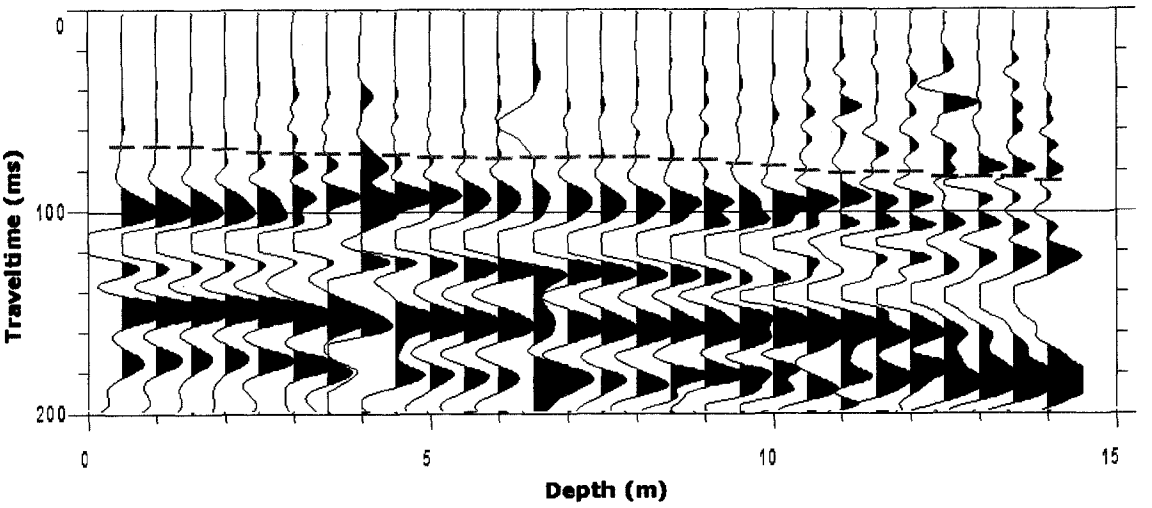

Figure 5.7: Survey 3. Vertical-component VSP data and first break picks obtained from the north borehole on Day 2 at a 10 m offset. Maximum trace scaling. Filtered 0-80/100 Hz.

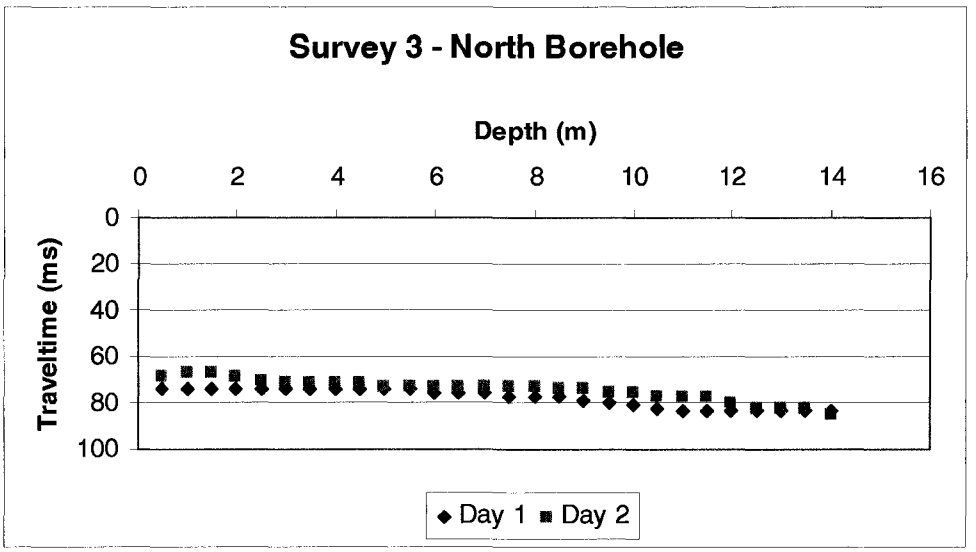

Figure 5.8: Survey 3. North borehole first break picks from Day 1 and Day 2.

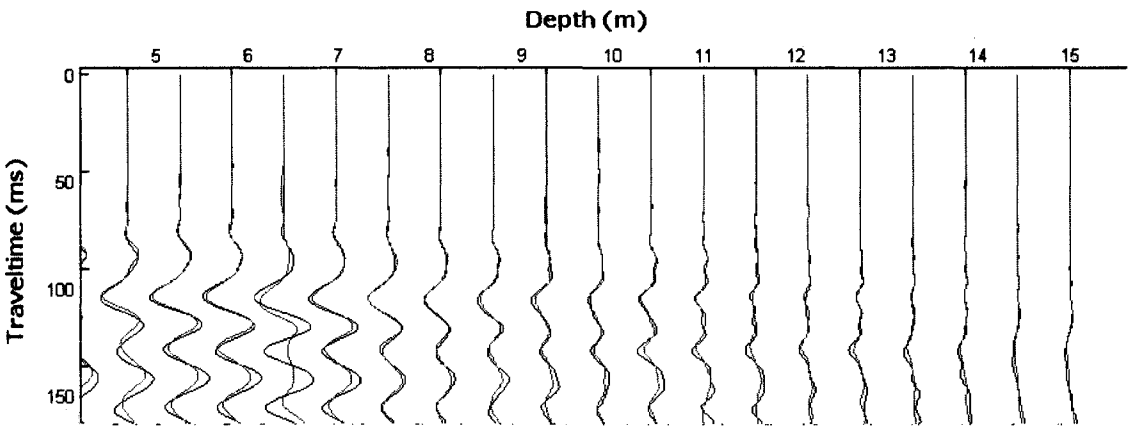

Figure 5.9: Survey 3. Vertical-component VSP data from north borehole on Day 1 (Blue) and VSP data from Day 2 (Green) at a 10 m offset. Maximum global scaling. Filtered 0-80/100 Hz.

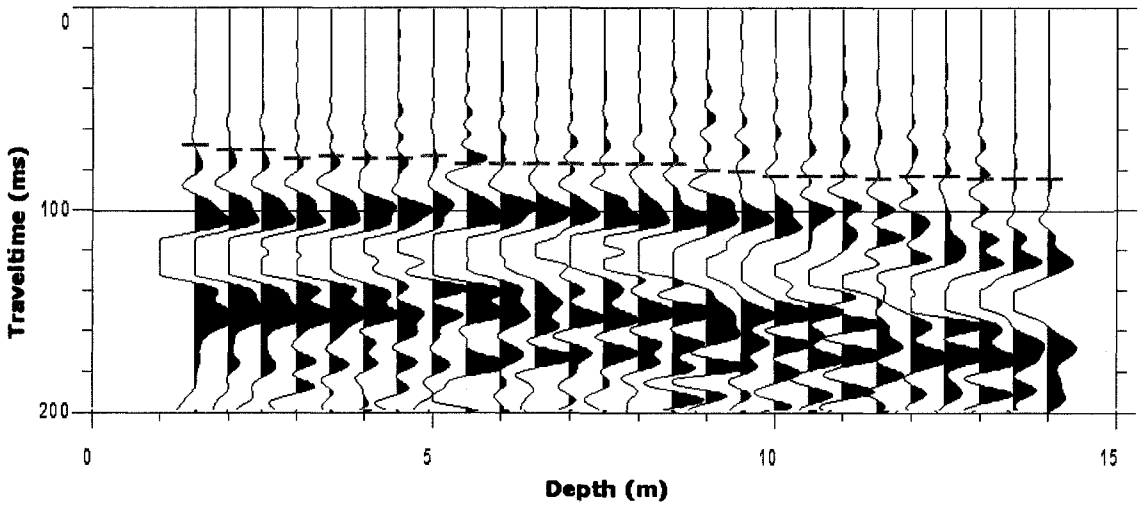

Figure 5.10: Survey 3. Vertical-component VSP data and first break picks obtained from the south borehole on Day 1 at a 10 m offset. Maximum trace scaling. Filtered 0-80/100 Hz.

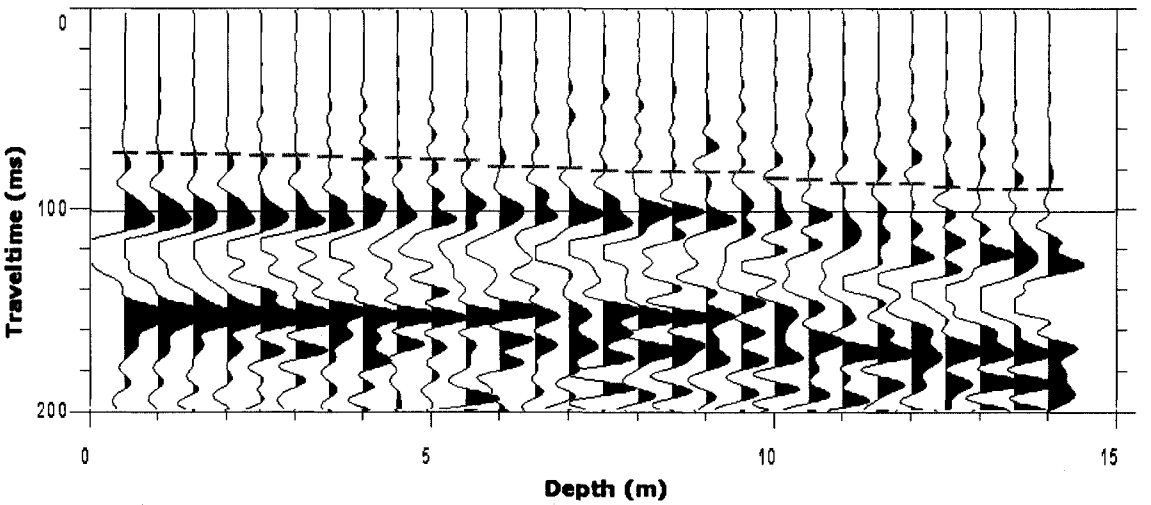

Figure 5.11: Survey 3. Vertical-component VSP data and first break picks obtained from the south borehole on Day 2 at a 10 m offset. Maximum trace scaling. Filtered 0-80/100 Hz.

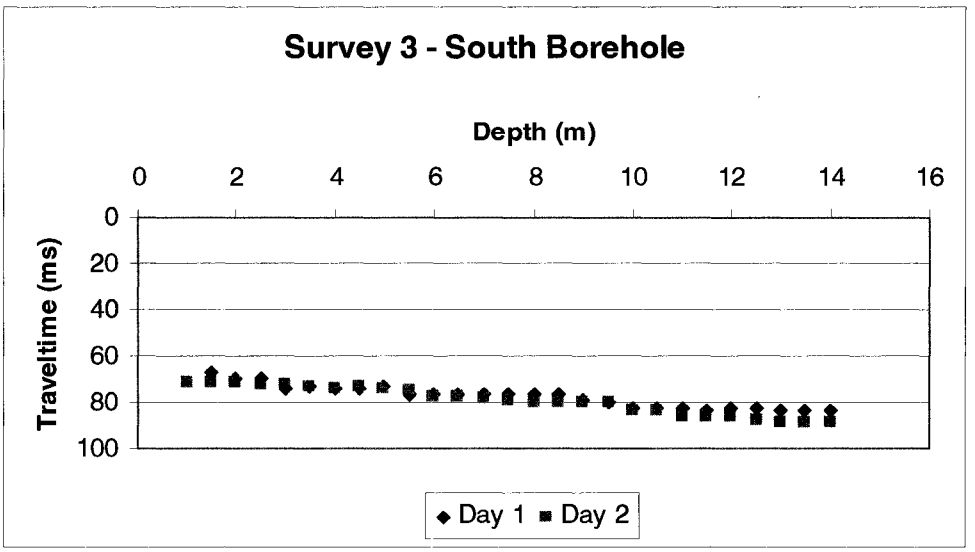

Figure 5.12: Survey 3. South borehole first break picks from Day 1 and Day 2.

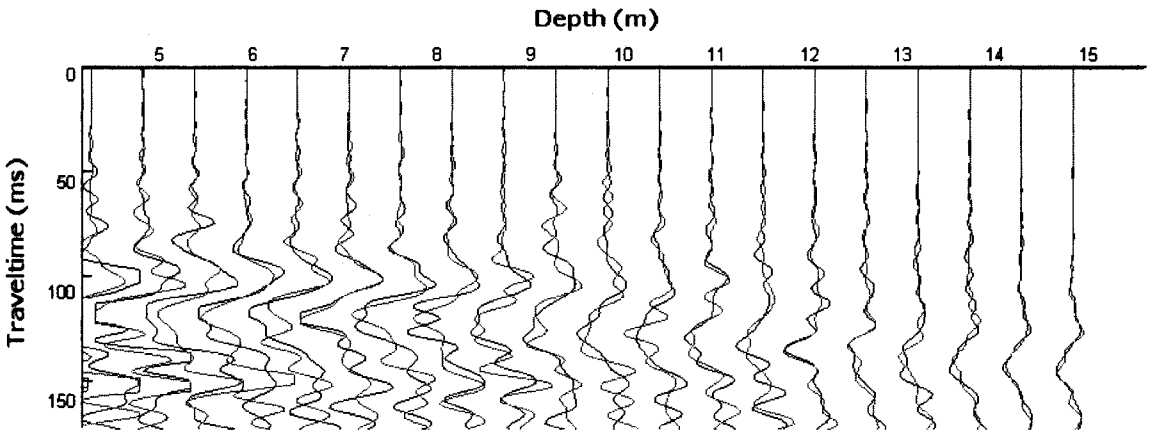

Figure 5.13: Survey 3. Vertical-component VSP data from south borehole on Day 1 (Blue) and VSP data from Day 2 (Green) at a 10 m offset. Maximum global scaling. Filtered 0-80/100 Hz.

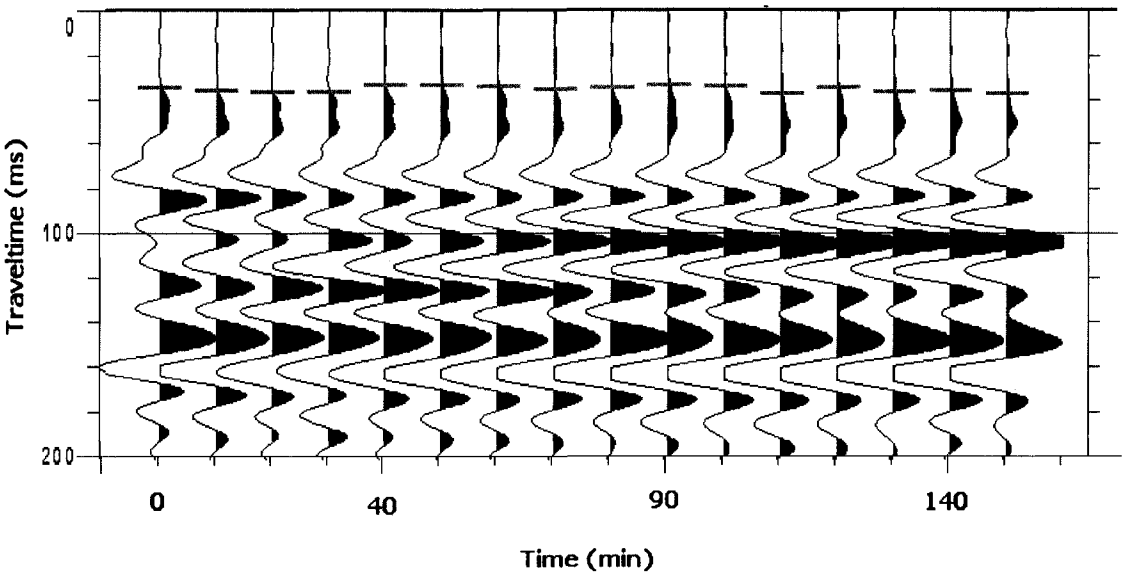

Figure 5.14: Survey 3. Vertical-component seismic traces from a 5 m depth in the north borehole obtained every 10 minutes at a 10 m offset. Maximum trace scaling. Filtered 0-80/100 Hz.

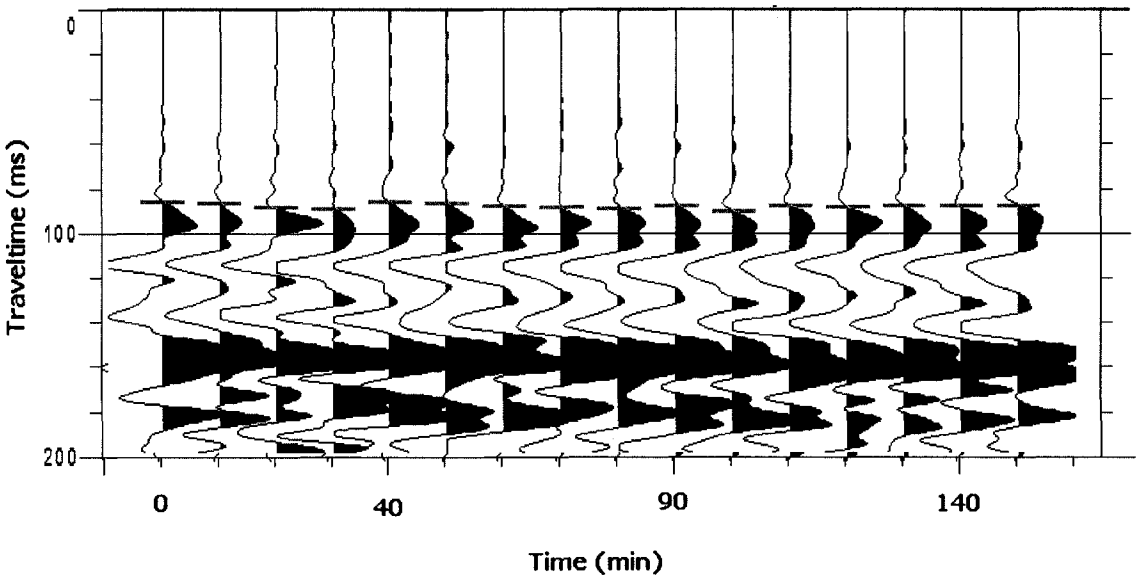

Figure 5.15: Survey 3. Vertical-component seismic traces from a 12 m depth in the north borehole obtained every 10 minutes at a 10 m offset. Maximum trace scaling. Filtered 0-80/100 Hz.

5.7 Discussion of Results

There were a few different reasons as to why it may not have been possible to conclusively detect an increase in P-wave velocity with the addition of water for any of the surveys. Again, the issue of wavelength relative to survey area arises. The water being added to the waste affects only a small part of the waveform. The P-wave wavelength may simply be too large to detect changes in waveform over the distances used in this survey.

Problems could arise when injecting water into the biogas collection trench. The collection trench may be slightly sloped in a westward direction, away from the plane of the boreholes. The trench is filled with gravel, through which water will likely flow at a much faster rate relative to the waste. Instead of the water being dispersed into the waste directly between the boreholes, it could preferentially flow westward through the trench and distribute itself into the waste over a much larger area than intended. In this case, a significant volume of the water added might never flow into the plane between the boreholes. During the transient test in Survey 3, the raypath for a geophone located at a 5 m depth travels directly through the trench. Even in this case, no velocity changes were detected. This could be due to the fact that the water injected to the waste percolates downward in a cone like fashion. Since the injection pipe is 2 m west of the plane of the boreholes (Figure 3.10), the area of influence of the cone probably intersects the borehole plane at a lower depth.

It was not possible to detect a signal using the borehole P-wave source. It was only possible to obtain a signal using the surface hammer source. As a result, it was not possible to obtain the desired raypath coverage and there is a large area where it is not possible to collect any data. Unfortunately this unsampled area corresponds to an area where it is most likely to be able to detect changes in velocity. A stronger surface or borehole source would allow for more of the area between the boreholes to be sampled and therefore a higher probably to detect changes in velocity.

The boreholes were only installed to a depth of 15 m, above the highest functional leachate recirculation trench series. Therefore, it is likely that the waste is maintained at field capacity and potentially at even lower moisture contents. The level of saturation in this area has been estimated at approximately 0.75. The level of saturation that is sensitive to changes in P-wave velocity falls within the range between 85-100%. If it is assumed that waste has a similar P-wave response to saturation as sand, and the added water dispersed over a large area, P-wave velocity in waste will remain stable between the boreholes. It was initially hoped that the P-wave response to changes in saturation would be more sensitive in a lower range compared to that of sand, however, this may not be the case.

Seismic techniques may be better suited for identifying saturated areas within the landfill as opposed to identifying areas that have not yet reached field capacity. Water has a P-wave velocity of approximately 1500 m/s, compared to roughly 400 m/s for compacted waste. This change would be easily detectable by either borehole or surface refraction

and reflection surveys to evaluate the level of mounding in the landfill. Provided a strong surface source was available, a surface seismic refraction or reflection survey would be a feasible alternative to determine the depth of mounding throughout the landfill.

6.0 Conclusions

6.1 Seismic Sources

Three different seismic sources were tested. The borehole P-wave source was not able to generate a detectable signal at a distance of 10 m. The borehole S-wave wave source generates an even weaker signal than the P-wave source. As a result, both borehole sources were not used for the remainder of the study although only having a surface source is very limiting in terms of the coverage between the boreholes. Two surface sources were compared. It was possible to generate a detectable signal in the borehole from a surface hammer source. The seismic gun which is traditionally known to be a strong source was also tested in hope that it would be possible to extend the offsets to larger distances and increase the coverage for the VSP survey. The seismic gun signal, however, has a slightly higher frequency content than that of the hammer and was therefore attenuated over shorter distances. There were also coupling and triggering issues with the seismic gun. Overall, the hammer provided a stronger signal in the waste.

6.2 Seismic Resolution

The seismic hammer was able to produce P-waves and S-wave with wavelengths of 40 m and 3.5 m respectively. This represents a major problem in terms of the survey area, which is able to record less than a single wavelength for P-waves and just a few wavelengths for S-waves. These conditions do not allow for adequate resolution of the velocity distribution in the waste. Moving to a higher frequency source could help resolve

this issue, however higher frequency source signals will attenuate over shorter distances in the landfill environment.

The limited coverage provided by the surface source reduces the multi-angular coverage throughout the waste and therefore reduces the resolution of velocity structures. A borehole source that is able to generate a detectable signal would help resolve this issue.

6.3 Seismic Wave Propagation Through Waste

During the three surveys conducted for this research, it was possible to generate and record both P-waves and S-waves propagating within the landfill. However since the survey area is considered to be in the near-field, the distinction between P-wave and S-wave modes is not as well defined compared to larger source-receiver distances. S-waves did not appear to be very well developed. The data recorded in waste are very noisy compared to those from media like rock or soils. Seismic waves are greatly attenuated due to the heterogeneous nature of solid waste. Accurately picking the first arrivals, becomes very difficult at a 15 m offset for P-waves and a 10 m offset for S-waves. The data appeared increasing noisy with each survey. During Survey 3, data was very noisy and it was not possible to accurately pick first breaks at offsets of even 10 m. This behaviour seems odd, when considering that Catley et al. (2006) were able to record reflections off the landfill base. In this case, the waves had travelled almost four times the distance compared to this study. There may have been issues with: (1) geophone coupling with the borehole; (2) attenuation through the borehole wall; and (3) attenuation through the bentonite grouting poured in between the borehole and the waste. The quality of this

grouting may have deteriorated over time due to changing conditions in the landfill. There is also the attenuating affect of the cover that was not present during the previous study.

6.4 Seismic Tomography

The seismic tomography approach was not as successful as hoped. The size of the wavelengths relative to study area reduces the level of detail that can be extracted using ray-based inversion methods. Seismic tomography relies on having a large amount of data and being able to very accurately pick these data. Unfortunately in this case, both the coverage is limited and the first breaks are noisy and difficult to pick. Single offset VSP inversions are severely under-constrained. The resulting velocity inversions should be considered preliminary. They provide a general overview of what the velocity distribution is, rather than detailed information. The P-wave tomogram has a velocity gradient increasing with depth which likely reflects increased compaction of the waste. The velocity through the cover is approximately 300 m/s, and then increases to approximately 500 m/s at a depth of 15 m. The S-wave tomogram exhibits a velocity inversion. The velocity through the cover is approximately 230 m/s. Just below the cover the velocity is about 140 m/s, which increases to about 210 m/s at a depth of 15 m.

6.5 Seismic Velocity Under Variable Moisture Conditions

It was estimated that the waste between the two boreholes has a moisture content either at or below field capacity because of the lack of leachate recirculation in that particular area. This corresponds to a saturation level of 0.75 or lower. It was not possible to detect

changes in P-wave velocity with the addition of 5 m^3 or 7 m^3 of water. This is due to a number of different possible reasons. The water being added covers a small distance relative to the distance of a single P-wave wavelength. This would not result in significant waveform changes. It is possible that a large portion of the water being added between the boreholes, preferentially flowed westward through the biogas collection trench. In this case, much of the water may not have reached the plane between the boreholes and the level of saturation was not increasing as much as we had anticipated. The range of saturation levels created may not have been very sensitive to changes in P-wave velocity. The limited coverage of the surface source created a large area between the boreholes that remained unsampled. Unfortunately it is this area where water was most likely to flow and therefore where velocity changes were most likely to occur. Due to the large P-wave velocity variation between waste at field capacity and saturated waste, however, it could potentially be feasible to utilize P-wave to detect mounding levels within the landfill in the future.

6.6 Recommendations

It was hoped that borehole seismic methods would be an improvement over the previous surface reflection study. It was originally assumed that a seismic tomography experiment would provide greater resolution of the velocity distribution within the landfill. The results from this study indicate a larger source is needed. It would then be possible to increase the size of the study area to address the issue of resolution. It would be useful to evaluate the effects of the borehole on the seismic signal. There was probably coupling issues between the borehole and the waste. Due to the issues discussed above, it seems

that a surface reflection survey may be a better alternative. It is possible to use tomography on surface reflection data. Surface reflection and refraction surveys offer advantages over boreholes surveys because they are more efficient. Surface geophones are more cost effective and can be employed in large arrays that allow for an entire gather to be collected at a single shot offset. More powerful sources, such as a weight drop, are available for surface studies, which allow for a larger distance between the source and receivers. In this case, larger distances can be covered and surveying the entire landfill becomes feasible. If chains of geophones could be installed within the landfill as waste is filled, this process would become much more efficient.

It would be useful to determine the relationship between P-wave velocity and moisture content in waste. This relationship would have to be determined in a controled laboratory environment. In a smaller environment, it may be possible to use a higher frequency source. It would then be more likely to notice changes in waveform with the addition of water. Ideally, a linear relationship between P-wave velocity and saturation would prove most useful. If it is determine that P-wave velocity is only sensitive to change in the upper levels of saturation, then P-waves could still have the useful application of detecting saturated areas throughout the landfill. It may also be possible to detect changes in dry density due to settlement from increased S-wave velocity. Although preliminary work has been done by Kavazanjian et al. (1996), more work would have to be done to calibrate the relationship between density and S-wave velocity.

7.0 References

Baria, R, Jackson, P.D., and McCann, D.M. (1989) Further development of a high frequency seismic source for use in boreholes. *Geophysical Prospecting* 37:31-52.

Bouazza, A. and Kavazanjian, Jr., E., (2000) Characterization of municipal solid waste sites using the continuous surface wave method. Proceedings International Conference on Geotechnical and Geological Engineering, GeoEng.2000, Melbourne, Australia. (CD-ROM)

Carpenter, P. J., Bruer, E., Higuera-Diaz, I. And Thompson, M. (2004) Seismic Tomographic Imaging of Buried Karst Features. Presented at the *2004 annual SAGEEP Conference*, Colorado Springs, CO, February 25, 2004.

Catley, A. J. (2006) Seismic velocity analysis to determine moisture distribution in a bioreactor landfill. Master's Thesis, Carleton University, Ottawa, Canada.

Catley, A., Samson, C., and van Geel, P. (2008) Seismic velocity analysis to determine moisture distribution in a bioreactor landfill. *J. of Solid Waste Technology and Management* 34(2): 81-90.

Choudhury, D. and Savoikar, P. (2009) Simplified method to characterize municipal solid waste properties under seismic conditions. *Waste Management* 29: 924:933.

Davis, J.L. and Annana, A.P. (1989) Ground-penetrating radar for high-resolution mapping of soil and rock stratigraphy. *Geophysical Prospecting* 37: 531-551.

Gardner, G. H. F., Gardner, L.W. and Gregory, A.R. (1974) Formation velocity and density – the diagnostic basics for stratigraphic traps. *Geophysics* 39: 770-80

Gawande, N.A., Reinhart, D.R., Thomas, P.A., McCreanor, P.T., and Townsend, T.G. (2003). Municipal solid waste in situ moisture content measurement using an electrical resistance sensor. *Waste Management* 23: 667-674.

Geometrics Inc., San Jose, California
Photo available from: www.geometrics.com/Seismographs/Geode/geode.html

Geostuff, Grass Valley, California. Geostuff borehole geophone data sheet. Accessed January 2009.

Gibson, R. L. Jr. & Peng, C. (1994) Low- and high-frequency radiation from seismic sources in cased boreholes. *Geophysics* 59:1780-1785.

Goulty, N.R. (1993) Controlled-source tomography for mining and engineering applications. Seismic Tomography: Theory and Practice, edited by Iyer, H.M. and Hirahara, K. 797:811, Chapman and Hall, London, UK.

Green, A. et. Al. (1999) A template for geophysical investigations of small landfill. *The Leading Edge* February 1999.

Guérin, R., Munoz, M.L., Aran, C., Laperrelle, C., Hidra, M., Drouart, E., and Grellier, S. (2004). Leachate recirculation: moisture content assessment by means of a geophysical technique. *Waste Management* 24: 785-794.

Hatanaka, M. and Masuda, T. (2008) Experimental study on the relationship between the degree of saturation and P-wave velocity in sandy soils. Geotechnical Engineering for Disaster Mitigation and Rehabilitation. Science Press, Bejing, China and Springer-Verlag, Berlin, Germany.

Kavazanjian, E., Jr., Matasovic, N., Stokoe, K.H.II, Bray, J.D. (1996) In situ shear wave velocity of solid waste from surface wave measurements. *Environmental Geotechnics* Kamon, (editor), 1996 Balkema, 1:97-102.

Korfiatis, G.P., Demetracopoulos, A.C., Bourodimos, E.L., and Nawy, E.G. (1984) Moisture transport in a solid waste column. *J. Environmental Engineering* 110: 780-796.

Li, R.S., and Zeiss, C. (1999) Automated moisture measurement system for in-situ moisture measurement in landfills. The International Conference on Solid Waste Technology and Management, Widener Univ School Eng, Chester, PA: 943-950.

Li, R.S., and Zeiss, C. (2001) In situ moisture content measurement in MSW landfills with TDR. *Environmental Engineering Science* 18: 53-66.

Miller, R.D., Pullan, S.E., and Waldner, J.S. (1986) Field comparison of shallow seismic sources, *Geophysics* 51(2): 2067-2092.

Phillips, C. Golder Associates Ltd., Mississauga, ON, Canada. Personal communication November 19, 2008.

Porsani, J.L. et. al. (2004) The use of GPR and VES in delineating a contamination plume in a landfill site: a case study in SE Brazil. *Journal of Applied Geophysics* 55: 199– 209.

Reinhart, D.R., and Townsend, T.G. (1998) Landfill Bioreactor Design and Operation. Lewis Publishers, Boca Raton, FL.

Rowe, K. R., Quigley, R. M., Booker, J. R. (1997) Clayey Barrier Systems for Waste Disposal Facilities, E & FN Spon. London, UK.

Schuck, A. and Lange, G. (2007) Seismic Methods, Environmental Geology: Handbook of Field Methods and Case Studies: 337-402, Springer, New York, NY.

Sharma, H.D., Dukes, M.T., and Olsen, D.M. (1990) Field Measurements of Dynamic Moduli and Poisson's Ratio of Refuse and Underlying Soils at a landfill Site. Geotechniques of Waste Fill – Theory and Practice, STP 1070, ASTM, Philadelphia, PA.

Sharma, P. (1997) Environmental and Engineering Geophysics, Cambridge University Press, New York, NY.

Sheean, J. R., Doll, W. E., Mandell, W.A. (2005) An Evaluation of Methods and Available Software for Seismic Refraction Tomography Analysis. *Journal of Environmental and Engineering Geophysics* 10(1): 21-34.

Sheriff, R. E., and Geldart, L. P. (1995). Exploration Seismology, Second Edition, Cambridge University Press, New York, NY.

Yang, J. (2002) Liquefaction Resistance of Sand in Relation to P-wave Velocity. *Geotechnique* 52:295-298.

Warith, M. (2002) Bioreactor landfills: experimental and field results. *Waste Management* 22:7-17.

Yang, J. & Sato, T. (2000) Interpretation of seismic vertical amplification at an array site. *Bulletin of the Seismological Society of America* 90:275–285.

Yuen, S.T.S., McMahon, T.A., and Styles, J.R. (2000) Monitoring In Situ Moisture Content of Municipal Solid Waste Landfills. *J. Environmental Engineering* 126: 1088-1095.

Yuen, S. T. S., and Styles J. R. (2000) Settlement and Characteristics of Waste at a Municiple Solid Waste Landfill in Melbourne. Proceedings of GeoEng2000 - International Conference on Geotechnical and Geological Engineering.